

Technical Report

**TR-23-25**

October 2023



# Alternative Buffer Material (ABM) experiment

Investigations of test packages ABM2 and ABM5

Daniel Svensson

Therese Bladström

Torbjörn Sandén

Ann Dueck

Ulf Nilsson

Viktor Jensen

SVENSK KÄRNBRÄNSLEHANTERING AB

SWEDISH NUCLEAR FUEL  
AND WASTE MANAGEMENT CO

Box 3091, SE-169 03 Solna  
Phone +46 8 459 84 00  
skb.se

SVENSK KÄRNBRÄNSLEHANTERING



ISSN 1404-0344

**SKB TR-23-25**

ID 2021598

October 2023

# **Alternative Buffer Material (ABM) experiment**

## **Investigations of test packages ABM2 and ABM5**

Daniel Svensson, Therese Bladström  
Svensk Kärnbränslehantering AB

Torbjörn Sandén, Ann Dueck, Ulf Nilsson, Viktor Jensen  
Clay Technology AB

This report is published on [www.skb.se](http://www.skb.se)

© 2023 Svensk Kärnbränslehantering AB



# Abstract

Bentonite clay is an integral part of the Swedish KBS-3 design for final repositories of high-level radioactive waste. In the KBS-3 concept, Wyoming bentonite, commercially known as MX-80 (American Colloid Co), has long been the standard reference for the buffer material. However, expanding the knowledge base of alternative buffer materials is crucial for optimizing safety, availability, and cost-effectiveness. To achieve this objective, the field experiment called Alternative Buffer Material (ABM) was initiated by SKB at the Äspö Hard Rock Laboratory, Sweden in 2006.

The primary goals of the ABM project were to characterize various clays in terms of their hydro-mechanical properties, mineralogy, and chemical composition. Furthermore, the project aimed to identify any differences in their behavior and long-term stability. Additionally, the inclusion of diverse clays and the presence of a heating steel component allowed for studying the interactions between iron and bentonite.

The installation of the ABM1–ABM3 experiments took place in 2006, followed by the installation of ABM4–ABM6 experiments in 2012. To date, three experiments have been retrieved: ABM1 in 2009, ABM2 in 2013, and ABM5 in 2017. This report focuses specifically on the findings from the ABM2 and ABM5 experiments. Based on the findings presented in this report and the collaborative research efforts with multiple groups and publications, the following was concluded:

1. No general significant alteration of smectite in the bentonite was observed in either ABM2 or ABM5.
2. Minor changes were detected in the cation exchange capacity (CEC). However, these changes do not seem to be correlated with smectite transformation or any significant impact on important properties of the bentonite, such as swelling pressure and hydraulic conductivity.
3. The crucial properties swelling pressure and hydraulic conductivity were largely unaffected by the extremely high temperatures in the ABM5 experiment.
4. Minor formation of trioctahedral smectite, most likely ferrosaponite, was observed in ABM2. However, the extent of formation was minimal and is not expected to affect the performance of the bentonite. It is important to note that this reaction has not been observed in experiments using copper heaters, which is the actual canister material in the SKB KBS-3 design.
5. Corrosion products were observed in both ABM2 and ABM5 (at the iron heater interface), as well as dissolution-precipitation and cation exchange reactions.
6. Magnesium redistribution was occasionally observed, and in some cases, it correlated with the formation of trioctahedral smectite and changes in the 060 region of the XRD patterns. Similar magnesium redistribution and accumulation towards the heater have also been observed in experiments with copper heaters to a minor extent, although the underlying mechanism is not yet fully understood.
7. Unexpected accumulation of halite was observed in the Kunigel block #22 of ABM2 and is attributed to the high temperature and a possible boiling event, possibly coupled with a pressure drop resulting from a local fracture.
8. Unexpected physical breakdown of some of the bentonite blocks were observed in ABM5 and is attributed to the extremely high temperature conditions during the experiment.

## Acknowledgement

The work concerning ABM5 has been part of the HITEC WP (Influence of temperature on clay-based material behaviour) which is part of the first phase of EURAD, and has received funding from Euratom research and training programme 2014–2018 under grant agreement No [847593].



Funded by  
the European Union



# Sammanfattning

Bentonit är en central del av SKBs KBS-3 design. I KBS-3-konceptet har Wyoming-bentonit, kommersiellt känd som MX-80 länge varit standard för buffert. Att utöka kunskapen om alternativa material är avgörande för att optimera säkerhet, tillgänglighet och kostnadseffektivitet. Därför initierades fältexperimentet Alternativa BuffertMaterial (ABM) av SKB vid Äspölaboratoriet år 2006. De primära målen med ABM-projektet var att karakterisera olika leror med avseende på deras hydro-mekaniska egenskaper, mineralogi och kemisk sammansättning. Dessutom syftade projektet till att identifiera eventuella skillnader i deras beteende och långsiktiga stabilitet. Dessutom möjliggjorde inkluderingen av olika leror och närvaron av en uppvärmd ståldel att studera interaktionerna mellan järn och bentonit.

Installationen av experimenten ABM1–ABM3 ägde rum år 2006, följt av installationen av experimenten ABM4–ABM6 år 2012. Hittills har tre experiment brutits: ABM1 år 2009, ABM2 år 2013 och ABM5 år 2017. Denna rapport fokuserar specifikt på resultaten från experimenten ABM2 och ABM5. Baserat på de resultat som presenteras i denna rapport och samarbetet med olika grupper och vetenskapliga publikationer som har genomförts dras följande slutsatser:

1. Ingen generell signifikant förändring av smektiten i bentoniten observerades varken i ABM2 eller ABM5.
2. Små förändringar upptäcktes i katjonutbyteskapaciteten (CEC). Dessa förändringar verkar dock inte vara korrelerade med smektittransformation eller någon betydande påverkan på viktiga egenskaper hos bentoniten, som svälltryck och hydraulisk konduktivitet.
3. De avgörande egenskaperna svälltryck och hydraulisk konduktivitet påverkades i stort sett inte av de extremt höga temperaturerna i ABM5-experimentet.
4. Små mängder trioctahedral smektit, troligen ferrosaponit, observerades i ABM2. Dock var omfattningen av bildandet minimal och förväntas inte påverka bentonitens prestanda. Det är viktigt att notera att denna reaktion inte har observerats i experiment med kopparvärmare, som är det faktiska kapselmaterialet i SKB KBS-3-designen.
5. Korrosionsprodukter observerades i både ABM2 och ABM5 (vid gränssnittet mot järnvärmaren), liksom upplösning-utfällnings- och katjonutbytesreaktioner.
6. Magnesiumomfördelning observerades ibland, och i vissa fall korrelerade den med bildandet av trioktaedrisk smektit och förändringar i 060-regionen av XRD-mönstren. Liknande magnesiumomfördelning och ansamling mot värmaren har också observerats i experiment med kopparvärmare i mindre utsträckning, även om den underliggande mekanismen ännu inte är helt förstådd.
7. Övåntad ansamling av halit observerades i Kunigel-blocket #22 i ABM2 och tillskrivs de höga temperaturerna och en möjlig kokhändelse, eventuellt kopplad till ett tryckfall som uppstod på grund av en lokal spricka.
8. Övåntad fysisk nedbrytning av vissa av bentonitblocken observerades i ABM5 och tillskrivs de extremt höga temperaturförhållandena under experimentet.



# Contents

<b>1</b>	<b>Introduction</b>	9
1.1	General	9
1.2	ABM test series	9
1.3	Objectives	10
	1.3.1 Chemical and mineralogical evolution	10
	1.3.2 Physical properties for important safety functions	10
<b>2</b>	<b>Experiment description</b>	11
2.1	General	11
	2.1.1 Experimental configuration	11
	2.1.2 Principles	11
2.2	Test packages	12
	2.2.1 General	12
	2.2.2 Test principle	12
	2.2.3 Central tubes	12
	2.2.4 Heaters	12
	2.2.5 Blocks	12
2.3	Instrumentation	14
	2.3.1 General	14
	2.3.2 Thermocouples	14
	2.3.3 Relative humidity	14
2.4	Artificial wetting system	14
2.5	Test sites	15
2.6	Buffer materials	16
	2.6.1 General	16
	2.6.2 Description of the different clay materials	16
<b>3</b>	<b>Method descriptions</b>	19
3.1	X-ray fluorescence (XRF) spectroscopy	19
3.2	Powder X-ray diffraction (XRD)	19
3.3	Specific cation exchange capacity (CEC) and extractable cations (EC)	19
3.4	Swelling pressure and hydraulic conductivity	20
<b>4</b>	<b>ABM2 evolution and excavation</b>	21
4.1	Test layout	21
4.2	Field operation	22
	4.2.1 Heating	22
	4.2.2 Temperature development	23
	4.2.3 Relative humidity measurements	26
	4.2.4 Artificial water saturation	26
4.3	Termination	28
	4.3.1 Releasing the test package	28
	4.3.2 Division and material handling	28
4.4	Water content and density determinations	33
	4.4.1 General	33
	4.4.2 Test procedure and evaluation	33
	4.4.3 Results	35
4.5	Comments	40
<b>5</b>	<b>ABM5 evolution and excavation</b>	41
5.1	Test layout	41
5.2	Field operation	42
	5.2.1 Heating	42
	5.2.2 Temperature development	42
	5.2.3 Artificial water saturation	45

5.3	Termination	47
5.3.1	Releasing the test package	47
5.3.2	Division and material handling	48
5.4	Water content and density determinations	50
5.4.1	General	50
5.4.2	Test procedure and evaluation	50
5.4.3	Results	50
5.5	Comments	55
<b>6</b>	<b>ABM2 results from analysis</b>	57
6.1	Chemical and mineralogical evolution in ABM2	57
6.1.1	MX-80	58
6.1.2	Calcigel	63
6.1.3	Deponit CA-N	65
6.1.4	IbecoSeal	66
6.1.5	Ikosorb	68
6.1.6	Kunigel	70
6.1.7	Febex	73
6.1.8	Rokle	78
6.1.9	Asha505	79
6.2	Conclusions and discussion ABM2	80
<b>7</b>	<b>ABM5 results from analysis</b>	81
7.1	Chemical and mineralogical evolution in ABM5	81
7.2	Swelling pressure and hydraulic conductivity in ABM5	87
<b>8</b>	<b>ABM5 external results</b>	93
8.1	Unconfined compression tests on bentonites from test package 5	93
8.1.1	General	93
8.1.2	Unconfined compression tests	94
8.1.3	Results	96
8.1.4	Concluding remarks	113
<b>9</b>	<b>Conclusions</b>	115
	<b>References</b>	117
<b>Appendix 1</b>	Photos of sampling for unconfined compression tests	121
<b>Appendix 2</b>	Results from unconfined compression tests	123

# 1 Introduction

## 1.1 General

Bentonite clay plays a crucial role in the Swedish KBS-3 design for final repositories of high-level radioactive waste. In this design, copper canisters are used as corrosion-resistant containers for the waste, placed at a depth of approximately 500 meters in crystalline rock. To minimize water flow and transport between the rock and the canister, compacted bentonite blocks are emplaced as buffer material. The swelling pressure of the clay ensures the canister remains in place and limits microbiological activity, while its plasticity prevents the transfer of forces from rock displacements.

The MX-80 bentonite from American Colloid Co (Wyoming) has long been the reference material for the buffer in the KBS-3 concept and has been utilized in various field experiments at Äspö, such as LOT (Karnland et al. 2009), Prototype (Olsson et al. 2013), and TBT (Åkesson et al. 2012). However, expanding the knowledge base on alternative buffer materials is essential for optimizing safety, availability, and cost-effectiveness. Consequently, the Alternative Buffer Material (ABM) field experiment was initiated at the Äspö Hard Rock Laboratory in 2006.

The main objectives of the ABM project were to characterize the mineralogical content of different clays and identify any variations in behavior or long-term stability after exposure to field conditions. Some studies, such as those conducted by Lantenois et al. (2005) and Carlson et al. (2007), suggest that the bentonite buffer may be sensitive to the presence of metallic iron, while others indicate a more moderate interaction (e.g., Kumpulainen 2010). This is of significant importance since the KBS-3 concept employs copper canisters with iron inserts, and iron is present in other components of the repository, such as rock reinforcement.

The ABM experiment offers valuable insights into iron-bentonite interactions due to the diversity of clays used, as well as the repository-like conditions implemented in the study (e.g., compacted clay, non-powdered metallic iron, swelling pressure from the clay, relatively large scale, in situ placement at repository depth, and natural water sourced from the bedrock). The initial ABM1 experiment has already been extensively studied and reported in publications (e.g. Svensson and Hansen 2013, Svensson 2015, Kaufhold et al. 2013). The ABM project is conducted by SKB, however various international partners are also involved in the analysis of the experiments.

This report provides a summary of observations from SKB's internal investigations, as well as cooperative efforts and publications, specifically focusing on the ABM2 and ABM5 experiments.

## 1.2 ABM test series

### **ABM 1–3**

The ABM 1–3 test series was installed in 2006. The experiment comprised three medium-scale test packages, each consisting of a central steel tube with heaters and a buffer of compacted clay. Eleven different clays were selected for the buffers to investigate the effects of smectite content, interlayer cations, and overall iron content. Additionally, bentonite pellets with and without additional quartz were tested.

Test package 1 (ABM1) was retrieved in 2009, and the status of the material investigations was reported by Svensson et al. in 2011. Test package 2 (ABM2) was retrieved in 2013, and the results from the initial analyses of the materials, as well as subsequent laboratory investigations, are described in this report. Test package 3 is still ongoing.

### **ABM 45**

A second test series, ABM 45, was installed in 2012. This new test series also included three test packages with the same design principle as the first test series, but some of the materials used in the first series were replaced with others.

Test package 5 (ABM5) was retrieved in 2017, and the results from the initial analyses of the materials, along with subsequent laboratory investigations, are presented in this report. Test packages 4 and 6 are still ongoing.

## **1.3 Objectives**

The overall objective of the ABM test series is to verify that the buffer material will retain its advantageous hydromechanical properties under “realistic” repository conditions. This is done:

1. Indirectly, by investigations of the chemical and mineralogical evolution of the materials.
2. Directly, by investigations of the physical properties that are related to the desired safety functions.

### **1.3.1 Chemical and mineralogical evolution**

One crucial property of the buffer material is its long-term mineralogical stability, which is essential for the buffer’s sustained functionality. The long-term stability of Wyoming montmorillonite in contact with a copper canister is being studied in another SKB project called LOT. The potential processes identified as relevant for the bentonite in the ABM experiments can be categorized as follows:

1. Smectite to illite conversion.
2. Dissolution and neof ormation of bentonite accessory minerals.
3. Cation exchange.
4. Salt dissolution/transport/precipitation.
5. Build-up of corrosion products.
6. Iron-bentonite interaction (impact on smectite mineral stability, important properties).

According to literature, corrosion and/or its products appear to react with clay minerals in some cases, leading to the formation of new non-swelling minerals (Lantenois et al. 2005).

In ABM, special focus is on iron-bentonite interaction and the other field experiments at Äspö use copper canisters.

Some possible scenarios for iron-bentonite interaction are:

- Formation of iron-montmorillonite through ion exchange.
- Reduction of iron within the octahedral sheet of the montmorillonite structure, potentially coupled with dehydroxylation (reversible or irreversible).
- Dissolution and/or transformation of montmorillonite.
- Formation of corrosion products that may contribute to buffer cementation.

All these scenarios are likely to impact the buffer’s performance to some extent. The rate and extent of smectite destabilization seem to depend on factors such as the nature of the smectite (dioctahedral/trioctahedral), counter ion presence, and Fe(III) content (Lantenois et al. 2005). The reduction of iron may negatively affect hydraulic conductivity and swelling properties. Additionally, an increase in cation fixation capacity has been observed (Khaled and Stucki 1991).

### **1.3.2 Physical properties for important safety functions**

The buffer material must meet several physical property requirements, including swelling pressure, hydraulic conductivity, and stiffness or plasticity. These properties are examined using three selected materials: MX-80, DepCAN, and Asha 505. Both re-compacted samples and drilled samples are utilized to differentiate between irreversible changes resulting from mineralogical alterations and reversible changes such as potential microstructural texture. These properties are expressed as a function of the compacted density of the buffer.

## 2 Experiment description

### 2.1 General

#### 2.1.1 Experimental configuration

The ABM test packages have been installed at Äspö HRL in two different test series:

1. **ABM 1–3.** These first test-packages were installed in November 2006. The design and installation of the three test packages are described in a report (Eng et al. 2007). Two of the tests have been dismantled:
  - a. Test Package 1, ABM 1. The test was terminated in May 2009. A status report describing the results from termination, dismantling and investigations of the materials are presented in Svensson et al. (2011).
  - b. Test Package 2, ABM 2. The test was terminated in April 2013. The results from the field test and initial investigations of the materials are presented in this report.
2. **ABM 45.** Three additional test packages were installed in November 2012. The design and installation of the three test packages are described in a report (Sandén et al. 2018). One of these tests has been dismantled:
  - a. Test Package 5, ABM 5. The test was terminated in June 2017. The results from the field test and initial investigations of the materials are presented in this report.

There was no intention in the ABM to study the hydration of the materials. In order to have a relatively rapid, even and controlled water saturation process a sand filter was installed between the buffer material and the rock. All test packages have had access to natural water from fractures in the rock via a sand filter surrounding the bentonite blocks. In addition, a system for artificial wetting has been installed which made it possible to inject water into the sand filter. Artificial water injection has been made for all test packages but ABM 3 and ABM 5.

Test package ABM 5 has had a considerably higher temperature than the other tests. The maximum temperature has been 130 °C in the other tests but 250 °C in ABM 5.

A compilation of the test program including time for installation, time for termination and the most important test conditions is provided in Table 2-1.

**Table 2-1. Test program for the Alternative Buffer Material project.**

Test series	Test no.	Installed	Terminated	Max temp.	Artificial wetting	Remark
ABM 1–3	ABM 1	Nov 2006	May 2009	130 °C	Yes	
ABM 1–3	ABM 2	Nov 2006	April 2013	130 °C	Yes	Heating after saturation
ABM 1–3	ABM 3	Nov 2006	Running	130 °C	No	
ABM 45	ABM 4	Nov 2012	Running	130 °C	Yes	
ABM 45	ABM 5	Nov 2012	June 2017	250 °C	No	High temperature
ABM 45	ABM 6	Nov 2012	Running	130 °C	Yes	

#### 2.1.2 Principles

The experiment layout of the ABM tests is similar to the Swedish KBS-3 concept with a copper canister surrounded by clay situated in crystalline bedrock at approximately 500 m depth. The differences are mainly the scale and that the simulated canister is made of carbon steel (P235TR1) instead of copper. The experiments consist of test-packages which were placed in separate vertical bore holes drilled in granitic rock. Each test package consisted of a central steel tube including heaters on the inside, ring shaped bentonite blocks and in addition also some instruments. The bentonite was during the test period exposed to conditions similar to the KBS-3 concept except for the temperature, which was higher, 130 °C in all packages except for ABM 5 where the maximum temperature was 250 °C (compared to 90 °C in the KBS-3 concept). The higher temperature will accelerate the alteration processes.

All test packages were prepared in order to use an artificial water saturation system. The outermost slot between bentonite blocks and rock was filled with sand in which titanium pipes, perforated with drilled holes at different levels, were placed. The pipes were connected to a water tank which could be pressurized.

## **2.2 Test packages**

### **2.2.1 General**

The installation and design of the first three test packages within the ABM experiment is described in Eng et al. (2007). The installation and design of the second test series, ABM 45, is described in Sandén et al. (2018). This chapter contains a brief description of the test design, the block manufacturing, instrumentation and a description of the system for artificial wetting.

### **2.2.2 Test principle**

All test packages have a similar design. The main differences are the material configuration, the test duration, the maximum temperature and if there have been an artificial wetting or not, see information provided in Table 2-1.

A schematic drawing of the test design is provided in Figure 2-1. The experiments consist of test-packages placed in separate vertical bore holes drilled in granitic rock. Each test package consists of a central steel tube including heaters on the inside, ring shaped bentonite blocks and some instruments, mainly thermocouples (twenty pcs per test package).

### **2.2.3 Central tubes**

The central tubes containing heaters were made of carbon steel, P235TR1. The tubes have a length of about four meters and an outer diameter of 108 mm. In order to facilitate installation and to be able to put together a complete test package, a steel plate was welded onto the tube at the bottom. The ring-shaped blocks were threaded onto the tube. The upper part of the tube extends into the tunnel and is accessible throughout the test.

### **2.2.4 Heaters**

Three heaters were installed in each of the test packages. There was one central heater (1 000 W), one heater at the top (500 W) and one at the bottom (500 W). The effect of each heater could be adjusted separately which made it possible to get an even temperature along the test package. The heaters were placed inside the central steel tube, which is favorable in case of failure, since then a damaged heater can be lifted up and a new installed very easily.

### **2.2.5 Blocks**

All bentonite blocks used in the tests were compacted in a special mould with a pressure of 100 MPa. The compaction technique was based on experiences from previous SKB projects concerning block production. The blocks had a slightly axial conical shape and chamfered edges between the mantle and end surfaces. In order to produce blocks of good quality it was also necessary to use a small amount of grease to reduce the friction and facilitate de-moulding. The grease used is based on molybdenum disulphide, MoS<sub>2</sub>. In ABM5 special effort was used to minimize the use of grease and the outermost approximately 1–3 mm of bentonite on the block surface towards the heater was removed by abrasion in order to make sure that no grease was present in the heater-bentonite interface.

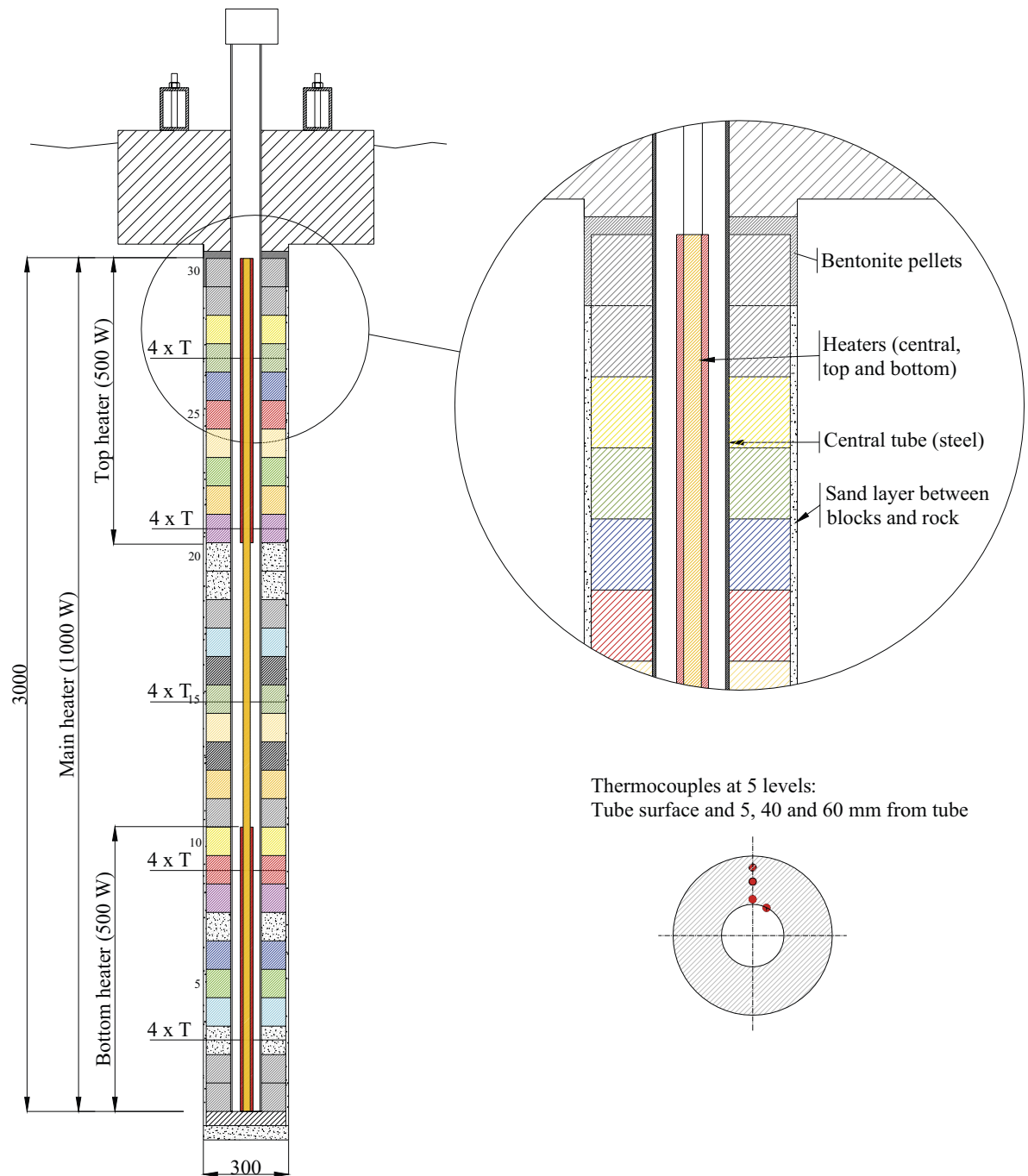


**Figure 2-1.** Schematic view of the principal test layout for the ABM experiments. Dimensions are given in mm.

The blocks were compacted with the as-delivered water content and granule size except for the Callovo-Oxfordian and the Asha material. The Callovo-Oxfordian material was delivered as hard rock shards and was crushed down to a maximum grain size of five mm by use of sledgehammer, jaw crusher and finally a roller mill. The Asha 505 material was delivered with a water content of 26.6 % and was before compaction dried to a water content of about 13 %. All manufactured blocks were after compaction weighed and measured, see data provided in the installation reports (Eng et al. 2007, Sandén et al. 2018).

## **2.3 Instrumentation**

### **2.3.1 General**

The ABM test packages were all sparsely instrumented, the reason for this is that the focus is on investigations after dismantling. The main objectives with the test series were to expose the different bentonite materials to conditions similar to a repository and to adverse conditions with respect to temperature. This means that measurements of the temperature distribution in the test packages were important.

The test program for the first series included that the heating of test package two, ABM 2, should not start before the bentonite was judged to be saturated. In order to get a rough estimation of how the saturation proceeded, this package was also equipped with four relative humidity sensors.

### **2.3.2 Thermocouples**

Twenty thermocouples were installed in each of the test packages. The thermocouples are of type K with the shield of the sensors made of cupronickel in order to withstand the tough conditions in the test holes.

#### ***Test package ABM 2***

The thermocouples in test package ABM 2 were positioned in block numbers 3, 9, 15, 22 and 28. Four thermocouples were positioned at each level, one inside the steel tube and three in the buffer. The thermocouples in the buffer were positioned at different radial distances from the heater; 5, 40 and 60 mm.

#### ***Test package ABM 5***

The thermocouples in test package ABM 5 were positioned almost as in test package ABM 2 with some minor changes:

- The thermocouples were positioned in block numbers 3, 9, 15, 21 and 27.
- The thermocouples that in previous packages were positioned inside the tube were instead positioned on the outside of the tube. (The new positions were chosen to avoid any direct contact with the electrical heater which may have been the case in previous packages.)

### **2.3.3 Relative humidity**

The test program, Table 2-1, included that the heating of test package two, ABM 2, should start when the bentonite was saturated. In order to get information regarding this process, four relative humidity sensors were installed. These sensors were positioned in block numbers 3, 9, 22 and 28. The sensors were installed in predrilled holes in the blocks about five cm down from the upper block surface and at a radial distance from the heater of thirty mm.

The relative humidity sensors were delivered by Vaisala Oy. Before installation the sensors were encapsulated in special housings in order to protect them physically.

## **2.4 Artificial wetting system**

All test packages were prepared in order to use an artificial water saturation system. The outermost slot between bentonite blocks and rock was filled with sand in which titanium tubes,  $d = 6$  mm, were placed. The sand served as a filter and distributed inflowing water around the outer mantle surface. Four titanium tubes were installed in each of the test packages. They were connected in pairs underneath the bottom buffer block, which made it possible to flush the system if needed. Holes were drilled in the titanium tubes every meter. In order to avoid sand to enter or clog the small holes, a perforated plastic "sock" was pulled over the pipes. The pipes were connected to a water tank which could be pressurized.

As mentioned in Section 2.1, test package ABM 2 was artificially wetted from test start while test package ABM 5 did not have any artificial wetting.

## 2.5 Test sites

### ABM 1–3

The test packages installed in 2006, ABM 1–3, were located in the TASQ tunnel at the –450 meter level at Äspö HRL, red ring in Figure 2-2. A niche, NASQ, was excavated on the eastern side of the tunnel and the three test holes were placed here. The bedrock consists of Äspö diorite and greenstone. The tunnel holds quite many water bearing fractures further in, but these were avoided in the test niche which was rather dry.

### ABM 45 (4–6)

The three test packages that were installed 2009 were placed in a tunnel named TASD, blue ring in Figure 2-2. The tunnel is located at the level –420 meters. The main requirements for the selection were that the depth should be similar to a repository and that the site should be reasonably dry.

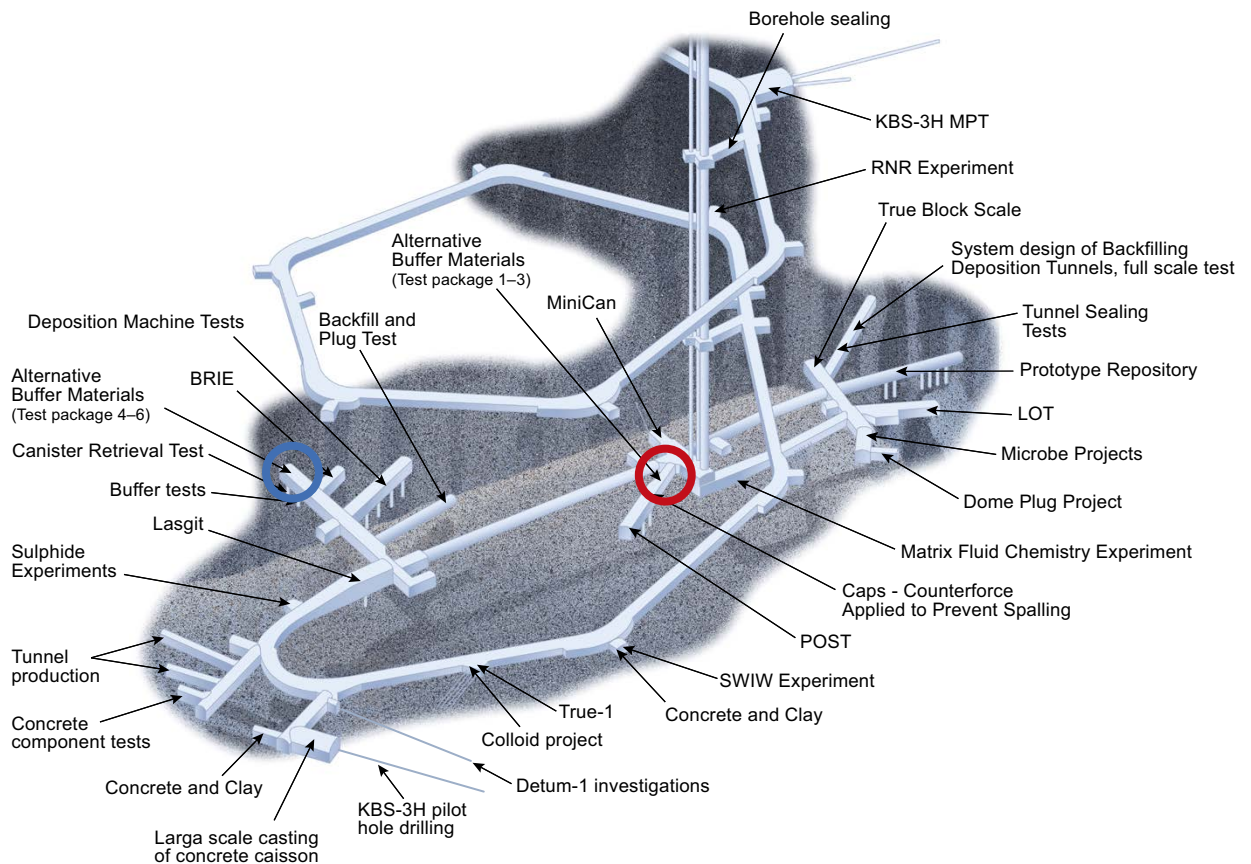


**Figure 2-2.** Test sites in the lower part of the Äspö HRL. The ABM 1–3 test series is located in the TASQ tunnel (red ring) and the ABM 45 test series is located in the TASD tunnel (blue ring).

## 2.6 Buffer materials

The materials for the ABM packages were selected on the basis that they should be interesting possible alternatives to MX-80, either as actual buffer materials or that they should have scientifically interesting properties. Some materials were selected on the interest from project partners.

### 2.6.1 General

ABM test package 2, ABM 2, included fourteen different types of blocks manufactured by eleven different materials. ABM test package 5, ABM 5, included twelve different materials which were compacted to blocks. Most of the materials in ABM 2 were also used in ABM 5 but there were some changes (see also compilation provided in Table 2-2):

- **Materials used in ABM 2 but not in ABM 5:** Callovo Oxfordian (discs and compacted blocks), Friedland, MX-80 granulate, and MX-80 granulates with quartz.
- **New materials in ABM 5:** Asha-NW BFL-L, Saponite and GMZ.

This chapter gives a short description of the materials regarding country of origin, the main content of clay minerals and the commercial name and abbreviations, see also Svensson et al. (2011) and Sandén et al. (2018).

**Table 2-2. Compilation of the different materials used in ABM 2 and ABM 5.**

Material	ABM 2	ABM 5
MX-80	yes	yes
Calcigel	yes	yes
Ikosorb	yes	yes
Rokle	yes	yes
Kunigel	yes	yes
Febex	yes	yes
Callovo Oxfordian	yes	
Asha 505	yes	yes
Friedland	yes	
Ibeco Seal	yes	yes
Deponit CAN	yes	yes
GMZ		yes
Saponite		yes
Asha NW BFL-L		yes

### 2.6.2 Description of the different clay materials

- **Asha 505** produced by Ashapura Minechem Co. is the commercial name of natural Na-bentonite that is quarried in the Kutch area, 60–80 km from the ports of Kandla and Mandvi on the northwest-coast of India. The bentonite is associated with the basaltic Deccan Trap rocks of Tertiary age and formed through hydrothermal alteration of volcanic ash in saline water (Shah 1997). The bentonite occurs in scattered pockets or layers within the basaltic rocks, with thicknesses ranging from a few meters up to 30 meters. Due to the high content of secondary iron oxides the color is normally dark reddish brown but there are also light colored variants low in iron.
- **Calcigel** is the commercial name of a natural Ca-bentonite produced from selected Bavarian bentonites by Süd-Chemie AG. The bentonites are quarried in the triangle between Mainburg, Moosburg and Landshut in southern Germany, where the most important commercial deposits in Germany are located. Most of the Bavarian bentonite deposits occur as scattered, rather thin ( $\leq 3$  m) lenses or layers in sedimentary sequences of late Miocene marls and tuffaceous sands, and are believed to have formed by in situ alteration of acid vitreous tuff, originating from the volcanic activity in the Carpathian Mountains (Süd-Chemie AG 2011). The bentonite quality varies from relatively pure montmorillonite (up to 70 %) to material with rather much kaolinite, mica and quartz.

- The **Callovo-Oxfordian (COX)** sedimentary formation in the eastern part of the Paris basin was selected by Andra to host the French underground laboratory in the Meuse/Haute-Marne region. This macroscopically homogeneous Jurassic formation (~150–160 Ma) of argillites is ~130 m thick and has a burial depth of more than 400 m below the ground surface in the region. The rock formation was selected because it's potential ability to act as barrier to radionuclide migration from the storage to the environment due to a very low hydraulic conductivity and large vertical extension on either side of the laboratory level. Quartz and calcite globally represent approximately 50 % of the bulk rock, whereas clay minerals, including mixed-layers as well as discrete smectite, illite, kaolinite and chlorite, represent 40–45 % (Claret et al. 2004).
- **IBECO Deponit CA-N** is the commercial name of a natural calcium bentonite mined by Imerys. The bentonite is quarried in the north-eastern part of the island of Milos, Greece, where some of the economically most important bentonite deposits in Europe are concentrated. The island of Milos is located in the central part of the South Aegean active volcanic arc. Pyroclastic tuffs and lavas of andesitic to rhyolitic composition are the main parent rocks of the bentonite, which forms irregular bodies within the pyroclastics (Kelepertsis 1989). The volcanic rocks have yielded K-Ar ages in the range 3.5–0.09 m.y. Based on isotope data, Decher et al. (1996) conclude that the bentonite formation is a result of hydrothermal reactions between the permeable volcanic rocks and percolating groundwater heated during volcanic activity, although there is some disagreement about the genesis e.g. Christidis et al. (1995).
- The **FEBEX** bentonite is a Mg-Ca bentonite extracted from the Cortijo de Archidona deposit in the southern part of Serrata de Nijar in Almería, Spain. The deposit has been exploited by the major Spanish bentonite producer, Minas de Gádor S.A (now Süd-Chemie Espana). Conditioning of the bentonite at the quarry/factory has been strictly mechanical. According to Caballero et al. (2005) the bentonites in Cortijo de Archidona are alteration products of rhyodacitic glasses and ignimbrites. Radiometric dating of the volcanic events indicates ages of 15 to 7 Ma. The FEBEX bentonite (also called S-2 or Serrata clay) had been chosen as reference bentonite by ENRESA before the start of the FEBEX project (Full-scale Engineered Barriers Experiment), among others because of the homogenous nature and very high montmorillonite content (ENRESA 1998). The subordinate amount of accessory minerals includes quartz, cristobalite, plagioclase and calcite.
- **Ikosorb Ca White** (actual commercial name: IBECO RWC White) is a Ca-Mg-Na bentonite, characterized by a high Montmorillonite content (> 80 %), a low sulphur content (< 0.1 %) and an off-white color which is related to a low content of iron in the smectite clay minerals. The subordinate amount of accessory minerals includes quartz, mica, ct-opal and feldspar. The bentonite was mined in Morocco in the Mount Tidienit area, where rhyolitic pyroclastic rocks related to a rhyodacitic intrusive body of Pliocene/Pre-Pliocene age have been altered to bentonite (Martin Vivaldi 1962).
- **Ibeco Seal M-90** (actual commercial name: IBECO RWN) is a natural sodium bentonite, characterized by a high Montmorillonite content (> 80 %) and a low sulphur content (< 0.1 %), produced by Imerys. in the Askana region in Georgia/CIS. The subordinate amount of accessory minerals includes quartz, illite and mica. The bentonite is derived from andesite-trachyte pyroclastic rocks of Jurassic to Tertiary age. There are several theories for the formation of the bentonite ranging from weathering or hydrothermal alteration to submarine alteration as described by Grim and Güven (1978).
- **Kunigel V1** is the commercial name of a sodium bentonite produced by Kunimine Industries Co., Ltd., Japan. The bentonite is quarried in under-ground mines in the Tsukinuno district, northern part of Japan, which is the largest bentonite production area in Japan. The Tsukinuno formation consists of stratified bodies of bentonitized felsic tuff beds intercalated in sedimentary hard shale and mudstone of Miocene age (Takagi 2005). There are more than 30 bentonite layers in the mining area, ranging in thickness from centimeters to several meters. The Tsukinuno bentonite is composed of Na smectite with subordinate quartz, feldspars, illite, calcite, and zeolite.
- The Wyoming bentonite **MX-80**, produced by American Colloid Co., is a blend of several natural sodium dominated bentonite horizons, dried and milled to millimeter-sized grains. The Wyoming bentonite occurs as layers in marine shales, and is widespread and extensively mined, not only in Wyoming but also in parts of Montana and South Dakota. The bentonite formed through alteration of rhyolitic tephra deposited in ancient Mowry Sea basin during the Cretaceous, more

than 65 million years ago (Slaughter and Earley 1965). There are strong evidence that the tephra altered in contact with the Mowry seawater (Elzea and Murray 1989, 1990), but palaeosalinity and palaeoredox conditions within the semi-restricted basin varied spatially and through time, which explains that the smectite composition varies both stratigraphically and laterally.

- The **Rokle** deposit within the north Bohemian volcanic areas NW of Prague, is one of the economically most important deposits in the Czech Republic. The deposit is part of a series of argillised volcanoclastic accumulations of Tertiary age, formed in shallow lacustrine basins within the stratovolcano complex of Doupovské Mountains (Konta 1986). The lens-shaped bentonite body has a maximum thickness of about 40 m. The volcanic glass is completely altered to smectite, but flakes of biotite, which is a primary constituent of the basaltic magma, are relatively frequent. The bentonite is highly variable in colour, ranging from olive-gray to yellow/red due to the admixture of secondary iron and manganese oxides.
- **Asha NW BFL-L** is produced by Ashapura Minechem Co, see Asha 505 for more data. This material is less refined and is planned to be used as a backfill material. The material has been investigated within another project (Sandén et al. 2014).
- **Geohellas saponite**. Saponite is a smectite as montmorillonite, but a trioctahedral mineral instead of a dioctahedral mineral as montmorillonite. It has a somewhat different structure than montmorillonite and also somewhat different properties. The material originates from Greece. Various methods point to the existence of a significant amount of tetrahedral charge, which is typical of ferruginous smectites. The major exchangeable cation is  $Mg^{2+}$  (73–90 %), which represents a special property of these materials compared with other bentonites (Kaufhold et al. 2019).
- The **GMZ-bentonite** deposit has been selected as the most potential buffer/backfill material supplier for China's HLW repository. The GMZ-bentonite deposit is a large-scale one, located in the northern China's Inner Mongolia Autonomous Region, 300 km northwest of Beijing. The deposit, with bedded ores, was formed in late Jurassic. The ore minerals include montmorillonite, quartz, feldspar, cristobalite etc (Liu et al. 2001, Chen et al. 2018).

## 3 Method descriptions

### 3.1 X-ray fluorescence (XRF) spectroscopy

The equipment used was a Panalytical Epsilon 3 XL spectrometer using a Rh X-ray tube. Helium gas was flowed over the sample during the measurement to reduce the absorption by the air, and the samples were analyzed as compacted discs of pure clay or as a milled sample placed on a mylar foil depending on the amount of sample available. The measurement setup and evaluation was the standard provided from the manufacturer (called Omnian). The XRF does not measure elements with atomic number lower than sodium. The reported elements are reported as e.g. oxides and the sum is normalized to 100 %.

### 3.2 Powder X-ray diffraction (XRD)

The XRD data was collected in reflection mode (theta-theta configuration) using a Panalytical X'Pert Pro system with a Co X-ray source (broad focus;  $\lambda = 1.789 \text{ \AA}$ ), a PIXcel1D linear detector and programmable divergency- and anti-scatter slits. In order to maximize the intensity no monochromator was used, however a thin Fe filter was used for suppression of white- and Co K-beta radiation, making the K-beta intensity < 1 % of the K-alpha. The samples were either back-loaded or prepared on a zero-background Si substrate, depending on the amount of sample available. Data collection was done for typically 1–3 hours per sample at 40 kV and 40 mA.

### 3.3 Specific cation exchange capacity (CEC) and extractable cations (EC)

Exchangeable cations (EC) were extracted with an  $\text{NH}_4\text{Cl}$  (or  $\text{NH}_4\text{OAc}$ ) solution in 76 % ethanol solution instead of water (Belyayeva 1967) to minimize dissolution of gypsum.

Exchangeable cations are extracted by shaking milled bentonite ( $1\,000 \text{ mg} \pm 10 \text{ mg}$ ) in ammonium chloride solution in 76 % ethanol (saturated 1 M  $\text{NH}_4\text{Cl}$ ; 12.5 ml) on a vibrating table for 30 minutes. After 5 minutes centrifugation at 2 700 RCF (relative centrifugal force) the supernatant is separated from the bentonite by decanting the extract to a sample tube. The extraction is repeated totally three times (i.e. same sample is extracted three times with a total volume of approximately 38 ml). After evaporation of the alcohol, the extract is filtrated ( $0.45 \mu\text{m}$  filter) and volume corrected with deionised water to 50 ml. The cations are analysed by inductively coupled plasma (ICP) at external laboratory. As EC are reported in relation to the dry weight of a bentonite sample water content of the material is determined by weighing a separate bentonite sample before and after drying at  $105 \text{ }^\circ\text{C}$  for 24 h.

The specific cation capacity (CEC) was measured using a  $\text{Cu}^{2+}$ -triethylenetetramine complex (Meier and Kahr 1999, Ammann et al. 2005). As the Cu-tri complex has a very strong blue colour this exchange was quantified using spectrophotometry. The measured CEC of pure montmorillonite (or other smectite) correspond very well to the calculated layer charge of Wyoming montmorillonite based on chemical composition (Karnland et al. 2006) hence it is well established that the  $\text{Cu}^{2+}$ -complex is adsorbed as a divalent cation in amounts corresponding to the permanent charge of the smectite. Milled bentonite ( $400 \text{ mg} \pm 10 \text{ mg}$ ) is dispersed in deionised water (33 ml) on a vibrating table for 30 minutes followed by ultrasonic treatment (15 minutes). The bentonite is then equilibrating with Cu (II)-triethylenetetramine solution (7 ml; 45 mM) and left on a vibrating table for 30 minutes. After 5 minutes of centrifugation at 3 000 RCF (relative centrifugal force) spectrophotometer measurement at 583 nm of the supernatant is performed against a calibration curve. The CEC is calculated by the difference in the copper concentration before and after ion exchange with the clay and is expressed as  $\text{cmol}(+)/\text{kg}$  dry weight. As the CEC is reported in relation to the dry weight of a bentonite sample the water content of the material is determined by weighing a separate bentonite sample before and after drying at  $105 \text{ }^\circ\text{C}$  for 24 h.

### 3.4 Swelling pressure and hydraulic conductivity

The tests are performed according to the following, for details see also Karnland et al. (2006) and Svensson et al. (2019), the total time for all steps is approximately six weeks:

1. A compacted clay disc is emplaced into the swelling pressure cell or alternatively the clay is compacted in situ in the cell. The compacted clay disc has a diameter of 35 mm and an approximate height of 5 mm, and a specific target density of choice.
2. The clay is saturated with deionised water and the swelling pressure is continuously measured with an external force cell. This is done over a time period of about one week. The swelling pressure is determined as the force divided with the cross-sectional area of the specimen and interpreted when the pressure (force) is considered to be stable.
3. The hydraulic conductivity of the specimen is determined with deionised water. The determination is made by applying a constant pore pressure gradient over the specimen while the amount of water per time unit is measured continuously. The gradient is defined as the applied pressure in meters of water column divided by the height of the sample. The evaluation is made according to Darcy's law. The measurement of the hydraulic conductivity continues for about one week and interpreted when the outflow is considered to be stable.
4. Step 2 is repeated but with a 1 M  $\text{CaCl}_2$  solution instead of deionised water, this will exchange the bentonite to Ca-form.
5. Step 3 is repeated with the 1 M  $\text{CaCl}_2$  solution.
6. Step 2 is repeated using deionised water (this removes the salt from the bentonite).
7. The specimen is taken out of the swelling pressure cell, and its bulk density and water content are determined. The bulk density is determined by weighing a sample both in air and submerged in paraffin oil with known density. The water content is determined by drying a sample in an oven at a temperature of 105 °C for 24 hours. With the known density and water content the dry density is calculated.

## 4 ABM2 evolution and excavation

### 4.1 Test layout

The schematic drawing provided in Figure 4-1 shows the block order in test package ABM 2.

### ABM test package 2

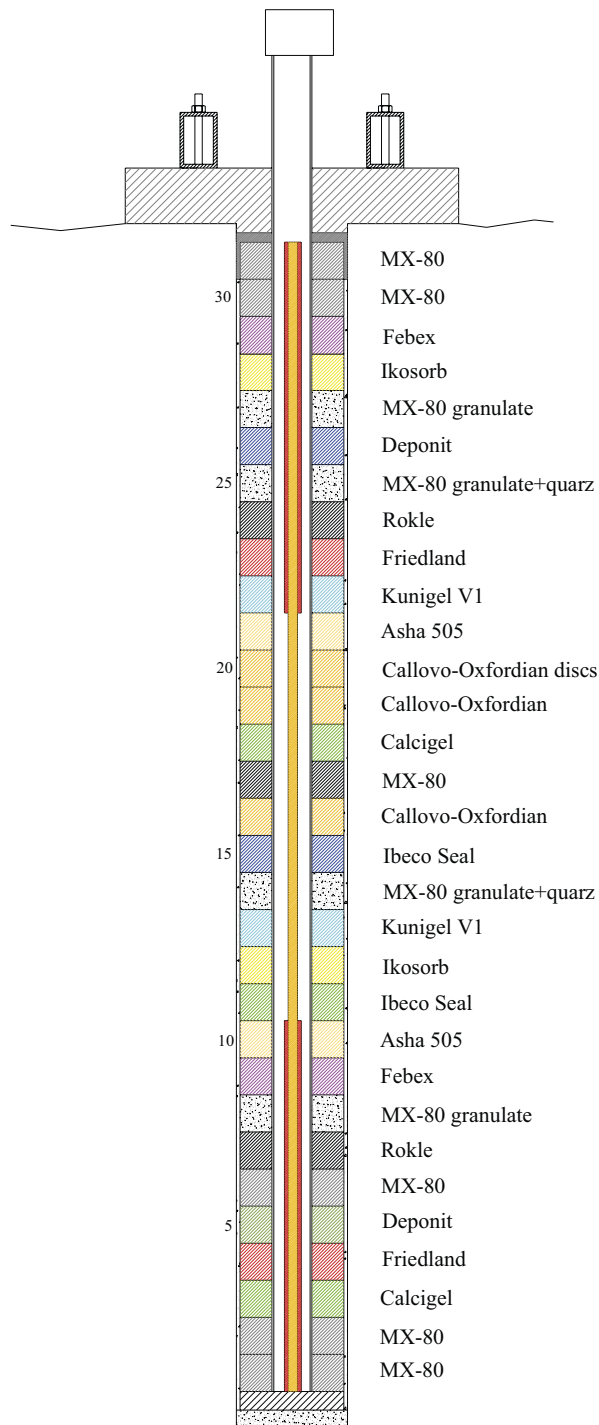


**Figure 4-1.** Schematic drawing of the ABM 2 test layout. The drawing shows how the different blocks (no. 1–31) were positioned in the test.

## 4.2 Field operation

The test included the following important milestones:

- 2006-12-04. Test package ABM 2 was installed in the test hole.
- 2006-12-07. The artificial saturation i.e. injection of water into the sand filter started three days after installation.
- 2008-08-26. The heating was started 631 days after installation.
- 2013-03-03. The heating was stopped 2234 days after installation.
- 2013-04-09. The test package was released from the test hole.

### 4.2.1 Heating

The original planning of this first test series included that the heating of the ABM 2 test should start after the bentonite was judged to be completely water saturated, Section 2.1.1. The bentonite was judged saturated after 631 days test duration and at this time the heating was started. The power to test package ABM 2 was increased in two steps, Figure 4-2. During the increase of power the achieved temperature was controlled in order to achieve as even temperature as possible along the test package, Figure 4-3 to Figure 4-7.

In conjunction with a restart of the computer, there was an interruption of the applied power to the central heater, see day 1410 in Figure 4-2.

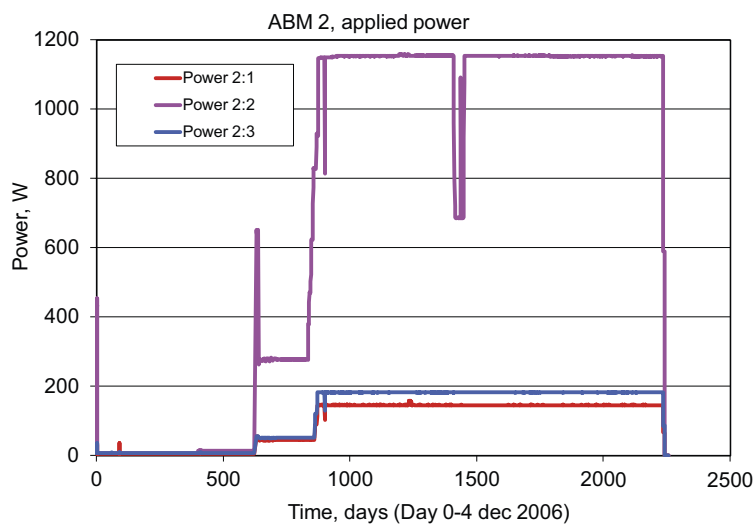


**Figure 4-2.** Applied power in ABM 2 plotted versus time.

### 4.2.2 Temperature development

The registered temperature data for the five levels with instruments (block no. 3, 9, 15, 22, 28) is presented in Figure 4-3 to Figure 4-7. The number of measuring points is limited but the registered data gives a fairly good picture of the temperature distribution within the test package.

The data from the thermocouples placed inside the steel tube is not presented in the graphs since the registered temperature was judged unrealistic (in the range 180–220 °C). The high temperatures registered for these thermocouples depends probably on that they have been in direct contact with the electrical heaters (the design was changed for the next test series, ABM 45, where the thermocouples instead were mounted on the outside surface of the tube).

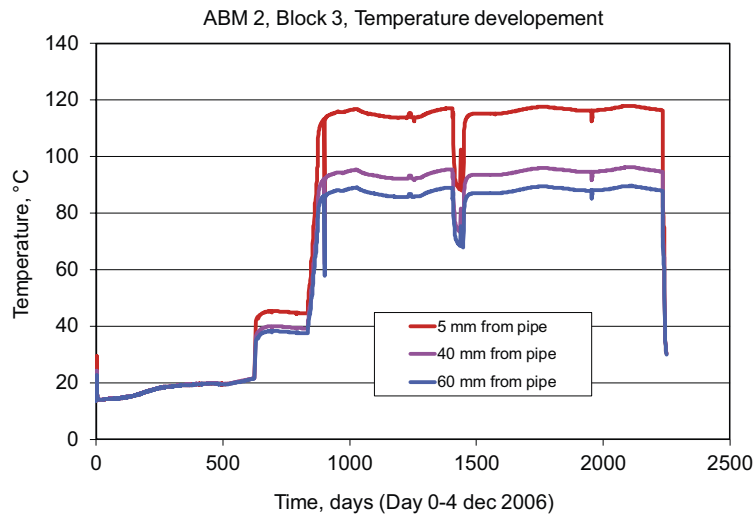


Figure 4-3. Temperature measurements in block no. 3 plotted vs. time.

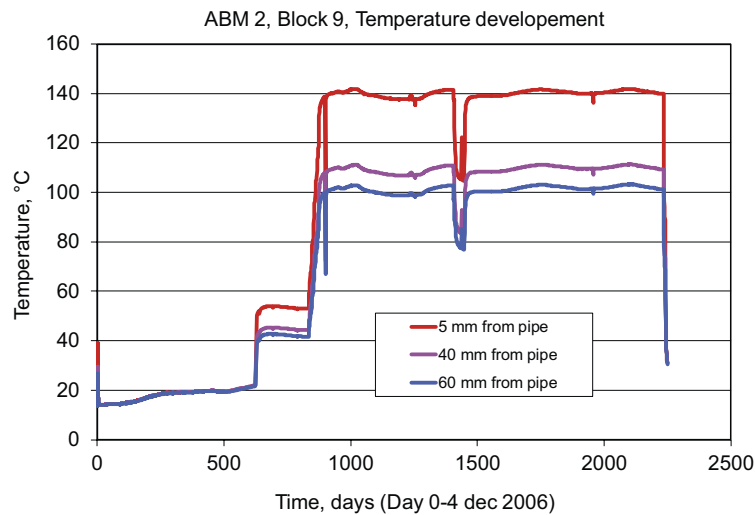
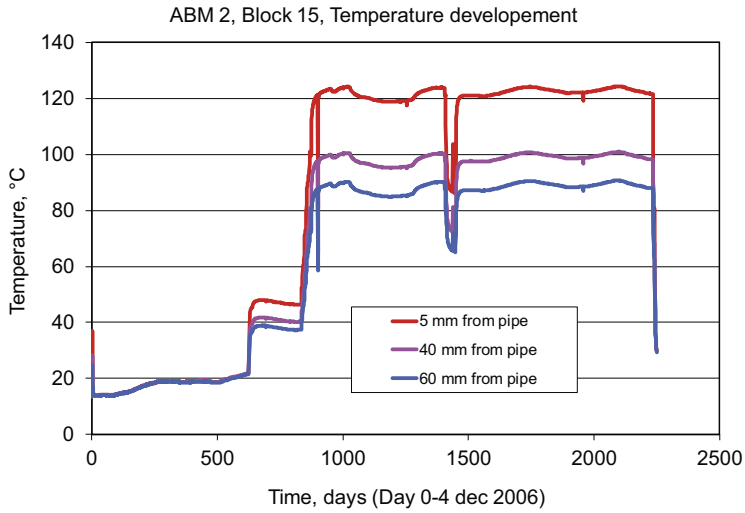
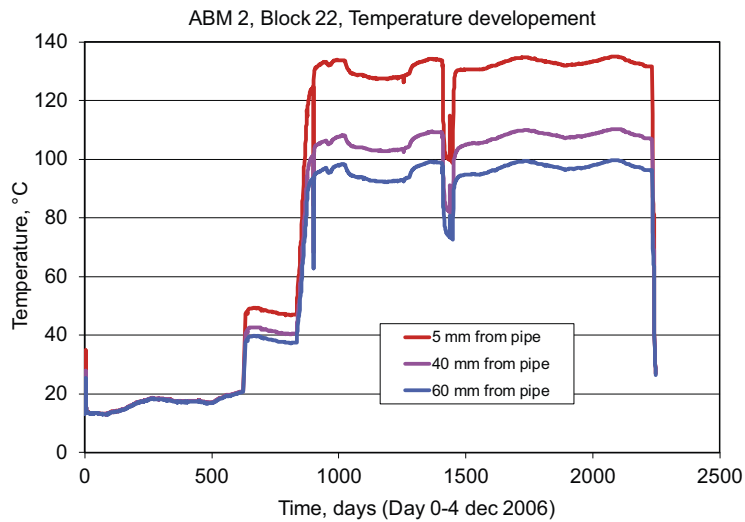


Figure 4-4. Temperature measurements in block no. 9 plotted vs. time.



**Figure 4-5.** Temperature measurements in block no. 15 plotted vs. time.



**Figure 4-6.** Temperature measurements in block no. 22 plotted vs. time.

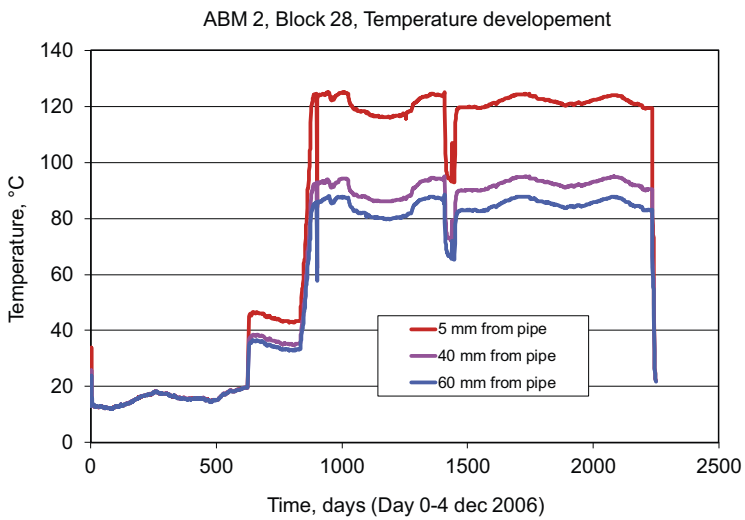


**Figure 4-7.** Temperature measurements in block no. 28 plotted vs. time.

To get an overview of the temperature distribution within the test package, a contour plot of the measured temperature was made using an interpolation program. The graph shows the temperature distribution 2013-03-02 i.e. the day before the heating was stopped.

The contour plot indicates that the temperature close to the surface of the central tube had been between 120 and 140 °C (on the section from 400–2700 mm from bottom). The temperature varied radially within the test package, roughly according to the following:

- 0–20 mm: in the range 120–140 °C
- 20–40 mm: in the range 110–120 °C
- 40–60 mm: in the range 90–110 °C
- 60–96 mm: in the range 70–90 °C

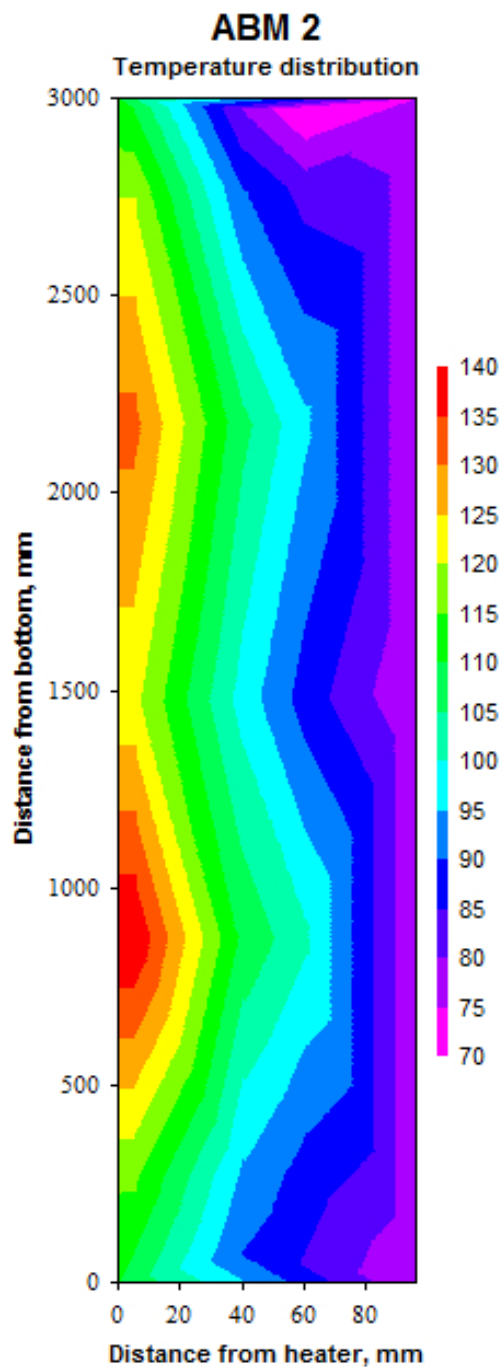


*Figure 4-8. Temperature distribution in ABM 2.*

### 4.2.3 Relative humidity measurements

The results from the measurements of relative humidity from the sensors positioned in block 3, 9, 22 and 28, are provided in Figure 4-9. All sensors indicated a rather fast increase in humidity within the first month and after approximately three months test duration they had all reached 100 % relative humidity. The sensors were positioned 30 mm from the heater which means that the radial wetting from the sand filter had reached 70 mm towards the heater after three months. The final wetting of the innermost 30 mm was, however, judged to take long time.

It was planned that the heating of the ABM 2 test should start after the bentonite was judged to be completely water saturated. The relative humidity measurements were intended to give an indication of how the saturation process proceeded. The heating of the test package was started 631 days after installation, see Figure 4-2.

### 4.2.4 Artificial water saturation

The water supply to test package 1 and 2 was made using the same system i.e. it was not possible to distinguish the total inflow for a certain test package (test package 3 had no artificial water saturation).

The water injection started three days after installation and at the same time, the increase of temperature was started in test package 1. The graph provided in Figure 4-10 shows the applied water pressure and the injected water volume from test start and until the termination of test package 2.

During the artificial saturation of test package 1 and 2 the following actions and decisions were made:

- During the first 50 days the inflow rate was very high (about 850 liters were injected) and in order to avoid strong erosion of the installed bentonite during long time the inflow was stopped for a period of about four months.
- After about four months a water pressure of 1.3 bar was applied and this was then increased in steps up to 2.7 bar. At this pressure the water inflow increased again and it was decided to again decrease the pressure. In order to avoid boiling at the intended test temperature (130 °C), 2.7 bar absolute pressure is needed. The applied pressure during the test period of ABM 1 was about 1.7 bar which is enough to prevent boiling up to 117 °C.
- The heating of ABM 2 was started after 631 days. This seems to have influenced the water injection that started to increase.
- In order to discover where the water flow took place; a small test was made on day 721. The valve feeding test package 2 was closed for about eight hours but this did not have any impact on the water consumption. The leakage therefore appears to mainly be linked to test package 1.
- The termination of test package 1 was done after 881 days. Before termination the heat was shut down on day 863 and the artificial water saturation on day 872.
- After termination of test package 1, it was possible to increase the applied pressure to above 4 bar. At the same time, the water injection rate was rather constant and at a lower level than earlier. However, after 1 407 days, a sampling of water from the borehole (KA2598A) was made. This disturbance resulted in a temporary increase of the inflow rate. The pressure was then decreased to about 3.3 bar. The inflow rate was after that rather constant for the remaining test duration of ABM 2.

The composition of the water used for the artificial saturation was investigated 2009-10-07 (day 1407) within the Äspö HRL campaigns and the results are given in Table 5-1.

**Table 4-1. Main elements in the water supply. The water was taken from bore hole KA2598A 2009-10-07.**

Na mg/L	K mg/L	Ca mg/L	Mg mg/L	HCO <sub>3</sub> mg/L	Cl mg/L	SO <sub>4</sub> mg/L	SO <sub>4</sub> -S mg/L	Br mg/L	F mg/L	Si mg/L	PH pH unit
2470.0	12.4	2560.0	64.8	51.7	8580.0	483.0	171.0	59.0	1.5	6.3	7.33

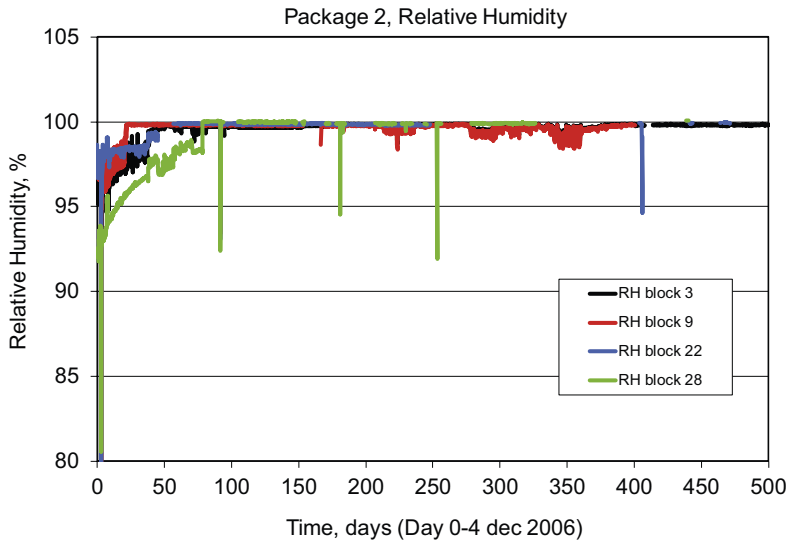


**Figure 4-9. Relative humidity plotted vs. time.**

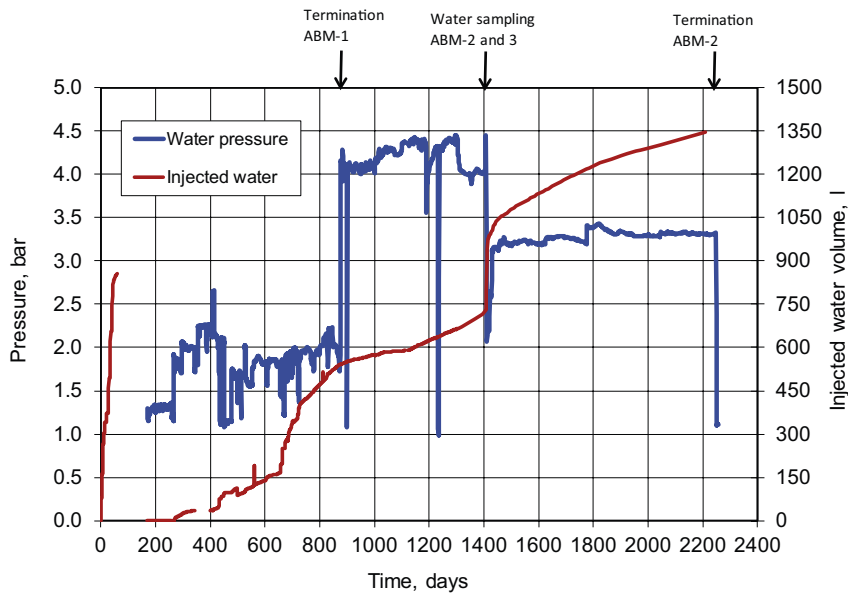


**Figure 4-10. Applied water pressure and injected water volume plotted vs. time.**

## 4.3 Termination

### 4.3.1 Releasing the test package

The test package was terminated and released from the surrounding rock using the same technique as had been used for earlier test packages of this type, see e.g. Svensson et al. (2011) for ABM-1 and Sandén and Nilsson (2020) for LOT S2 and A3. The heater power was closed 2013-03-03, about one month before the uplifting.

The test package was released by seam drilling in the surrounding rock, Figure 4-11. The diameter of the holes was 89 mm and the depth around 3.5 meters. After finishing the overlapping drilling, two core-drilled holes with a diameter of 300 mm were drilled at one side. In these holes wire sawing equipment was installed which was used in order to release the rock column at the bottom, under the package.

The core drilling showed that the rock was very fractured which could cause problems when lifting the package. In order to keep the package together it was covered with boards and then surrounded by straps. The lifting of the package was made by positioning three wires with loops around the package and outside the boards. The wires were used as lassos i.e. when lifting in the free end the loops were stretched harder around the package. The free ends of the wires were led through a special cap placed on the central steel tube. The lifting of the test package was made by a lorry with a crane, see left photo in Figure 4-12. As shown in the close-up photo on the right side in Figure 4-12, there were a lot of fractures in the rock surrounding the test package. As a result, the lower part of the rock cover was left in the test hole when the package was lifted up, see left photo in Figure 4-12. All bentonite blocks were, however, intact and after having covered them with boards, the complete package could be lifted. The test package was then placed on the flatbed of the lorry and transported up to the ground.

### 4.3.2 Division and material handling

After retrieval the test package was immediately transported to the laboratory at Äspö HRL where the work with division of the rock column and uncovering the bentonite blocks was made, Figure 4-13.



**Figure 4-11.** Photo showing the released test package. After the seam-drilling, two core drilled holes with a diameter of 300 mm were drilled in order to make it possible to install the wire-sawing equipment and saw off the rock column at the bottom.

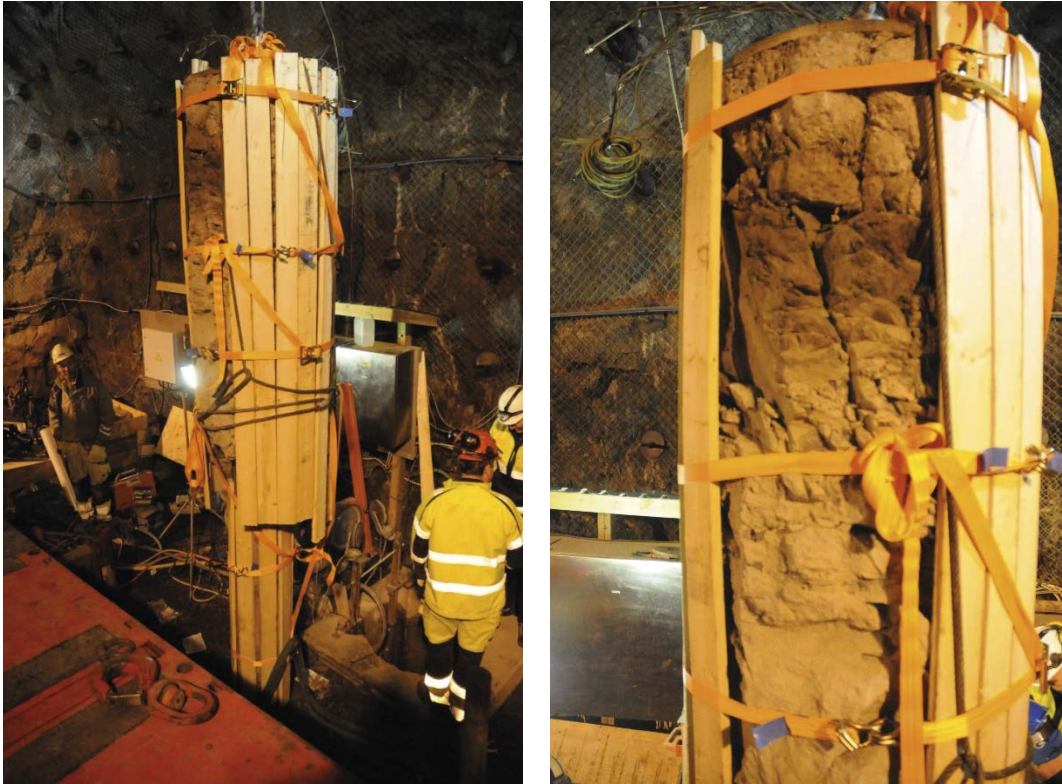


*Figure 4-12. Left: The test package was lifted up in one piece. In order to avoid pieces from falling off during the handling, the test package was surrounded by boards and straps. Right: Photo showing the rock cover at the top.*



*Figure 4-13. The test package was transported to the laboratory at Äspö HRL.*

The division of the test package started from the bottom where the bentonite blocks were already exposed (the bottom part of the rock cover was left in the test hole), Figure 4-14. The bottom plate that was welded to the central steel tube was cut off and then the bentonite blocks were removed using a special alligator saw. The blocks were cut at the interfaces between the different materials and also along the block height so that they could be threaded off from the steel tube, Figure 4-15.

The rock surrounding the upper part of the test package was in general very fractured which facilitated the dismantling. Some of the blocks were very fragile and fell into pieces in conjunction with the removal of the rock cover.



*Figure 4-14. The lower part of the test package.*



*Figure 4-15. The bottom plate has been cut off from the steel tube and some of the blocks have been removed.*



**Figure 4-16.** In the ABM2 (a) the rock was locally highly fractured, (b) some of the blocks were very fragile and fell into parts when the rock cover was removed, and (c) the iron heater was showing a different corrosion pattern in contact with different bentonites.

Examples of different blocks and how they looked like are provided in Figure 4-17:

- The upper left photo shows block no. 30 which was a block made of MX-80 bentonite. The block was complete with only a few fractures.
- The upper right photo shows block no. 26 which was made of Deponit CA-N. This block was rather complete with only a few fractures.
- The lower left photo shows block no. 22 which was made of Kunigel V1. The block had fallen in parts and consisted of many pieces.
- The lower right photo shows block no. 16 made of Callovo Oxfordian. This block was fractured and consisted of a lot of small pieces.

The initial sampling (see description in Section 4.4) included that a slice with a thickness of about 20 mm was cut from each block. This slice was then used to determine the radial water content and density distribution at five positions. After having cut out this slice from every block, the remaining block parts were placed in a sack made of alumina laminate which were evacuated and welded together. The sacks were then placed in airtight barrels. A number of samples were also distributed to other organizations for further analysis.



**Figure 4-17.** Examples of how the different blocks could look like. Upper left: Block no. 30, MX-80. Upper right: Block no. 26, Deponit CA-N. Lower left: Block no. 22, Kunigel V1. Lower right: Block no. 16, Callovo-Oxfordian.

## 4.4 Water content and density determinations

### 4.4.1 General

Basic properties of the bentonite test materials were determined in many positions of the test package to achieve a picture of the water content and density distribution. This data was then used to calculate the degree of saturation. Samples were taken at the mid-height of each block at five different radial distances from the heater, Figure 4-18.

In total, the water content and density were determined at 155 positions.

### 4.4.2 Test procedure and evaluation

#### Water content

The water content is defined as mass of water per mass of dry substance. The dry mass is obtained by drying the wet specimen at 105 °C for 24 hours or until no more mass loss occurs.

The sample was placed in an aluminum tin and the bulk mass ( $m_b$ ) of the sample was determined by use of a laboratory balance. The sample was placed in an oven for 24 h (or until no more mass loss is observed) at a temperature of 105 °C. The dry mass of the sample ( $m_s$ ) was determined immediately after removal from the oven. From these measurements the water mass ( $m_w$ ) was calculated:

$$m_w = m_b - m_s \quad (\text{Equation 4-1})$$

and the water content ( $w$ ) of the sample determined:

$$w = \frac{m_w}{m_s} \quad (\text{Equation 4-2})$$

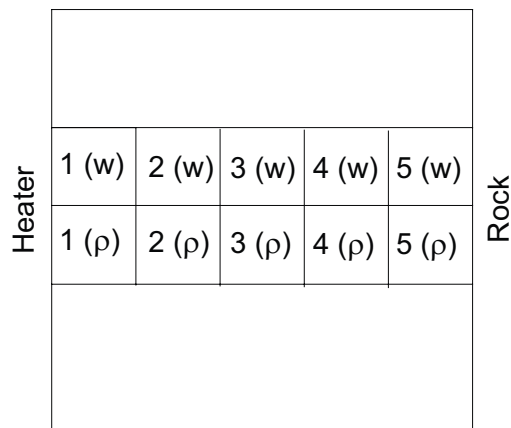


**Figure 4-18.** Schematic view of a slice from a block, showing how samples were cut out at different radial distances from the inner surface closest to the heater and out to the rock surface. The distance from the rock to the heater was approximately 100 mm.

### **Bulk density, dry density and degree of saturation**

The bulk density ( $\rho_b$ ) was determined by hanging the sample in a thin thread under a balance. The sample was then weighed, first in air ( $m_b$ ) and then submerged into paraffin oil ( $m_{bp}$ ). The volume of the sample was then calculated:

$$V = \frac{(m_b - m_{bp})}{\rho_p} \quad (\text{Equation 4-3})$$

where  $\rho_p$  is the paraffin oil density. The bulk density of the sample was then calculated:

$$\rho_b = \frac{m_b}{V} \quad (\text{Equation 4-4})$$

After determining the water content and the bulk density of each sample it was possible to calculate the dry density ( $\rho_d$ ):

$$\rho_d = \frac{\rho_b}{1 + w} \quad (\text{Equation 4-5})$$

Since the grain density ( $\rho_s$ ) and the density of the water ( $\rho_w$ ) are known the degree of saturation (Sr) can be calculated:

$$Sr = \frac{w \cdot \rho_b \cdot \rho_s}{[\rho_s \cdot (1 + w) - \rho_b] \rho_w} \quad (\text{Equation 4-6})$$

In the calculations different value of the grain density ( $\rho_s$ ) have been used for the different materials, see next section.

### **Grain density**

In the calculations of the degree of saturation, different values of the grain density have been used, see Table 4-2, from Svensson et al. (2011). The grain density of the materials was determined by using volumetric flasks. After determining the volume of the flasks very carefully, dried material was mixed with 1 M NaCl solution (in order to prevent swelling of the bentonite). When the mass of the solids, the total volume, the total mass (solids and flask) and the density of the liquid is known, it is possible to calculate the grain density of the material (Svensson et al. 2011).

**Table 4-2. Grain density for the different materials used in ABM 2 (Svensson et al. 2011).**

<b>Material</b>	<b>Grain density kg/m<sup>3</sup></b>
MX-80	2780
Calcigel	2695
Ikosorb	2740
Rokle	2940
Kunigel	2681
Febex	2735
Callovo Oxfordian	2682
Asha 505	2869
Friedland	2828
Ibeco Seal	2753
Deponit CAN	2750

### 4.4.3 Results

The results from the determinations of water content and density distribution are presented in Table 4-3 and Table 4-4. The calculated degree of saturation for each position is presented in Table 4-5.

Contour plots of the measured and calculated variables water content, dry density and degree of saturation were made using an interpolation program. The results are presented in Figure 4-19 (water content and dry density) and in Figure 4-20 (degree of saturation).

Since the test package consisted of blocks (and granulate) made of eleven different materials, with different compaction properties but compressed with the same pressure, there were rather large variations in the as-placed dry density of the blocks, see installation report (Eng et al. 2007). The differences were to varying degree still present and there were thus large variations in water content and dry density within the test package. The water content varied between 11 and 43 % and the dry density varied between 1 250 and 2 100 kg/m<sup>3</sup>. The degree of saturation was however high in the complete test package, between 93 and 100 %.

**Table 4-3. Results from radial water content measurements in ABM 2.**

Water content distribution in test package ABM 2, %						
Block no.	Material	Center position of sample, mm from heater				
		10	29	48	67	86
31	MX-80	26.0	26.9	27.3	28.5	29.8
30	MX-80	24.5	25.8	26.7	28.0	27.0
29	Febex	23.9	25.8	27.0	29.3	30.2
28	Ikosorb	22.9	23.6	26.2	29.8	30.0
27	MX-80 granulate	26.1	31.4	34.4	36.2	38.3
26	Deponit CA-N	26.2	27.1	33.1	35.9	37.2
25	MX-80 granulate+quarz	19.9	24.1	28.1	29.9	30.9
24	Rokle	24.5	28.4	34.1	38.6	39.4
23	Friedland	10.6		17.5	19.5	22.0
22	Kunigel V1		18.2	19.1	20.0	23.4
21	Asha 505			30.1	32.2	31.7
20	Callovo-Oxfordian discs					
19	Callovo-Oxfordian	13.8	13.4	13.2	13.7	15.4
18	Calcigel	30.1	31.2	32.2	34.3	37.1
17	MX-80	31.3	30.6	31.2	31.9	35.9
16	Callovo-Oxfordian	11.8	12.8	12.7	13.1	14.6
15	Ibeco Seal	34.7	33.8	34.1	35.2	37.7
14	MX-80 granulate+quarz	26.4	26.7	27.5	28.3	28.8
13	Kunigel V1	22.5	23.4	23.8	24.6	26.3
12	Ikosorb	27.9	28.2	28.7	30.7	30.4
11	Ibeco Seal	27.9	28.2	28.6	30.3	32.2
10	Asha 505	27.0	28.0	28.6	30.9	33.0
9	Febex	26.9	28.5	33.0	36.7	35.7
8	MX-80 granulate	31.3	32.6	35.6	39.9	42.9
7	Rokle	30.4	31.7	34.1	35.4	37.6
6	MX-80	25.7	26.6	28.5	32.9	32.3
5	Deponit CA-N	27.8	28.4	29.6	31.3	33.0
4	Friedland	14.6	15.9	15.6	17.2	17.5
3	Calcigel	27.3	28.2	30.2	32.0	31.0
2	MX-80	26.2	27.1	28.8	33.1	32.1
1	MX-80	27.7	28.2	30.7	34.2	31.5

**Table 4-4. Results from radial density measurements in ABM 2.**

Dry density distribution in test package ABM 2, kg/m <sup>3</sup>						
Block no.	Material	Center position of sample, mm from heater				
		10	29	48	67	86
31	MX-80	1587	1586	1576	1552	1536
30	MX-80	1633	1593	1569	1539	1559
29	Febex	1641	1596	1564	1517	1474
28	Ikosorb	1649	1634	1556	1499	1486
27	MX-80 granulate	1568	1478	1425	1377	1318
26	Deponit CA-N	1534	1540	1440	1389	1360
25	MX-80 granulate+quarz		1596	1503	1466	1482
24	Rokle	1654	1553	1462	1361	1384
23	Friedland	2088		1872	1800	1741
22	Kunigel V1		1800	1777	1739	1664
21	Asha 505			1534	1432	1467
20	Callovo-Oxfordian discs					
19	Callovo-Oxfordian	1984	1995	1990	1962	1921
18	Calcigel	1517	1497	1475	1429	1374
17	MX-80	1489	1483	1471	1454	1386
16	Callovo-Oxfordian	2072	2008	1988	1978	1926
15	Ibeco Seal	1408	1431	1423	1404	1351
14	MX-80 granulate+quarz	1571	1575	1555	1526	1512
13	Kunigel V1	1673	1661	1646	1621	1582
12	Ikosorb	1540	1539	1521	1488	1476
11	Ibeco Seal	1553	1549	1541	1512	1458
10	Asha 505	1608	1577	1568	1519	1466
9	Febex	1552	1525	1437	1352	1334
8	MX-80 granulate	1497	1458	1319	1293	1229
7	Rokle	1548	1513	1471	1412	1392
6	MX-80	1611	1591	1549	1457	1423
5	Deponit CA-N	1565	1547	1521	1486	1404
4	Friedland	1979	1943	1927	1878	1872
3	Calcigel	1573	1540	1516	1471	1479
2	MX-80	1595	1574	1542	1443	1459
1	MX-80	1572	1541	1502	1428	1465

**Table 4-5. Results from calculations of the degree of saturation in ABM 2.**

Degree of saturation in test package ABM 2, %						
Block no.	Material	Center position of sample, mm from heater				
		10	29	48	67	86
31	MX-80	96.1	99.4	99.2	99.9	102.1
30	MX-80	97.0	96.2	96.3	96.7	95.9
29	Febex	97.8	98.7	98.7	99.8	96.6
28	Ikosorb	94.7	95.4	94.5	98.5	97.4
27	MX-80 granulate	94.0	99.2	100.8	98.7	96.0
26	Deponit CA-N	91.0	94.8	99.9	100.7	100.1
25	MX-80 granulate+quarz		92.2	93.4	94.2	99.8
24	Rokle	92.6	93.5	99.2	97.7	103.1
23	Friedland	89.2		100.4	99.7	102.3
22	Kunigel V1		99.4	100.6	99.1	102.5
21	Asha 505			99.4	92.0	95.2
20	Callovo-Oxfordian discs					
19	Callovo-Oxfordian	103.5	102.5	100.0	98.0	102.4
18	Calcigel	104.5	105.1	104.8	104.4	104.0
17	MX-80	100.4	97.2	97.4	97.3	99.2
16	Callovo-Oxfordian	105.4	100.0	95.8	96.9	98.2
15	Ibeco Seal	99.8	100.6	100.5	100.8	100.0
14	MX-80 granulate+quarz	97.2	98.9	98.7	97.5	97.2
13	Kunigel V1	100.0	102.0	101.7	100.8	101.7
12	Ikosorb	98.2	99.2	98.2	100.0	97.3
11	Ibeco Seal	99.4	100.0	100.1	101.5	99.8
10	Asha 505	98.6	98.1	99.0	99.8	98.8
9	Febex	96.6	98.4	99.9	98.0	92.9
8	MX-80 granulate	101.5	99.8	89.3	96.6	94.5
7	Rokle	99.4	98.8	100.4	96.1	99.4
6	MX-80	98.5	98.9	99.5	100.7	94.3
5	Deponit CA-N	100.8	100.4	100.6	101.2	94.7
4	Friedland	100.3	102.6	98.1	99.6	100.4
3	Calcigel	103.0	101.4	104.6	103.5	101.6
2	MX-80	98.2	98.4	99.6	99.3	98.5
1	MX-80	100.3	97.7	100.4	100.4	97.5

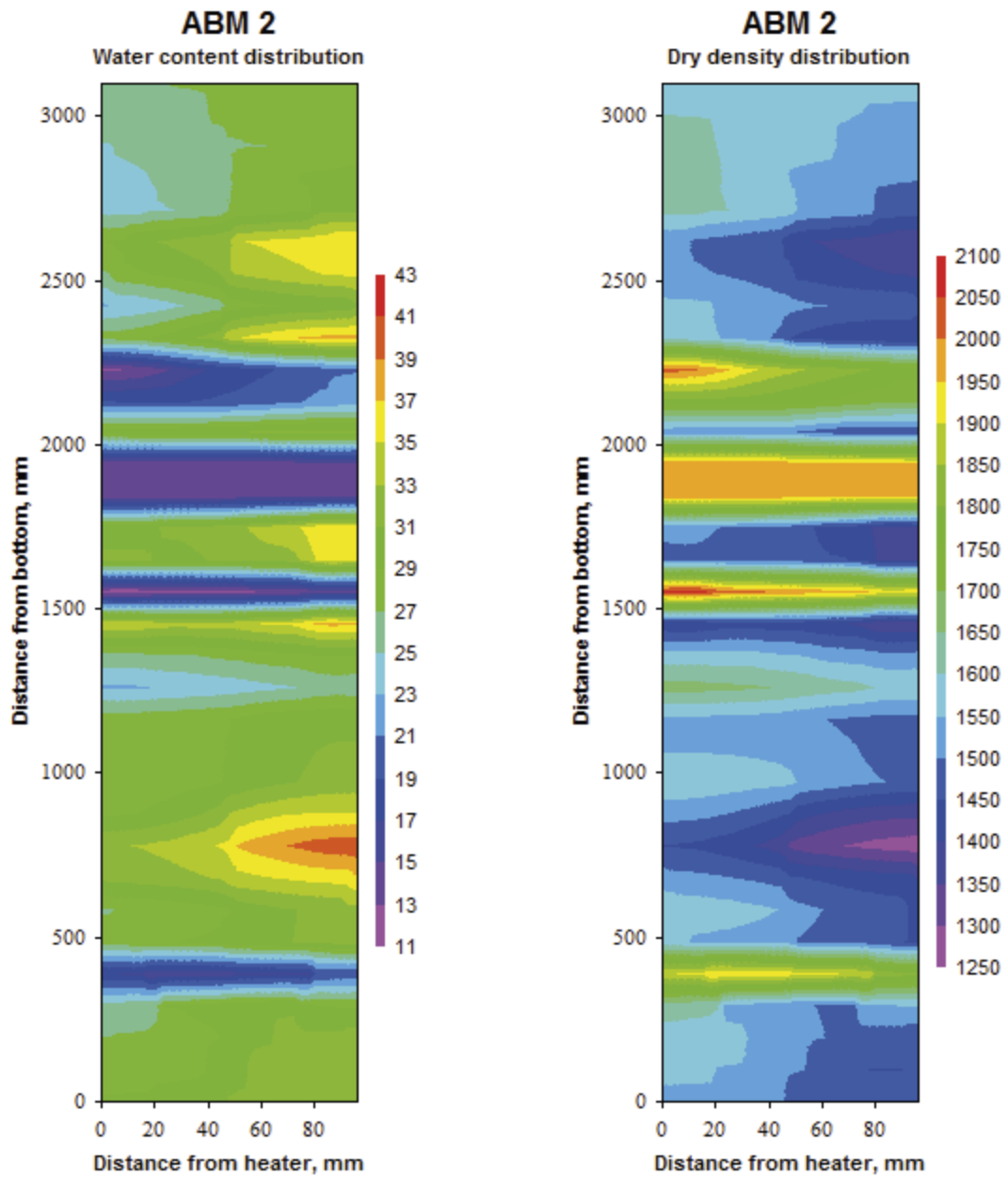
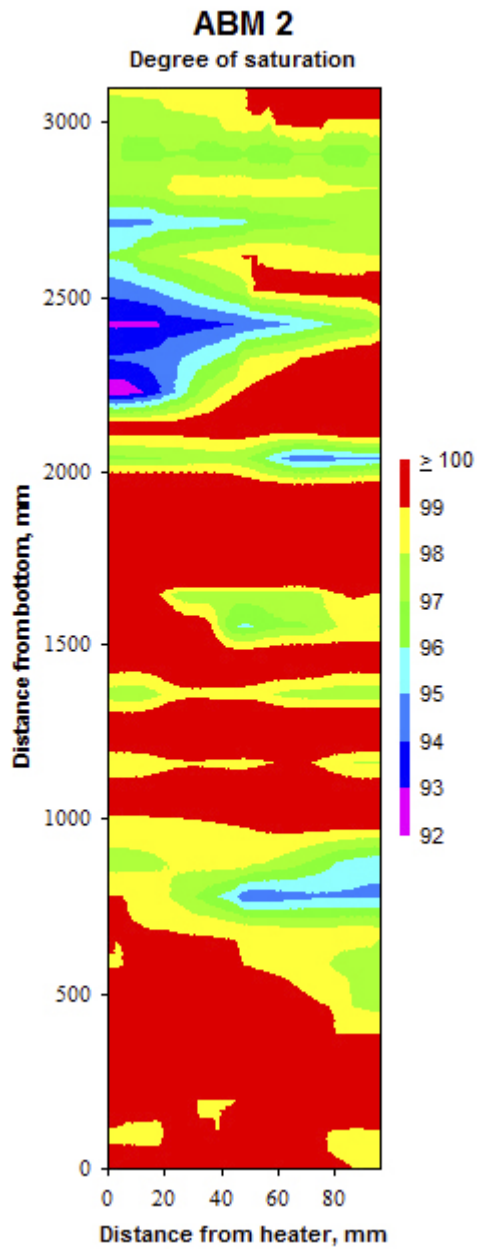


Figure 4-19. Water content distribution (left) and dry density (right) for test package ABM 2.



*Figure 4-20. Degree of saturation for test package ABM 2.*

## 4.5 Comments

The ABM 2 test package has been artificial wetted from test start. A water pressure between 1.2 and 4.5 bar has been applied in the surrounding sand filter. The heating of the ABM 2 test package was started after 631 days test duration when the bentonite was judged to be completely saturated. The temperature close to the surface of the central tube (5 mm from the tube into the clay) had been between 120 and 140 °C (on the section from 400–2700 mm from bottom).

The dismantling of the test and the following initial analyzes of the different blocks have shown that:

- Since the test package consisted of blocks (and granulate) made of eleven different materials, with different compaction properties, there was rather large variation in the as-placed dry density of the blocks, see installation report (Eng et al. 2007). The differences were to varying degree still present at the dismantling and there were thus large variations in water content and dry density within the test package. The water content varied between 11 and 43 % and the dry density varied between 1250 and 2100 kg/m<sup>3</sup>.
- The degree of saturation was high in the entire test package. Most blocks had a degree of saturation of between 95 and 100 %. The lowest degrees of saturation, between 89 and 95 % were found close to the heater at a length section between 2200 and 2600 mm from the bottom. The blocks in this section were made of Friedland, Rokle, MX-80 granulate+quarz and Deponit CA-N. The general high degree of saturation in Calcigel was probably caused by an error in the determination of the grain density.
- In many blocks there were several fractures dividing the block into 3–5 large pieces, see photos in Figure 4-17 (upper left and right). Other blocks were very fragile and fell into many small pieces, see photos in Figure 4-17 (lower left and right). The most fragile blocks were block no. 3–5 and no. 19–24.

## 5 ABM5 evolution and excavation

### 5.1 Test layout

The schematic drawing provided in Figure 5-1 shows the block order in test package ABM 5.

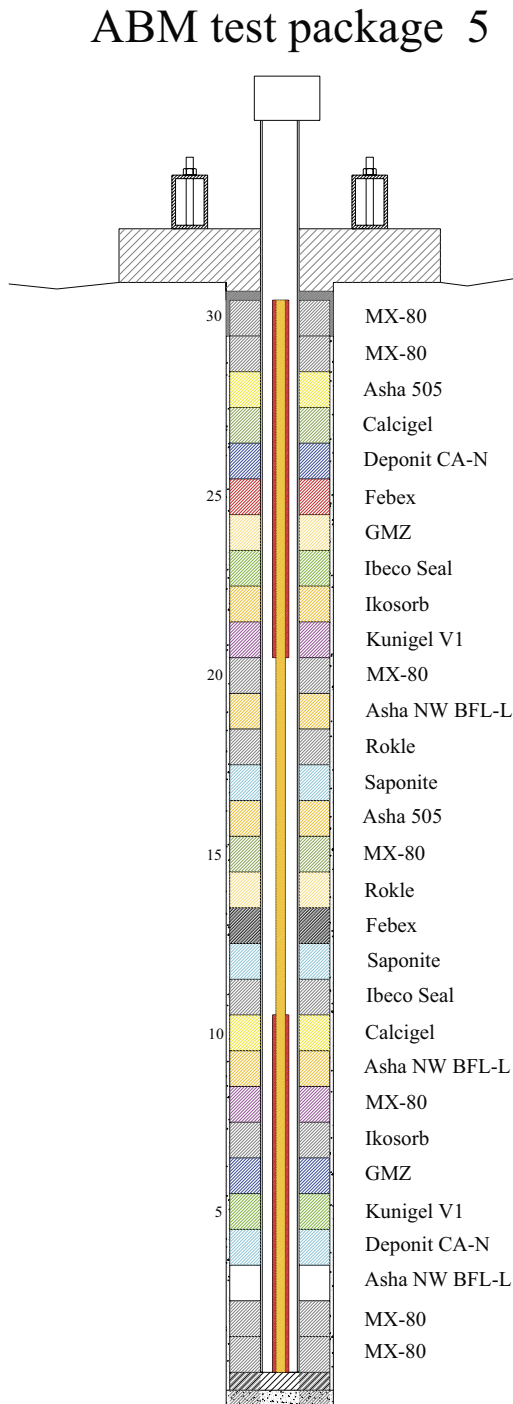


**Figure 5-1.** Schematic drawing of the ABM 5 test layout. The drawing shows how the different blocks (no.1–30) were positioned in the test.

## 5.2 Field operation

The test included the following important milestones:

- 2012-11-08. Test package ABM 5 was installed in the test hole.
- 2012-11-13. The filter (sand filter) surrounding the three new test packages were filled with water. The injected volume to ABM 5 was only 2 liters (about 29–30 liters in the other two packages), then water started to leak out through the floor. It was judged that the filter already was filled with inflowing formation water. See detailed description in Section 5.2.3.
- 2013-09-27. The heating was started 316 days after installation.
- 2017-04-10. The heating was stopped 1 608 days after installation.
- 2017-06-26. The test package was released from the test hole.

### 5.2.1 Heating

The heating of the ABM 5 test started 316 days after installation. The applied power was increased in steps to 340 W, Figure 5-2. This power was then applied for about 900 days. A new increase was made after 1 283 days. The power was increased in steps up to 1 800 W. This power was then applied until the test was stopped, 1 608 days after installation.

### 5.2.2 Temperature development

The registered temperature data for the five levels (block no. 3, 9, 15, 21, 27) is presented in Figure 5-3 to Figure 5-7. The number of measuring points is limited but the registered data gives a fairly good picture of the temperature distribution in the test package. In this test package, the innermost thermocouples were positioned outside the tube and in contact with the tube surface which resulted in reliable measurements, see also Section 4.2.2.

To get an overview of the temperature distribution within the test package, a contour plot of the measured temperature was made using an interpolation program. The graph shows the temperature distribution the day before the heating was stopped.

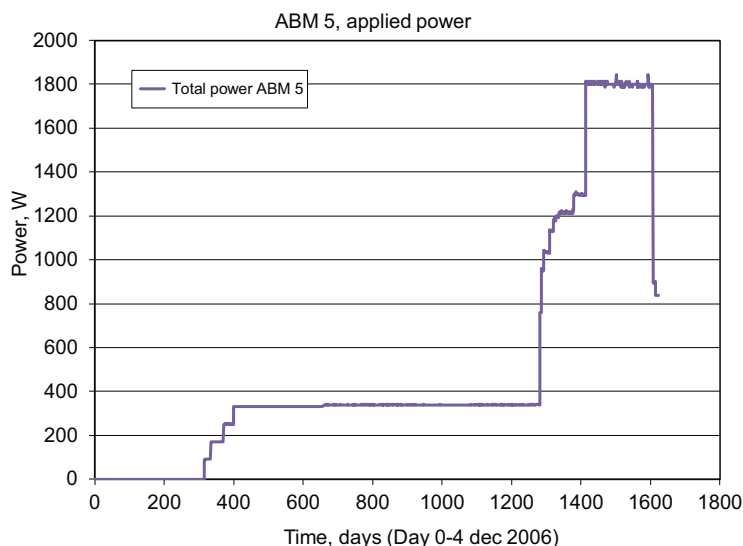


**Figure 5-2.** Applied power to the heaters in ABM 5 plotted versus time.

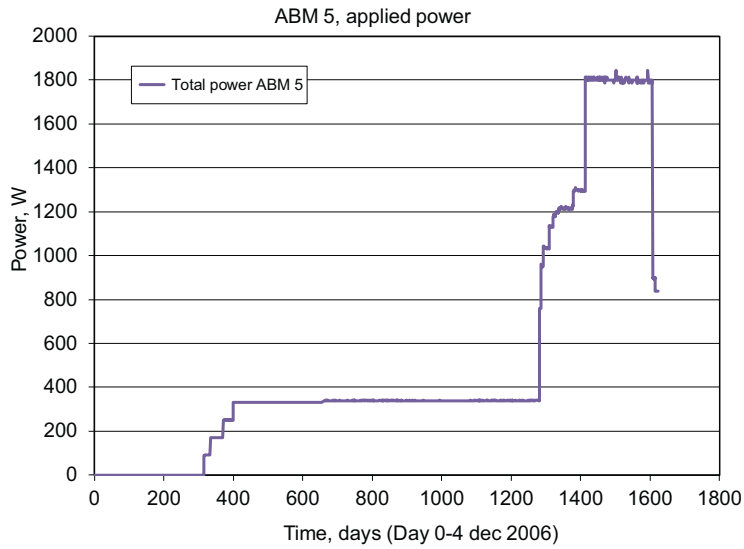


**Figure 5-3.** Temperature measurements in block no. 3 plotted vs. time.

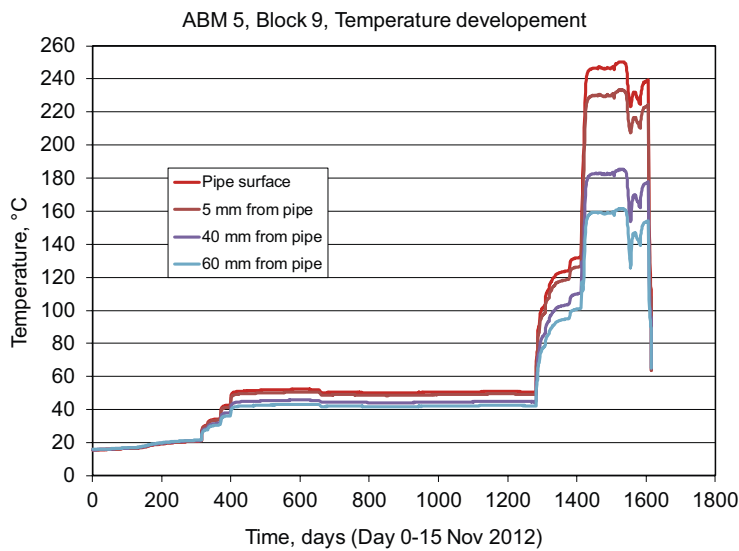


**Figure 5-4.** Temperature measurements in block no. 9 plotted vs. time.

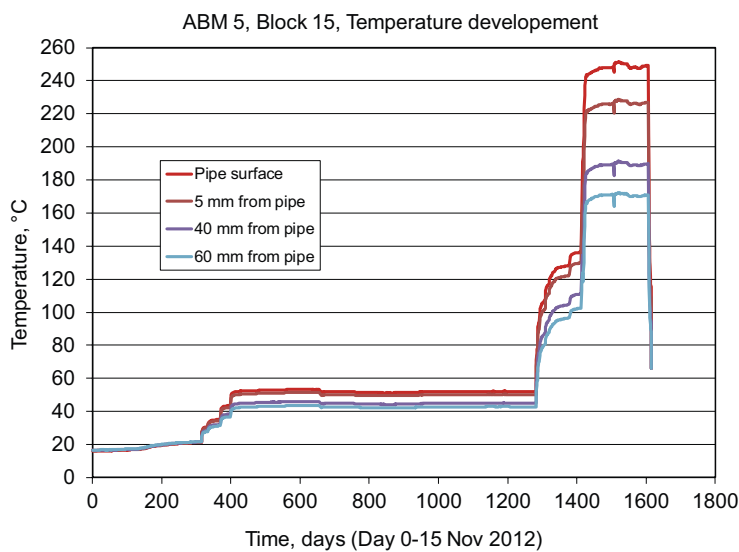


**Figure 5-5.** Temperature measurements in block no. 15 plotted vs. time.

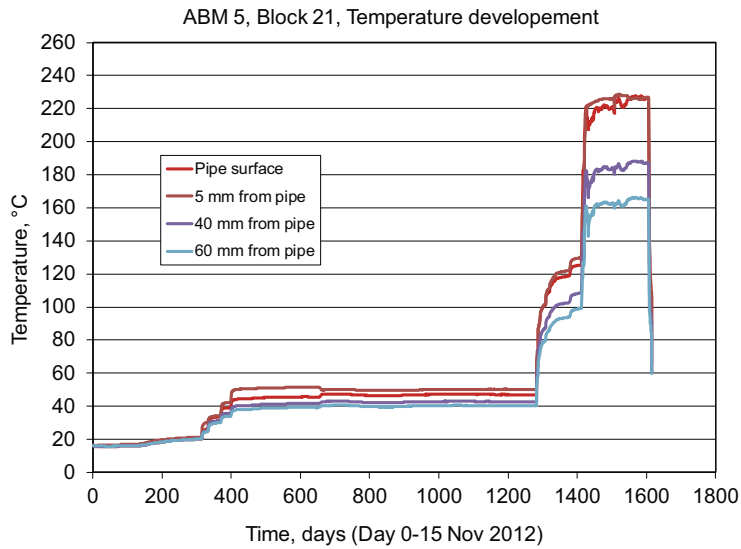


**Figure 5-6.** Temperature measurements in block no. 21 plotted vs. time.

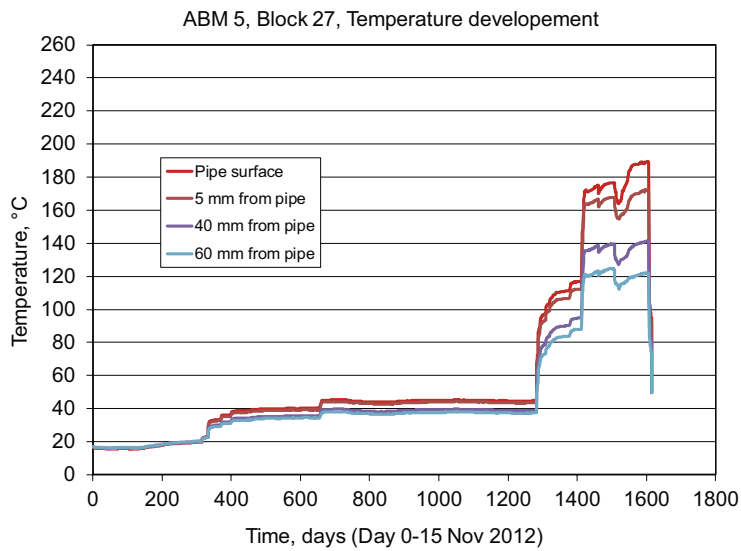


**Figure 5-7.** Temperature measurements in block no. 27 plotted vs. time.

The contour plot indicates that the temperature on the surface of the central tube had been between 200 and 240 °C (on the section from 600–2 500 mm from bottom). The temperature varied radially within the test package, roughly according to the following:

- 0–20 mm: in the range 200–240 °C
- 20–40 mm: in the range 180–200 °C
- 40–60 mm: in the range 150–180 °C
- 60–96 mm: in the range 90–150 °C

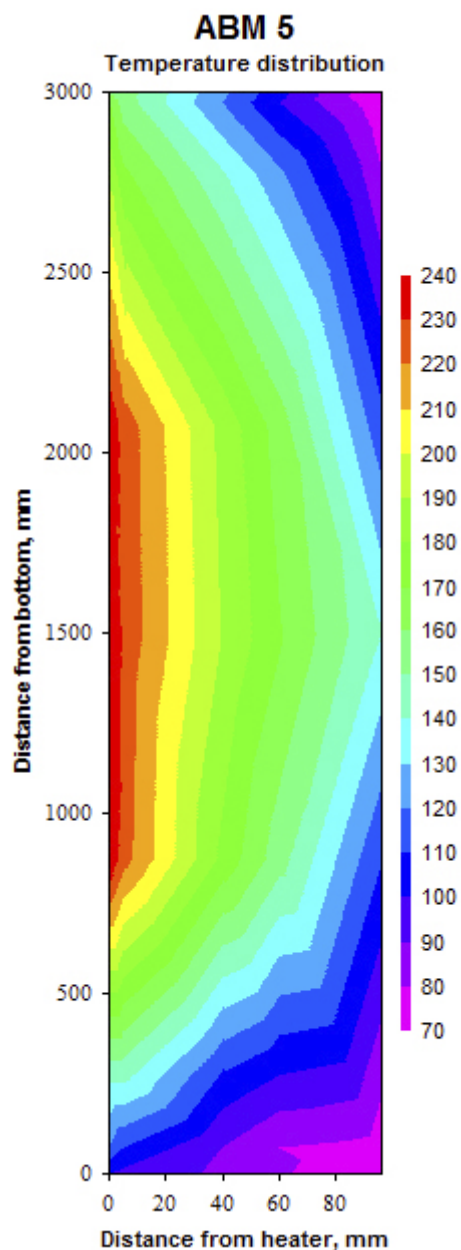


Figure 5-8. Temperature distribution in ABM 5.

### 5.2.3 Artificial water saturation

#### *Inflow measurements*

After completion of the three test holes, the natural water inflow into each test hole was measured (Sandén et al. 2018). Two of the test holes were very dry while one (the ABM 5 test hole) had a water inflow of approximately 8.5 liters/24 hours. All inflow was judged to come from one fracture located 0.8 meter down from the floor.

### Test start ABM 45

The test packages were installed 2012-11-08. Five days later, after having cast the concrete lids and mounted the steel beams, an attempt was made to artificially fill up the filters in the three tests. Water was injected through the titanium tubes into the sand filters. The injected water volume was 29.3 liters to ABM 4 and 28.9 liters to ABM 6. The injected volume to ABM 5 was about 2 liters and then water started to leak out on the floor above the test hole. It was judged that the filter already had been filled up with water from the earlier identified fracture. Since the fracture also had connections to the floor, it was not possible to apply a water pressure in the filter. This was also the reason why the temperature was kept below 100 °C for the first 1 300 days. It was not possible to maintain a sufficient pressure in the filter to avoid boiling. It was therefore decided to close the water injection to ABM 5. The artificial water injection system has thereafter not been used in this test. The ABM 5 test package has thus only had access to formation water, probably mainly from the earlier identified fracture. It is judged that the composition of the formation water was the same as from the borehole HD0025A that was used to supply the Canister Retrieval Test with water. This borehole is located only a few meters from the ABM 45 test site. The composition of this water is presented in Table 5-1 (Dueck et al. 2011).

### Artificial water injection to test packages ABM 4 and ABM 6

The water supply to test packages ABM 4 and ABM 6 have been made using one system. The water has been taken from a water supply coming from the ground (freshwater). After the initial filling of the sand filters a water pressure of 50 kPa has been applied.

**Table 5-1. Main elements in the water supply. The water was taken from bore hole HD0025A (Dueck et al. 2011).**

Date	Na mg/L	K mg/L	Ca mg/L	Mg mg/L	HCO <sub>3</sub> mg/L	Cl mg/L	SO <sub>4</sub> mg/L	SO <sub>4</sub> -S mg/L	Br mg/L	F mg/L	Si mg/L
1999-04-12	1830.0	16.8	1284.0	96.8	114.0	5530.0	363.0	112.0	36.1	1.56	4.70
1999-10-04	1730.0	20.7	987.0	123.1	147.0	4590.0	382.0	115.0	25.3	1.31	5.50
2001-09-26	1390.0	30.7	286.0	125.0	195.0	2540.0	261.0	98.9	12.1	1.20	5.51
2002-09-24	1590.0	27.8	629.0	120.0	164.0	3841.3	316.2	99.6	21.9	1.64	5.40
2004-09-21	1480.0	29.3	611.0	106.0	170.0	3360.0	325.0	105.0	29.8	1.45	5.63
Mean	1604.0	25.1	759.4	114.2	158.0	3972.3	329.5	106.1	25.0	1.43	5.35
Std	179.11	6.01	384.10	12.24	30.02	1145.81	46.8	7.23	8.98	0.18	0.37

Date	Fe <sub>tot</sub> mg/L	Fe(II) mg/L	Mn mg/L	Li mg/L	Sr mg/L	pH mg/L	COND mg/L	DOC mg/L	NH <sub>4</sub> -N mg/L
1999-04-12	0.703	0.707	0.580	0.7000	16.10	7.40	1250.0	4.5	0.3978
1999-10-04	0.912	0.912	0.845	0.4975	14.00	7.40	1310.0	5.4	0.6766
2001-09-26	0.937	0.941	0.683	0.1200	4.39	7.50	830.0	5.6	0.6900
2002-09-24	0.897	0.904	0.667	0.3780	9.95	7.45	1178.0	5.1	0.8547
2004-09-21	0.843	0.841	0.590	0.4070	9.51	7.45	1020.0	5.6	0.9430
Mean	0.858	0.861	0.674	0.421	10.79	7.4	1117.6	5.2	0.712
Std	0.09	0.09	0.11	0.21	4.52	0.04	193.93	0.46	0.21

## 5.3 Termination

### 5.3.1 Releasing the test package

The test package was terminated and released from the surrounding rock using the same technique as had been used for earlier test packages of this type. The heater power was closed 2017-04-10, and the test package was lifted 2017-06-26.

The lifting of the test package was made by a lorry with a crane. There were some fractures running along the rock cover, but the test package was successfully lifted from the rock, Figure 5-9. The left photo in Figure 5-10 shows the test package from the bottom. As shown in the photo a small rock piece had fallen off from the bottom part of the package. The right photo in Figure 5-10 shows the rock surface after retrieval of the test package. From the photo it is easy to understand the technique used to release the test package from the rock i.e. seam drilling around the periphery and then two large core drilled holes that have been used to install the wire sawing equipment which was used to saw off the rock column at the bottom.



*Figure 5-9. Photo showing the released test package during the uplift.*



*Figure 5-10. Left: The test package was lifted up almost in one piece. A minor rock piece close to the bottom fell off during the uplift. Right: Photo showing the rock after retrieval of the test package.*

### 5.3.2 Division and material handling

After retrieval the test package was immediately transported to an experiment hall at the surface of the Äspö HRL where division of the rock package and uncovering the bentonite blocks were made. The photo provided in Figure 5-11 shows the upper part of the test package. As shown in the photo there was some fractures in the rock cover which facilitated the work with the removal of the rock.

The photo in Figure 5-12 shows the bottom of the test package where a small rock piece had fallen off in conjunction with the uplift, see also Figure 5-10 to the left. The large fracture that runs along the test package can also be seen in the photo. The division of the test package started by removing the upper parts of the rock cover. After exposure of the bentonite, one could see that large fractures were running along the complete package also in the bentonite, see example in Figure 5-13.



*Figure 5-11. The test package was transported to the laboratory at Äspö HRL.*



*Figure 5-12. The bottom of the test package. A minor rock piece fell off during the uplift.*



**Figure 5-13.** Large fractures in the bentonite were present along the complete test package. The photo shows the situation for block no. 20 (left) to block no. 11 (right).

The bentonite was removed from the central tube as long sections containing parts from different blocks, see examples in the photos provided, Figure 5-14 and Figure 5-15. Some blocks were rather intact while others were highly fractured and very fragile due to the high temperature.

The initial sampling (see description in Section 5.4) included that a slice with a thickness of about 20 mm was cut out from each block. This slice was then used to determine the radial water content and density distribution at five positions. After having cut out this slice, the remaining block parts were placed in a sack made of alumina laminate which were evacuated and welded together. The sacks were then placed in airtight barrels.



**Figure 5-14.** Parts of blocks 6 to 9.



*Figure 5-15. Part of blocks 18-23.*

## **5.4 Water content and density determinations**

### **5.4.1 General**

Basic properties of the bentonite test material were determined in many positions of the test package to achieve a picture of the water content and density distribution. This data was then used to calculate the degree of saturation. Samples were taken at the mid-height of each block at five different radial distances from the heater, Figure 4-18.

In total, the water content and density were determined at 150 positions in the ABM 5 test package.

### **5.4.2 Test procedure and evaluation**

#### ***Water content, dry density and degree of saturation***

See description in Section 4.4.2.

#### ***Grain density***

For the calculations of the degree of saturation, different values of the grain density have been used, see Table 4-2 (Svensson et al. 2011). In the ABM 45 test packages there were two new materials, GMZ and Saponite. The grain density used for GMZ was  $2710 \text{ kg/m}^3$  (Sun et al. 2014) and for Saponite  $2300 \text{ kg/m}^3$  (Engineering ToolBox 2021).

### **5.4.3 Results**

The results from the determinations of water content and density distribution are presented in Table 5-2 and Table 5-3. The calculated degree of saturation for each position is presented in Table 5-4.

**Table 5-2. Results from radial water content measurements in ABM5.**

Water content distribution in test package ABM 5, %						
Block no.	Material	Center position of sample, mm from heater				
		10	29	48	67	86
30	MX-80	20.0	21.8	22.5	25.1	19.2
29	MX-80	14.4	16.3	17.7	19.8	14.2
28	Asha 505	16.5	17.9	18.8	18.7	18.9
27	Calcigel	12.1	11.8	12.7	13.3	13.0
26	Deponit CAN	16.4	18.2		20.3	21.6
25	Febex	17.1	17.7		18.5	19.7
24	GMZ	14.2	16.2	16.9		18.8
23	Ibeco SEAL	15.2	17.7		19.4	20.1
22	Ikosorb	14.5	15.7		16.7	18.5
21	Kunigel V1	11.1	11.8		12.2	12.7
20	MX-80	15.7	16.4	18.0	19.5	18.8
19	Asha NW BFL-L	18.4	18.1		18.8	20.0
18	Rokle	17.1	19.0	20.1	22.3	21.4
17	Saponite	11.8	12.8		13.5	12.4
16	Asha 505	18.1	19.6	19.2	19.3	20.2
15	MX-80	18.5	18.7	18.6	18.0	16.7
14	Rokle	15.4	17.0	17.5	17.8	17.3
13	Febex	18.3	18.8	19.6	17.5	18.1
12	Saponite	11.7	13.4		12.8	14.8
11	Ibeco SEAL	21.6		21.7	23.0	24.1
10	Calcigel	14.7	14.6	14.7	17.0	16.8
9	Asha NW BFL-L	18.7	19.5	20.6	21.0	22.2
8	MX-80	17.8	19.2	18.5	19.7	20.3
7	Ikosorb	18.9	19.9	20.4	21.3	18.2
6	GMZ	20.4	20.5	20.2	21.4	23.0
5	Kunigel V1	17.8	18.0	18.4	19.8	
4	Deponit CAN	17.4	19.8	20.7	21.2	25.6
3	Asha NW BFL-L	20.6	21.6	22.1	26.5	28.6
2	MX-80	21.7	22.7	25.3	29.1	26.9
1	MX-80	23.9	26.1	27.9	30.2	31.3

**Table 5-3. Results from radial density measurements in ABM5.**

Dry density distribution in test package ABM 5, kg/m <sup>3</sup>						
Block no.	Material	Center position of sample, mm from heater				
		10	29	48	67	86
30	MX-80	1612	1611	1626	1592	1713
29	MX-80	1843	1810	1774	1740	1767
28	Asha 505	1826	1798	1773	1760	1775
27	Calcigel	1836	1798	1782	1776	1759
26	Deponit CAN	1758	1724		1670	1626
25	Febex	1792	1784		1754	1684
24	GMZ	1847	1810	1801		1734
23	Ibeco SEAL	1727	1763		1730	1715
22	Ikosorb	1829	1806		1798	1743
21	Kunigel V1	1882	1888		1888	1906
20	MX-80	1802	1799	1765	1747	1751
19	Asha NW BFL-L	1797	1814		1780	1725
18	Rokle	1839	1789	1763	1699	1717
17	Saponite	1819	1789		1793	1811
16	Asha 505	1840	1782	1717	1781	1735

**Table 5-3. Continued.**

Dry density distribution in test package ABM 5, kg/m <sup>3</sup>						
Block no.	Material	Center position of sample, mm from heater				
		10	29	48	67	86
15	MX-80	1765	1783	1757	1769	1805
14	Rokle	1890	1842	1825	1811	1805
13	Febex	1741	1728	1714	1752	1716
12	Saponite	1787	1782		1799	1812
11	Ibeco SEAL	1692		1734	1657	1633
10	Calcigel	1790	1806	1804	1747	1739
9	Asha NW BFL-L	1814	1784	1737	1733	1707
8	MX-80	1808	1776	1785	1754	1731
7	Ikosorb	1754	1725	1697	1674	1772
6	GMZ	1744	1732	1747	1718	1657
5	Kunigel V1	1802	1790	1771	1733	
4	Deponit CAN	1788	1735	1712	1687	1553
3	Asha NW BFL-L	1750	1710	1685	1614	1556
2	MX-80	1715	1682	1623	1533	1559
1	MX-80	1644	1606	1560	1500	1506

**Table 5-4. Results from calculations of the degree of saturation in ABM5.**

Degree of saturation in test package ABM 5, %						
Block no.	Material	Center position of sample, mm from heater				
		10	29	48	67	86
30	MX-80	76.6	83.7	88.1	93.3	85.6
29	MX-80	78.9	84.8	86.6	92.2	68.8
28	Asha 505	82.8	86.2	87.4	85.3	88.1
27	Calcigel	69.4	64.0	66.9	69.4	65.7
26	Deponit CAN	83.9	88.3		90.2	89.3
25	Febex	88.8	90.7		90.3	86.6
24	GMZ	82.3	88.2	90.7		90.7
23	Ibeco SEAL	75.1	93.2		96.5	97.9
22	Ikosorb	79.6	83.1		87.4	88.8
21	Kunigel V1	70.0	75.2		77.6	84.0
20	MX-80	80.2	83.7	87.1	91.7	88.7
19	Asha NW BFL-L	88.3	89.5		88.2	86.3
18	Rokle	83.9	87.0	88.4	89.9	88.2
17	Saponite	102.8	103.0		109.5	106.0
16	Asha 505	92.9	92.4	82.2	90.5	88.5
15	MX-80	89.6	92.9	89.1	87.7	85.7
14	Rokle	81.2	83.7	84.0	84.0	80.9
13	Febex	87.5	88.2	90.2	85.5	83.3
12	Saponite	93.4	106.1		106.0	126.6
11	Ibeco SEAL	101.2		108.9	101.9	102.8
10	Calcigel	78.6	79.8	80.3	84.2	82.2
9	Asha NW BFL-L	92.1	91.9	90.8	91.9	93.6
8	MX-80	92.1	94.2	92.3	93.9	93.0
7	Ikosorb	92.1	92.4	91.2	91.5	91.1
6	GMZ	99.9	98.5	99.1	100.6	98.0
5	Kunigel V1	97.7	97.2	95.7	96.9	
4	Deponit CAN	93.5	97.4	98.4	96.7	94.4
3	Asha NW BFL-L	92.4	91.5	90.3	97.7	97.2
2	MX-80	96.9	96.4	98.6	99.3	95.4
1	MX-80	96.1	99.2	99.1	98.3	103.0

Contour plots of the measured and calculated variables water content, dry density and degree of saturation were made using an interpolation program. The results are presented in Figure 5-16 (water content and dry density) and in Figure 5-17 (degree of saturation).

Since the test package consists of blocks made of twelve different materials, with different compaction properties but compressed with the same pressure, there was rather large variation in the as-placed dry density of the blocks, see installation report (Sandén and Nilsson 2018). The differences were to varying degree still present and there are thus large variations in water content and dry density within the test package. The high temperature at the heater has also resulted in large water content gradients. The water content varied between 11 and 31 % and the dry density varied between 1 500 and 1 906 kg/m<sup>3</sup>. The degree of saturation varied between 64 and 100 %.

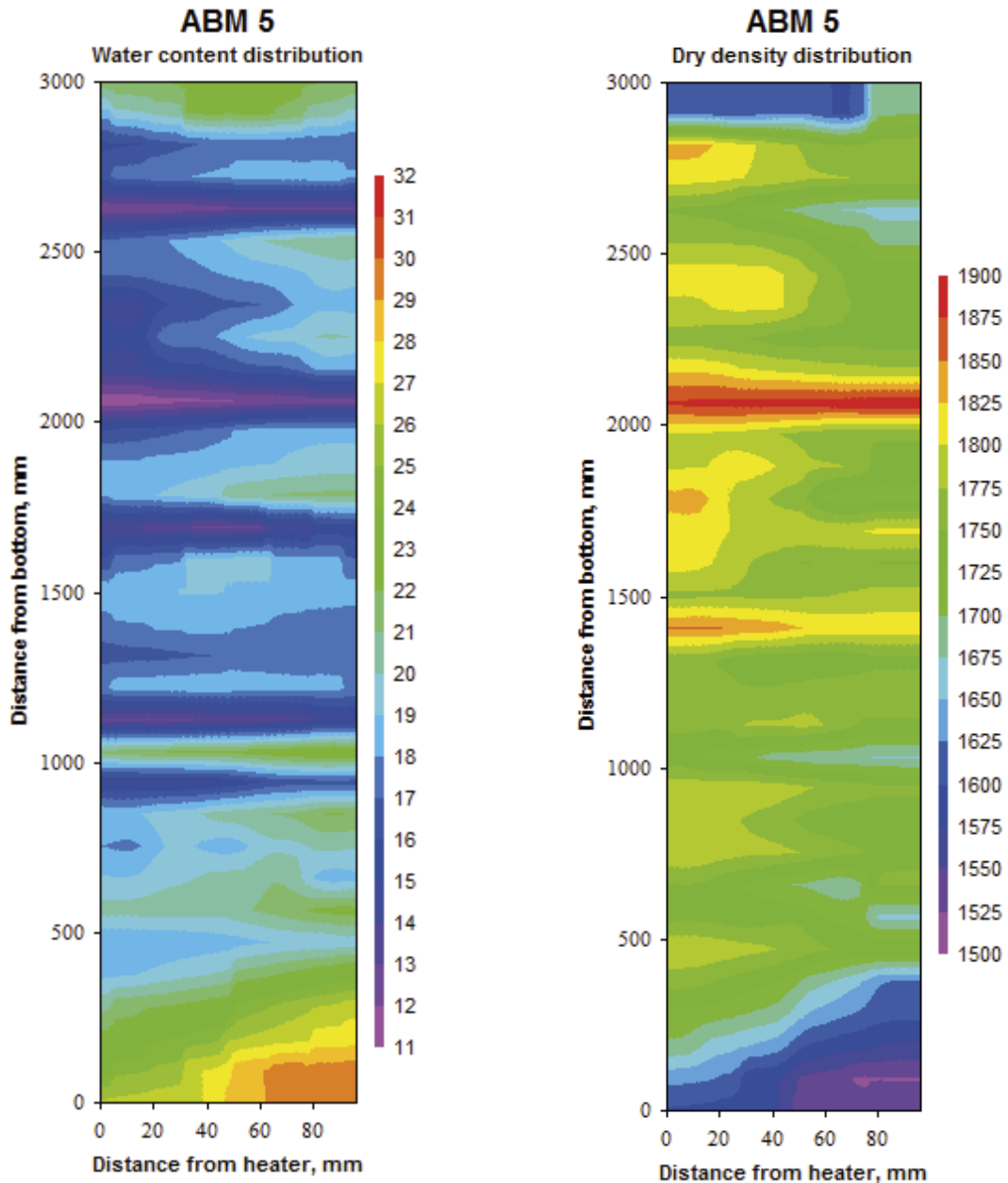


**Figure 5-16.** Water content distribution (left) and dry density (right) for test package ABM 5.

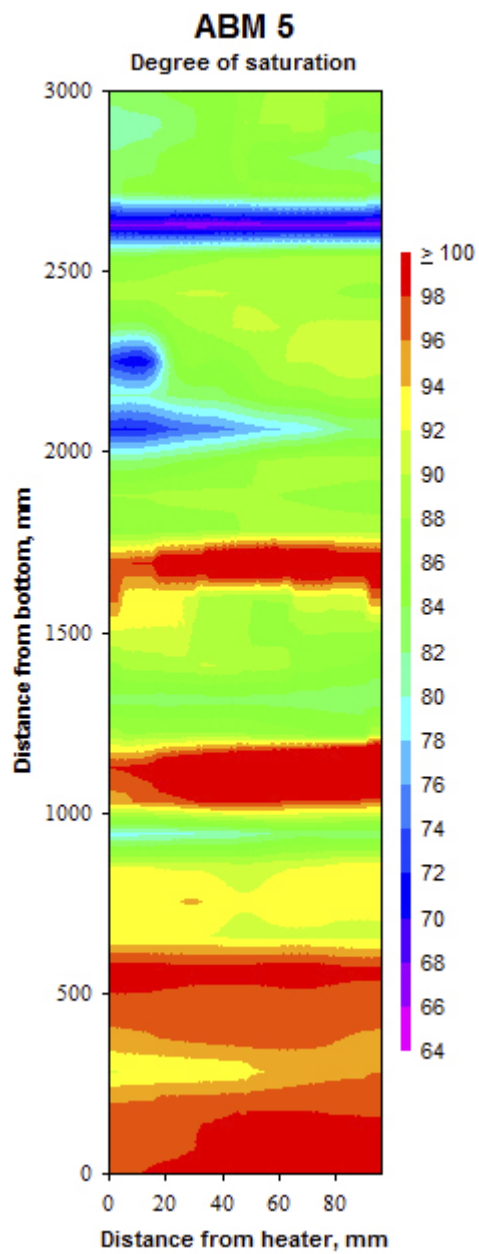


*Figure 5-17. Degree of saturation for test package ABM 5.*

## 5.5 Comments

The ABM 5 test package did not have access to artificial water injection. A water bearing fracture, positioned about 0.8 meter down from the floor has, however, been in connection with the sand filter. The heating of the ABM 5 test started 316 days after installation. The power was increased in steps to 340 W, Figure 5-2. This power was then applied for about 900 days. A new increase was made after 1 283 days. The power was increased in steps up to 1 800 W. This power was then applied until the test was stopped, 1 608 days after installation. The temperature on the surface of the central tube had been between 200 and 240 °C (on the section from 600–2 500 mm from bottom).

The dismantling of the test and the following initial analyzes of the different blocks have shown that:

- Since the test package consisted of blocks made of twelve different materials, with different compaction properties, there was rather large variation in the as-placed dry density of the blocks, see installation report (Sandén and Nilsson 2018). The differences are to varying degree still present and there are thus large variations in water content and dry density within the test package. The high temperature at the heater has also resulted in radial water content gradients, but the differences between different blocks (materials) are higher. The water content varies between 11 and 31 % and the dry density varies between 1 500 and 1 906 kg/m<sup>3</sup>.
- The differences regarding the degree of saturation were large within the test package, between 64 and 100 %. The lowest values were found in the upper half of the test package while the degree of saturation in the sections between 0 and 900 mm from bottom and between 1 100 and 1 700 mm from the bottom were close to saturation, between 90 and 100 %.
- The applied power to the heaters resulted in high temperatures in the buffer. Since there wasn't any water pressure applied into the surrounding filter, the bentonite has dehydrated which in turn has led to lower thermal conductivity and thus higher temperature in the bentonite.
- After the exposure of the bentonite, in conjunction with the dismantling, one could see that large fractures were running along the entire package in the bentonite, see example in Figure 5-13. The bentonite was removed from the central tube as long sections containing parts from different blocks, see examples in the photos provided in Figure 5-14 and Figure 5-15. Some blocks were rather intact while others were highly fractured and very fragile due to the high temperature.



## 6 ABM2 results from analysis

### 6.1 Chemical and mineralogical evolution in ABM2

Due to the extensive variety of clays and the complexity of the experiment, for us it was not feasible to analyze all clays in detail to the same extent. The approach taken was to conduct a screening of numerous samples and identify significant deviations in the mineralogy of clay minerals by observing changes in the XRD pattern in the low-angle region (basal spacing region) or in the region of the 060 reflection (dioctahedral vs. trioctahedral clay minerals). If any changes were detected, further investigation was conducted to better understand the details.

Table 6-1 provides an overview of the CEC (Cation Exchange Capacity) of the ABM2 samples. In MX-80 block #2, it appears that the samples closest to the rock exhibit higher CEC compared to the reference, while the samples closer to the heater show lower CEC than the reference. In Deponit CAN block #5, all field test samples have higher CEC than the reference clay. In the remaining blocks, the CEC of the field samples is similar to the reference clays. To summarize the CEC results of the ABM2 samples, no significant general trend is apparent. Most of the differences can be attributed to the relatively low reproducibility of the CEC measurement in combination with minor dissolution-precipitation (internal transport) of sulfates and carbonates. There is no indication of any significant overall change in smectite content in the ABM2 samples based on CEC measurements.

**Table 6-1. CEC of ABM2 samples.**

Sample	Sample id	CEC cmol(+)/kg (n = 2)	SD (n = 2)
MX-80 ABM Reference	c65d42	83.2	0.2
MX-80 ABM2 #2 0–2 mm	d5eda7	77.7	0.6
MX-80 ABM2 #2 2–10 mm	d5eda8	88.3	1.1
MX-80 ABM2 #2 10–20 mm	d5eda9	80.9	1.1
MX-80 ABM2 #2 20–50 mm	d5edaa	85.7	0.3
MX-80 ABM2 #2 50–70 mm	d5edab	88.5	3.4
MX-80 ABM2 #2 70–100 mm	d5edac	90.3	0.7
Calcigel ABM Reference	c65d56	70.2	0.2
Calcigel ABM2 #3 0–2 mm	d5edad	71.8	0.5
Calcigel ABM2 #3 2–10 mm	d5edae	70.5	0.1
Calcigel ABM2 #3 10–20 mm	d5edaf	61.3	0.2
Calcigel ABM2 #3 20–50 mm	d5edb0	68.4	0.7
Calcigel ABM2 #3 50–70 mm	d5edb1	68.2	0.1
Calcigel ABM2 #3 70–100 mm	d5edb2	67.9	0.5
Deponit CAN ABM Reference	c65d52	83.3	1.1
Deponit CAN ABM2 #5 0–2 mm	d5edb9	89.9	0.7
Deponit CAN ABM2 #5 2–10 mm	d5edba	90.8	1.7
Deponit CAN ABM2 #5 10–20 mm	d5edbb	84.8	0.1
Deponit CAN ABM2 #5 20–50 mm	d5edbc	86.7	0.5
Deponit CAN ABM2 #5 50–70 mm	d5edbd	85.1	0.1
Deponit CAN ABM2 #5 70–100 mm	d5edbe	84.2	1.2
Febex ABM Reference	c65d5e	98.3	0.1
Febex ABM2 #29 0–2 mm	d5ee49	96.0	2.0
Febex ABM2 #29 2–10 mm	d5ee4a	103.9	0.2
Febex ABM2 #29 10–20 mm	d5ee4b	96.6	1.2
Febex ABM2 #29 20–50 mm	d5ee4c	101.2	3.1
Febex ABM2 #29 50–70 mm	d5ee4d	100.2	0.5
Febex ABM2 #29 70–100 mm	d5ee4e	98.9	0.9

**Table 6-1. Continued.**

Sample	Sample id	CEC cmol(+)/kg (n = 2)	SD (n = 2)
Ibeco Seal ABM Reference	c65d8f	87.5	0.1
IbecoSeal ABM2 #15 0–2 mm	d5edf5	91.0	0.6
IbecoSea ABM2 I #15 2–10 mm	d5edf6	89.5	1.7
IbecoSea ABM2 I #15 10–20 mm	d5edf7	83.8	0.7
IbecoSeal ABM2 #15 20–50 mm	d5edf8	85.7	0.6
IbecoSeal ABM2 #15 50–70 mm	d5edf9	83.0	1.6
IbecoSeal ABM2 #15 70–100 mm	d5edfa	84.8	0.2

### 6.1.1 MX-80

In the XRD data of the MX-80 samples (Figure 6-1 to Figure 6-6), a reflection associated with illite/mica at around 10 Å (approximately 10 degrees two theta) was observed. Its presence varied, sometimes being absent, mostly minor, and occasionally somewhat larger. No correlation was observed between the intensity of this reflection and the sample's position relative to the heater. It is more likely that the reflection was influenced by small grains of mica crystals that were oriented differently in relation to the X-ray beam. Regarding the 060 reflection at around 75 degrees two theta, no changes were observed when comparing the ABM2 samples with the reference data. No other reflections indicating the formation of new clay minerals were found in the low-angle region. In summary, the XRD analysis of the MX-80 samples in ABM2 did not reveal any significant qualitative changes in the clay minerals present. The basal spacing reflection changed somewhat between the different samples, as a consequence of different amount of hydration of the montmorillonite interlayer cations.

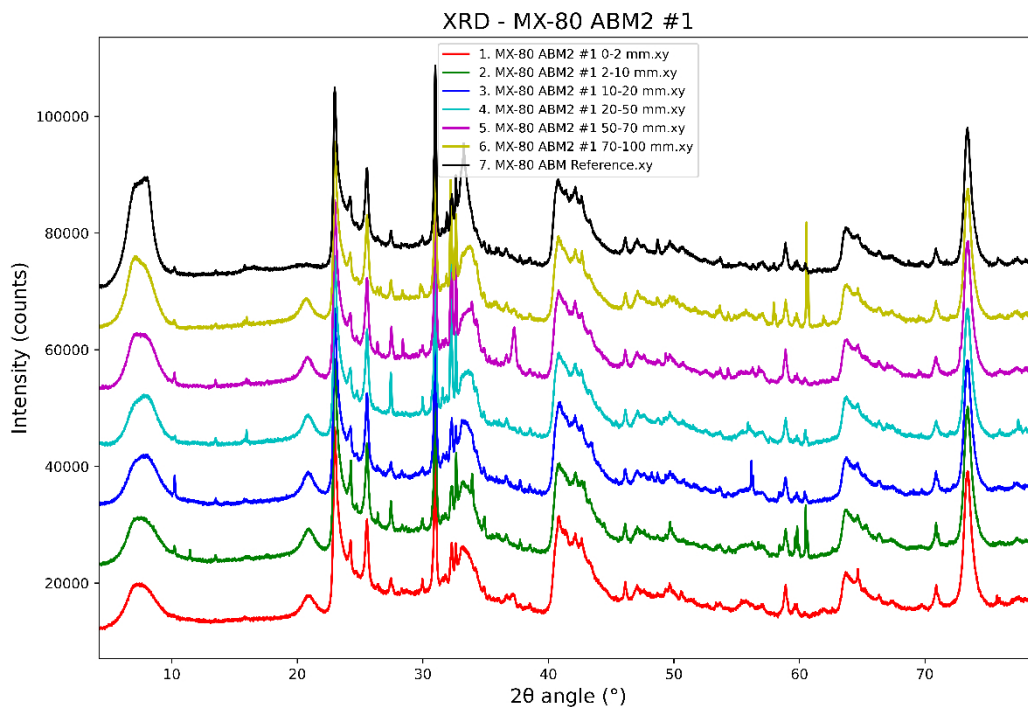


**Figure 6-1.** XRD patterns of the ABM2 MX-80 block 1. Co K $\alpha$  radiation.

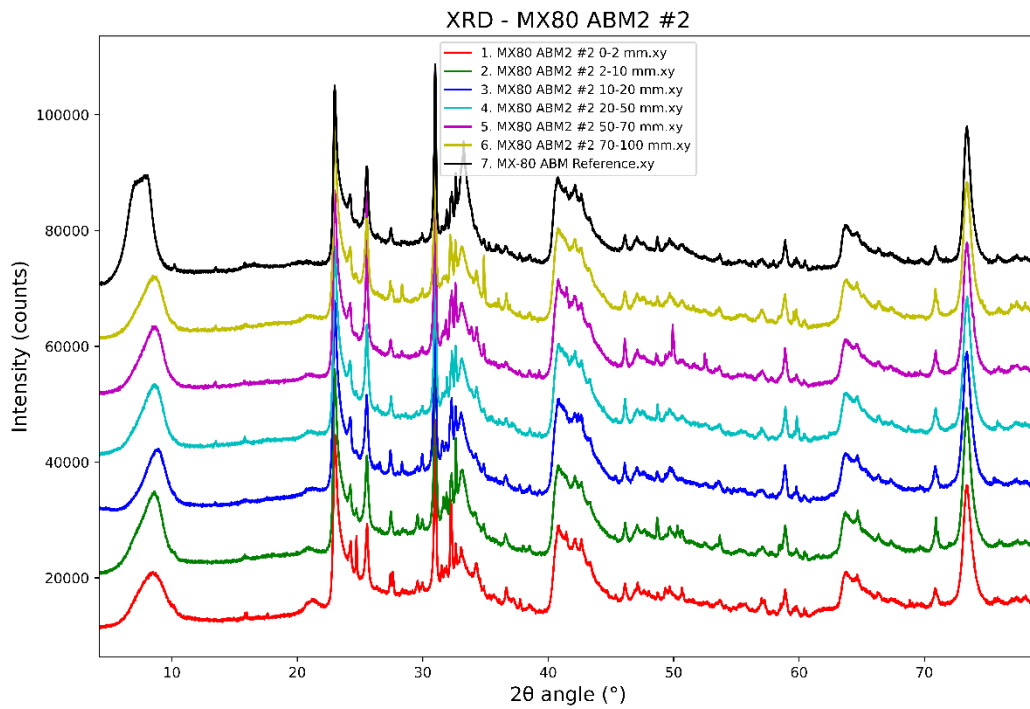


**Figure 6-2.** XRD patterns of the ABM2 MX-80 block 2. Co K $\alpha$  raditation.

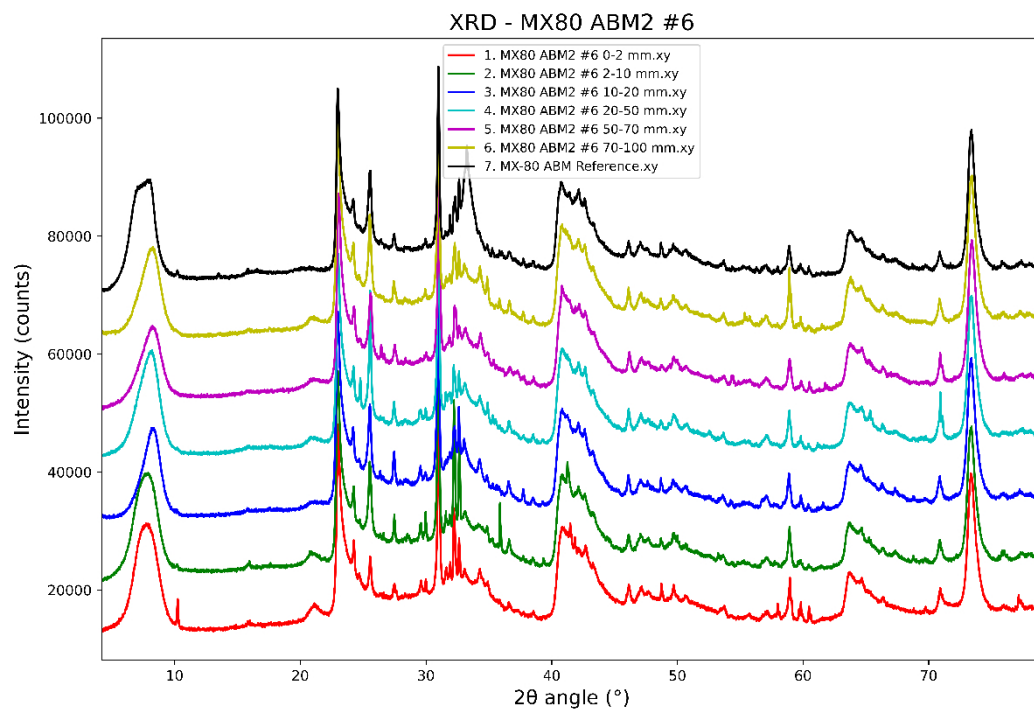


**Figure 6-3.** XRD patterns of the ABM2 MX-80 block 6. Co K $\alpha$  raditation.

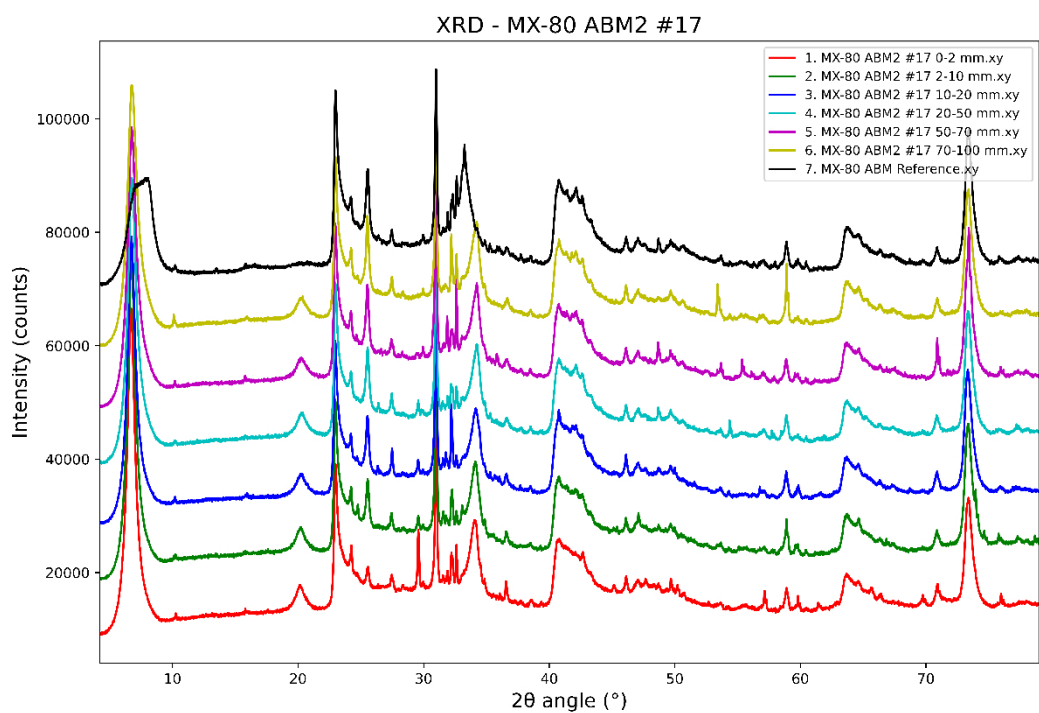


Figure 6-4. XRD patterns of the ABM2 MX-80 block 17. Co K $\alpha$  raditation.

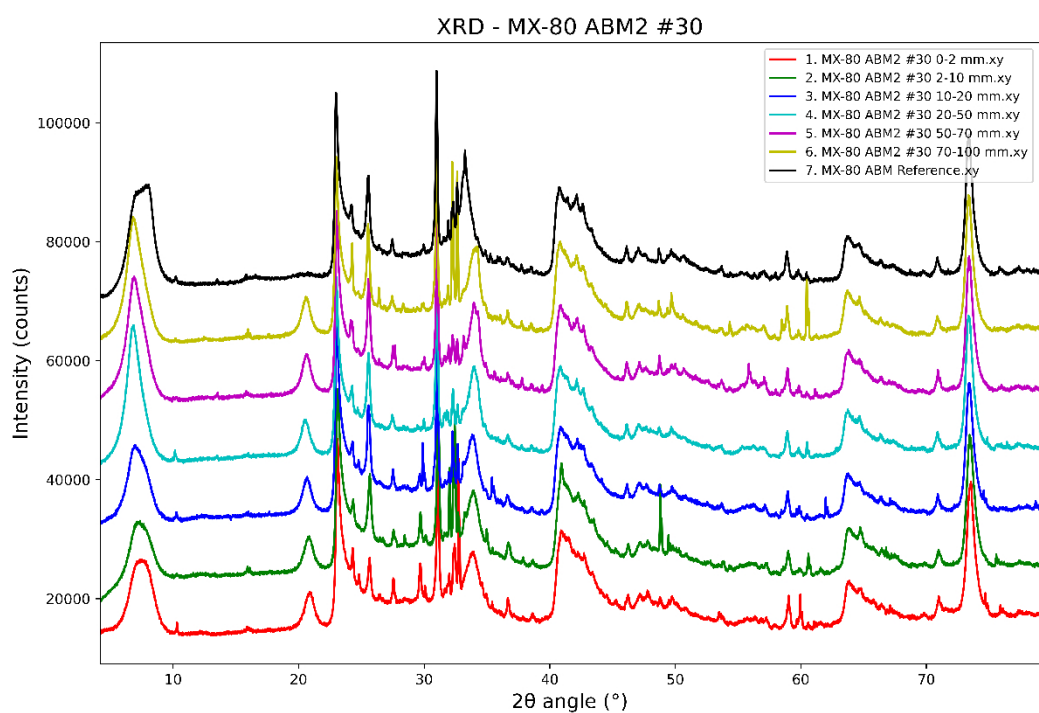
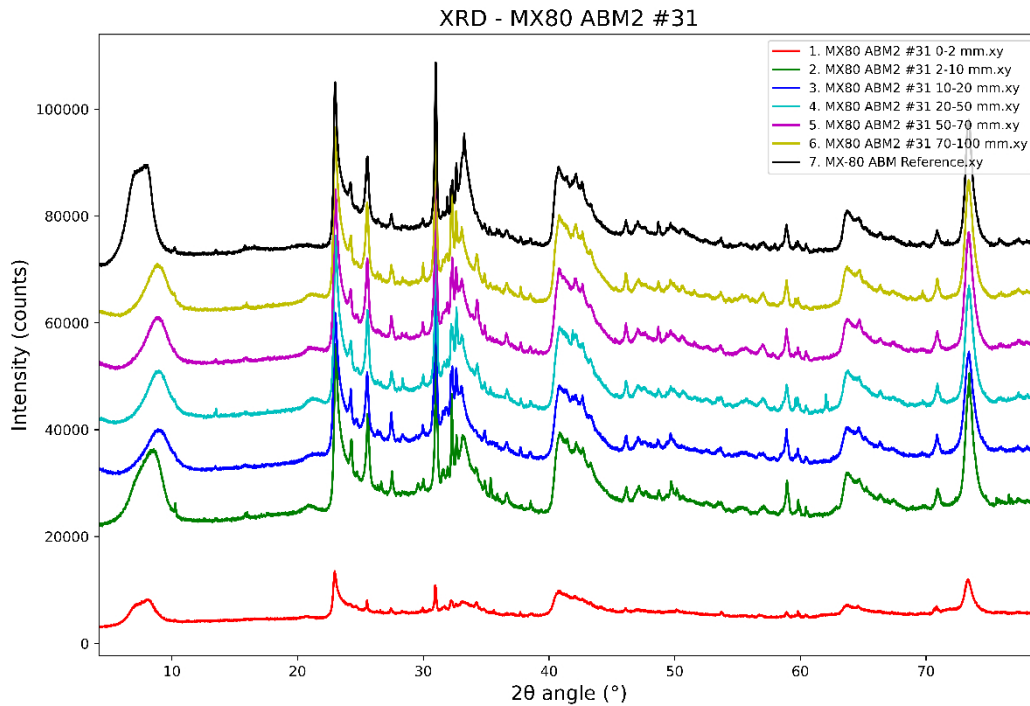


Figure 6-5. XRD patterns of the ABM2 MX-80 block 30. Co K $\alpha$  raditation.



**Figure 6-6.** XRD patterns of the ABM2 MX-80 block 31. Co K $\alpha$  raditation.

Chemical data of the ABM2 MX-80 samples is presented in Table 6-2 for bulk samples and Table 6-3 for clay fractions. There was no notable general trend observed for Mg. Fe typically increased in the samples closest to the heater due to corrosion. Ca and Cl generally increased, while Na decreased due to interactions with the Äspö water. The chloride content is higher in the two top blocks (#1 and #2) than in the MX-80 blocks further down, which could indicate that there has been more interaction with the groundwater in the top of the package. The Ca increase and the Na decrease is higher in the lower blocks, which may be caused by exchange with the neighbouring blocks. The clay fractions exhibited slightly higher Mg content in samples closer to the heater compared to those closer to the rock.

**Table 6-2. ABM2 MX-80 Chemical composition (XRF).**

Sample	MgO	Al <sub>2</sub> O <sub>3</sub>	SiO <sub>2</sub>	SO <sub>3</sub>	K <sub>2</sub> O	CaO	Fe <sub>2</sub> O <sub>3</sub>	Cl	Na <sub>2</sub> O	TiO <sub>2</sub>
MX-80 Reference – I	2.5	21.6	66.5	1.3	0.5	1.7	4.2	0.0	1.5	0.2
MX-80 Reference – II	2.5	21.6	66.8	1.0	0.5	1.6	4.2	0.0	1.6	0.2
MX-80 Reference – III	2.5	21.6	66.7	0.8	0.6	1.6	4.2	0.0	1.7	0.2
MX-80 Reference – IV	2.5	21.6	66.6	0.8	0.6	1.6	4.4	0.0	1.7	0.2
MX-80 Reference – V	2.6	21.6	66.9	0.8	0.6	1.4	4.4	0.0	1.7	0.2
MX-80 ABM2 #1 0–2 mm	2.4	21.2	65.5	0.4	0.6	2.3	5.9	0.4	1.2	0.2
MX-80 ABM2 #1 2–10 mm	2.4	21.3	66.2	0.6	0.6	2.4	4.7	0.4	1.3	0.2
MX-80 ABM2 #1 10–20 mm	2.4	21.2	66.1	0.6	0.6	2.5	4.7	0.4	1.2	0.2
MX-80 ABM2 #1 20–50 mm	2.4	21.4	66.5	0.6	0.6	2.5	4.3	0.4	1.1	0.2
MX-80 ABM2 #1 50–70 mm	2.4	21.3	66.4	0.6	0.6	2.6	4.3	0.4	1.2	0.2
MX-80 ABM2 #1 70–100 mm	2.4	21.3	66.6	0.5	0.5	2.6	4.3	0.5	1.2	0.2
MX-80 ABM2 #2 0–2 mm	2.5	21.1	64.8	0.6	0.5	2.9	6.1	0.3	1.1	0.2
MX-80 ABM2 #2 2–10 mm	2.4	21.1	66.1	0.7	0.6	2.3	5.0	0.4	1.2	0.2
MX-80 ABM2 #2 10–20 mm	2.4	21.6	66.6	0.5	0.5	2.1	4.7	0.3	1.1	0.2
MX-80 ABM2 #2 20–50 mm	2.4	21.7	66.7	0.5	0.5	2.4	4.2	0.4	1.1	0.2
MX-80 ABM2 #2 50–70 mm	2.4	21.6	66.5	0.6	0.5	2.6	4.3	0.4	1.1	0.2
MX-80 ABM2 #2 70–100 mm	2.4	21.6	66.6	0.4	0.5	2.5	4.3	0.4	1.1	0.2

**Table 6-2. Continued.**

Sample	MgO	Al <sub>2</sub> O <sub>3</sub>	SiO <sub>2</sub>	SO <sub>3</sub>	K <sub>2</sub> O	CaO	Fe <sub>2</sub> O <sub>3</sub>	Cl	Na <sub>2</sub> O	TiO <sub>2</sub>
MX-80 ABM2 #6 0–2 mm	3.3	21.2	64.8	0.7	0.4	3.2	5.6	0.2	0.5	0.2
MX-80 ABM2 #6 2–10 mm	2.4	21.5	66.3	0.7	0.4	3.1	4.6	0.3	0.6	0.2
MX-80 ABM2 #6 10–20 mm	2.3	21.8	66.7	0.6	0.5	3.0	4.3	0.2	0.5	0.2
MX-80 ABM2 #6 20–50 mm	2.3	22.0	66.8	0.4	0.4	2.9	4.2	0.2	0.5	0.2
MX-80 ABM2 #6 50–70 mm	2.3	21.9	66.8	0.3	0.5	3.0	4.3	0.2	0.5	0.2
MX-80 ABM2 #6 70–100 mm	2.3	21.8	67.0	0.4	0.5	2.9	4.3	0.3	0.6	0.2
MX-80 ABM2 #30 0–2 mm -1	2.4	20.3	62.2	1.6	0.5	3.5	8.7	0.1	0.6	0.2
MX-80 ABM2 #30 0–2 mm -2	2.4	19.8	62.1	1.5	0.5	3.6	8.9	0.1	0.6	0.2
MX-80 ABM2 #30 2–10 mm -1	2.1	21.2	65.6	1.2	0.5	3.4	5.1	0.2	0.6	0.2
MX-80 ABM2 #30 2–10 mm -2	2.1	20.6	65.3	1.3	0.6	3.5	5.4	0.1	0.7	0.2
MX-80 ABM2 #30 10–20 mm -1	2.2	20.9	66.0	0.7	0.5	3.1	5.4	0.2	0.6	0.2
MX-80 ABM2 #30 10–20 mm -2	2.2	20.7	66.2	0.7	0.5	3.2	5.4	0.2	0.6	0.2
MX-80 ABM2 #30 20–50 mm -1	2.2	20.9	66.4	0.6	0.5	3.1	4.9	0.2	0.7	0.2
MX-80 ABM2 #30 20–50 mm -2	2.2	20.8	66.4	0.6	0.5	3.2	5.0	0.2	0.7	0.2
MX-80 ABM2 #30 50–70 mm -1	2.2	20.9	66.6	0.5	0.5	3.4	4.6	0.2	0.6	0.2
MX-80 ABM2 #30 50–70 mm -2	2.2	20.9	66.5	0.7	0.5	3.3	4.6	0.2	0.6	0.2
MX-80 ABM2 #30 70–100 mm -1	2.2	21.0	66.8	0.3	0.5	3.3	4.7	0.3	0.6	0.2
MX-80 ABM2 #30 70–100 mm -2	2.2	20.9	66.8	0.3	0.5	3.2	4.8	0.2	0.7	0.2
MX-80 ABM2 #31 0–2 mm -1	2.2	21.1	64.6	0.6	0.6	2.9	6.8	0.2	1.0	0.2
MX-80 ABM2 #31 0–2 mm -2	2.1	21.0	64.4	0.9	0.7	2.8	6.7	0.2	1.0	0.2
MX-80 ABM2 #31 2–10 mm -1	2.1	21.3	66.1	0.6	0.6	2.5	5.3	0.2	1.1	0.2
MX-80 ABM2 #31 2–10 mm -2	2.1	21.3	66.2	0.6	0.6	2.5	5.2	0.2	1.1	0.2
MX-80 ABM2 #31 10–20 mm -1	2.1	21.7	66.4	0.5	0.6	2.3	5.0	0.2	1.1	0.2
MX-80 ABM2 #31 10–20 mm -2	2.1	21.7	66.4	0.5	0.6	2.3	5.0	0.2	1.0	0.2
MX-80 ABM2 #31 20–50 mm -1	2.2	21.6	66.6	0.6	0.6	2.7	4.4	0.2	1.0	0.2
MX-80 ABM2 #31 20–50 mm -2	2.2	21.6	66.5	0.6	0.6	2.7	4.5	0.2	1.0	0.2
MX-80 ABM2 #31 50–70 mm -1	2.2	21.7	66.7	0.5	0.6	2.7	4.2	0.2	1.0	0.2
MX-80 ABM2 #31 50–70 mm -2	2.2	21.7	66.6	0.5	0.6	2.7	4.3	0.2	1.0	0.2
MX-80 ABM2 #31 70–100 mm -1	2.2	21.7	66.9	0.3	0.6	2.6	4.3	0.3	1.0	0.2
MX-80 ABM2 #31 70–100 mm -2	2.2	21.7	66.9	0.3	0.6	2.6	4.3	0.3	1.0	0.2

**Table 6-3. ABM2 MX-80 Clay fraction (< 0.2 μm) Chemical composition (XRF).**

Sample	MgO	Al <sub>2</sub> O <sub>3</sub>	SiO <sub>2</sub>	SO <sub>3</sub>	K <sub>2</sub> O	CaO	Fe <sub>2</sub> O <sub>3</sub>	Cl	Na <sub>2</sub> O	TiO <sub>2</sub>
MX-80 ABM2 #30 CF 0–2 mm d5ee5b-1	2.5	22.2	65.2	0.0	0.1	0.1	7.2	0.0	2.6	0.1
MX-80 ABM2 #30 CF 0–2 mm d5ee5b-2	2.4	22.1	65.0	0.0	0.1	0.1	7.7	0.0	2.4	0.2
MX-80 ABM2 #30 CF 2–10 mm d5ee5d-1	2.3	22.5	66.4	0.1	0.1	0.1	5.6	0.0	2.8	0.2
MX-80 ABM2 #30 CF 2–10 mm d5ee5d-2	2.3	22.5	66.4	0.1	0.1	0.1	5.5	0.0	2.8	0.2
MX-80 ABM2 #30 CF 10–20 mm d5ee5f-1	2.3	22.6	66.6	0.1	0.1	0.1	5.3	0.0	2.8	0.2
MX-80 ABM2 #30 CF 10–20 mm d5ee5f-2	2.3	22.6	66.6	0.1	0.1	0.1	5.3	0.0	2.8	0.2
MX-80 ABM2 #30 CF 20–50 mm d5ee61-1	2.3	23.0	66.8	0.0	0.1	0.2	4.7	0.0	2.8	0.2
MX-80 ABM2 #30 CF 20–50 mm d5ee61-2	2.3	23.0	66.7	0.0	0.1	0.2	4.7	0.0	2.8	0.2
MX-80 ABM2 #30 CF 50–70 mm d5ee63-1	2.3	23.0	67.0	0.0	0.1	0.2	4.5	0.0	2.7	0.2
MX-80 ABM2 #30 CF 50–70 mm d5ee63-2	2.3	23.0	67.0	0.0	0.1	0.2	4.5	0.0	2.7	0.2
MX-80 ABM2 #30 CF 70–100 mm d5ee65-1	2.3	23.1	67.0	0.0	0.1	0.2	4.6	0.0	2.6	0.2
MX-80 ABM2 #30 CF 70–100 mm d5ee65-2	2.3	23.0	66.9	0.0	0.1	0.2	4.8	0.0	2.6	0.2

### 6.1.2 Calcigel

The Calcigel samples in ABM2 typically exhibited a dark reaction zone towards the iron heater (Figure 6-7). In the XRD data of the Calcigel samples (Figure 6-7 to Figure 6-8), an illite/mica reflection at around 10 Å (approximately 10 degrees two theta) was consistently observed with similar intensity. No correlation was found between the intensity of this reflection and the sample's position relative to the heater. The 060 reflection at around 75 degrees two theta did not show any changes when comparing the ABM2 samples with the reference data. No other reflections indicating the formation of new clay minerals were detected in the low-angle region. In summary, the XRD analysis of the Calcigel samples did not reveal any significant qualitative changes in the clay minerals present.



*Figure 6-7. ABM2 Calcigel block 3. Showing a dark reaction zone towards the contact with the iron heater.*

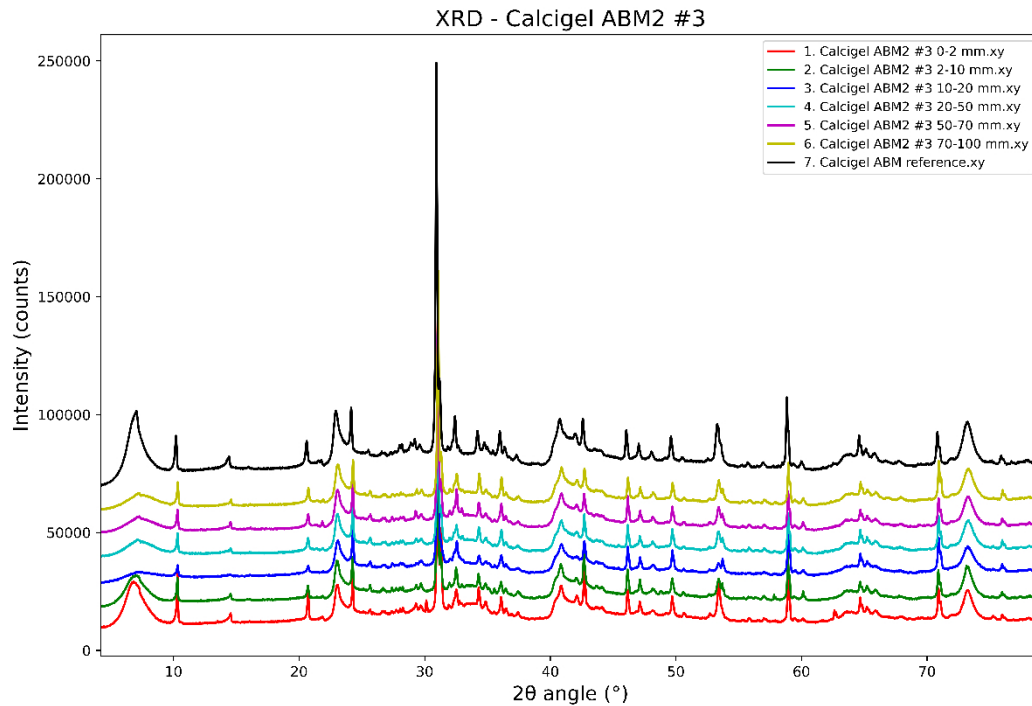


*Figure 6-8. XRD patterns of the Calcigel block #3 profile of samples. Co Kα radiation.*

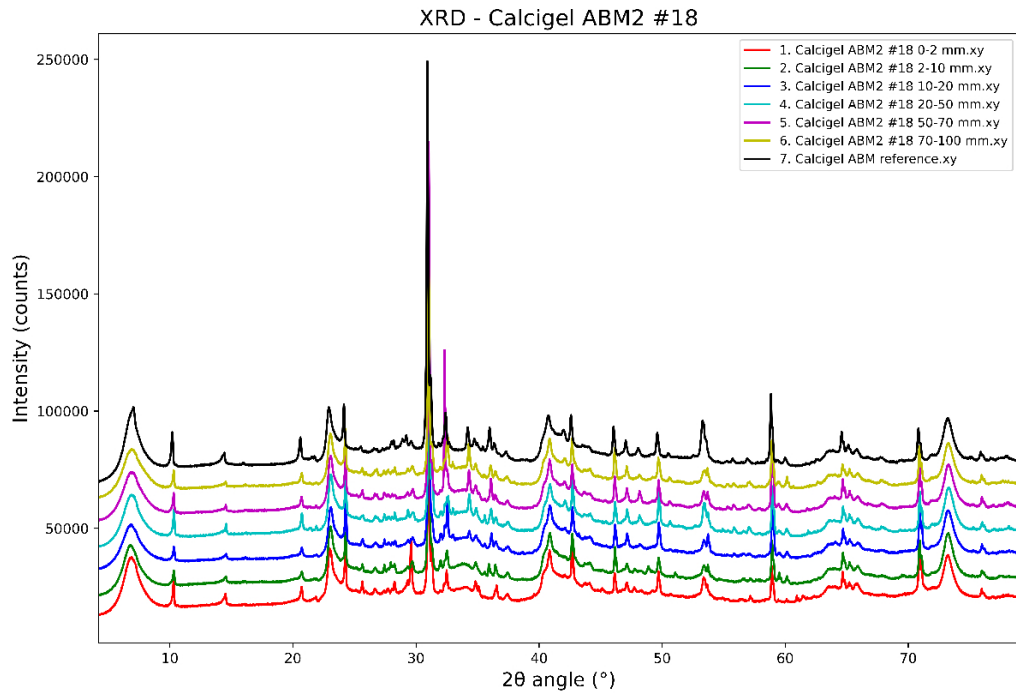


**Figure 6-9.** XRD patterns of the Calcigel block #18 profile of samples. Co K $\alpha$  radiation.

Chemical data for the ABM2 Calcigel samples can be found in Table 6-4. There was a minor redistribution of Mg, with a slight accumulation towards the heater. Fe content typically increased in the samples closest to the heater due to corrosion. Cl generally increased, while Ca and Na showed little change. Sulfate is strongly enriched towards the heater in block #18, but not in block #3.

**Table 6-4. ABM2 Calcigel Chemical composition (XRF).**

Sample	MgO	Al <sub>2</sub> O <sub>3</sub>	SiO <sub>2</sub>	P <sub>2</sub> O <sub>5</sub>	SO <sub>3</sub>	K <sub>2</sub> O	CaO	MnO	Fe <sub>2</sub> O <sub>3</sub>	Cl	Na <sub>2</sub> O	TiO <sub>2</sub>
Calcigel ABM2 #3 0–2 mm	3.62	21.47	60.01	0.01	0.11	1.93	3.36	0.04	7.58	0.42	0.96	0.49
Calcigel ABM2#3 0–2 mm	3.50	21.18	59.13	0.01	0.10	1.63	4.10	0.04	8.78	0.35	0.78	0.40
Calcigel ABM2 #3 2–10 mm	3.69	20.89	60.83	0.00	0.06	1.86	3.39	0.04	7.05	0.47	0.98	0.48
Calcigel ABM2 #3 2–10 mm	3.57	20.76	59.97	0.00	0.05	1.61	3.95	0.04	8.12	0.39	0.89	0.43
Calcigel ABM2 #3 10–20 mm	3.47	20.29	62.41	0.00	0.01	1.77	3.14	0.04	6.59	0.36	0.95	0.52
Calcigel ABM2 #3 10–20 mm	3.33	19.97	61.89	0.00	0.02	1.49	3.76	0.03	7.57	0.31	0.79	0.45
Calcigel ABM2 #3 20–50 mm	3.53	20.32	62.21	0.00	0.01	1.77	3.28	0.03	6.65	0.41	0.98	0.49
Calcigel ABM2 #3 20–50 mm	3.38	20.03	61.48	0.00	0.00	1.54	3.96	0.03	7.72	0.34	0.81	0.43
Calcigel ABM2 #3 50–70 mm	3.36	19.98	61.13	0.00	0.02	1.53	4.17	0.03	7.87	0.40	0.83	0.41
Calcigel ABM2 #3 50–70 mm	3.47	20.61	61.64	0.00	0.00	1.81	3.44	0.04	6.75	0.48	0.96	0.49
Calcigel ABM2 #3 70–100 mm	3.35	20.00	60.89	0.02	0.03	1.50	4.39	0.03	7.80	0.44	0.81	0.42
Calcigel ABM2 #3 70–100 mm	3.42	20.56	61.36	0.00	0.04	1.80	3.60	0.04	6.78	0.54	0.98	0.52
Calcigel ABM2 #18 0–2 mm	3.17	19.39	56.04	0.01	1.35	1.57	3.19	0.05	13.43	0.68	0.69	0.44
Calcige ABM2l #18 0–2 mm	3.17	19.69	55.90	0.01	1.08	1.64	3.08	0.05	13.57	0.69	0.68	0.45
Calcigel ABM2 #18 2–10 mm	3.19	21.15	59.47	0.02	0.52	1.73	3.12	0.04	8.61	0.96	0.73	0.47
Calcigel ABM2 #18 2–10 mm	3.19	21.35	59.25	0.01	0.51	1.81	3.09	0.04	8.63	0.94	0.72	0.45
Calcigel ABM2 #18 10–20 mm	3.31	20.90	61.20	0.03	0.04	1.69	3.24	0.04	7.37	0.96	0.75	0.48
Calcigel ABM2 #18 10–20 mm	3.31	20.94	61.35	0.03	0.05	1.66	3.17	0.04	7.27	0.95	0.74	0.49
Calcigel ABM2 #18 20–50 mm	3.40	21.56	60.45	0.02	0.02	1.69	4.07	0.04	6.50	1.06	0.72	0.50
Calcigel ABM2 #18 20–50 mm	3.42	21.55	60.63	0.01	0.02	1.72	3.97	0.04	6.40	1.07	0.70	0.48
Calcigel ABM2 #18 50–70 mm	3.38	21.39	60.80	0.02	0.01	1.70	3.99	0.04	6.38	1.06	0.74	0.50
Calcigel ABM2 #18 50–70 mm	3.38	21.38	60.83	0.02	0.01	1.68	4.02	0.04	6.31	1.10	0.73	0.50
Calcigel ABM2 #18 70–100 mm	3.31	21.29	60.46	0.02	0.02	1.67	4.05	0.04	6.64	1.29	0.74	0.48
Calcigel ABM2 #18 70–100 mm	3.30	21.34	60.53	0.01	0.01	1.67	4.01	0.04	6.61	1.24	0.77	0.48
Calcigel ABM reference c65d56	3.5	20.9	61.4	0.10	0.4	1.8	4.1	0.5	7.5	0.1	0.9	0.5

### 6.1.3 Deponit CA-N

DepCAN (Deponit CA-N) samples typically showed a dark reaction zone towards the iron heater and white precipitation bands (Figure 6-10). In the XRD data of the DepCAN samples (Figure 6-11 to Figure 6-12) no change could be seen in the low angle region or in the area of the 060 reflection around 75 degrees two theta. XRD of the samples did not show any significant qualitative changes of the clay minerals present. There is an observation of a 10 Å reflection in one instance, that most likely is associated with a mica mineral present in the bentonite.

Chemical data of the ABM2 DepCAN samples is seen in Table 6-5. Mg showed a clear redistribution with minor accumulation towards the heater. Fe did not change significantly. Cl and Ca generally increased, Na decreased somewhat.



**Figure 6-10.** ABM2 DepCAN. Some of the blocks showed centro-symmetrical white precipitates with a fairly constant distance to the iron heater.

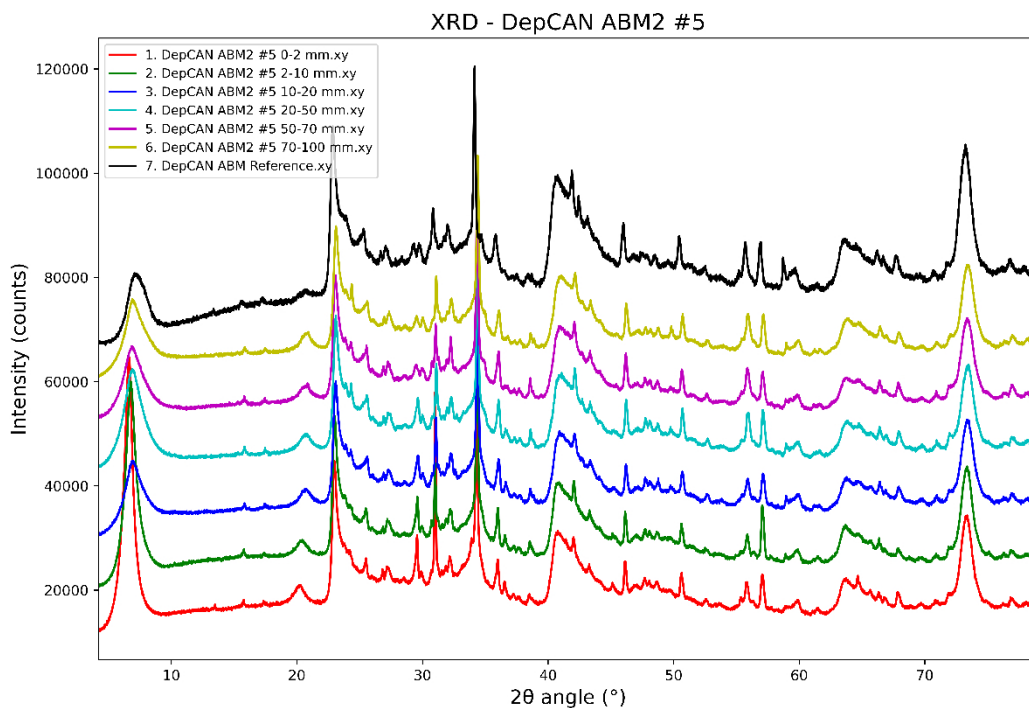


**Figure 6-11.** XRD patterns of the DepCAN block #5 profile of samples. Co K $\alpha$  radiation.

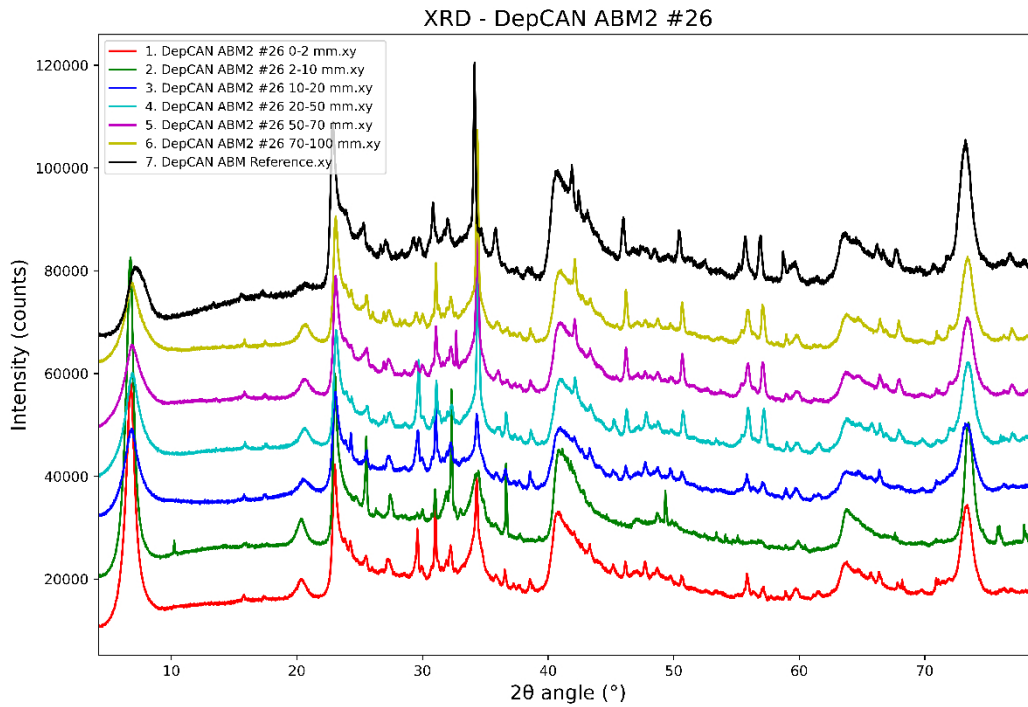


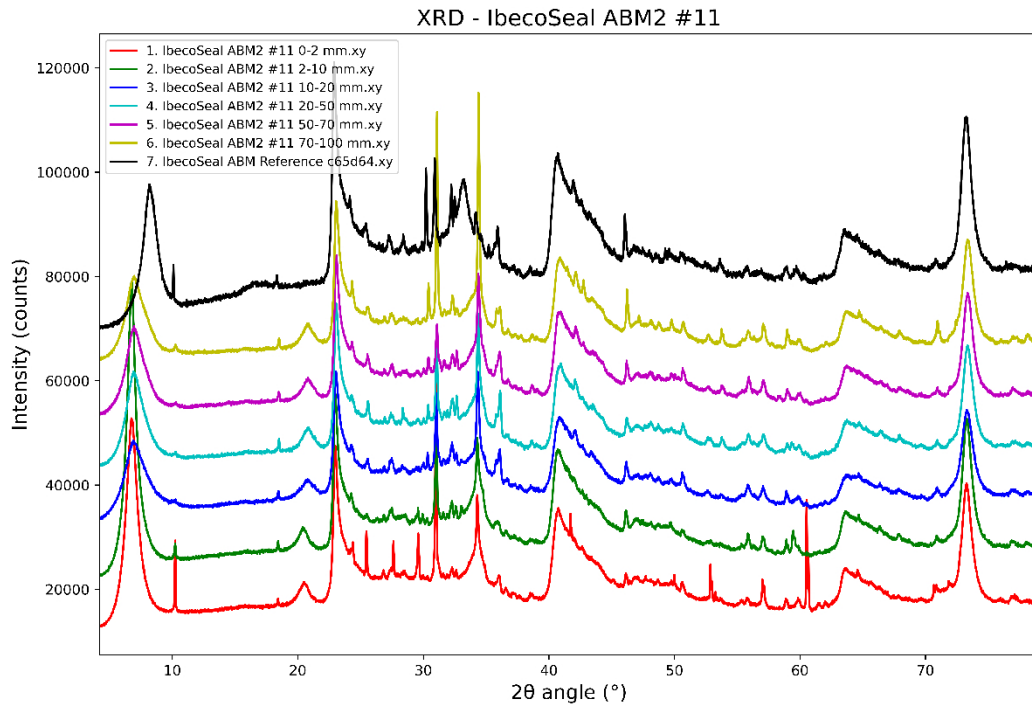
Figure 6-12. XRD patterns of the DepCAN block #26 profile of samples. Co K $\alpha$  raditation.

Table 6-5. DepCAN ABM2 Chemical composition (XRF).

Sample	MgO	Al <sub>2</sub> O <sub>3</sub>	SiO <sub>2</sub>	P <sub>2</sub> O <sub>5</sub>	SO <sub>3</sub>	K <sub>2</sub> O	CaO	MnO	Fe <sub>2</sub> O <sub>3</sub>	Cl	Na <sub>2</sub> O	TiO <sub>2</sub>
Deponit CAN ABM2 #5 0–2 mm	3.47	20.1	58.5	0.23	1.54	0.95	7.57	0.00	6.04	0.26	0.52	0.92
Deponit CAN ABM2 #5 0–2 mm	3.46	20.2	58.7	0.20	1.52	0.96	7.37	0.00	6.03	0.25	0.45	0.91
Deponit CAN ABM2 #5 2–10 mm	3.03	20.5	59.8	0.33	1.26	0.99	6.63	0.77	5.87	0.29	0.57	0.93
Deponit CAN ABM2 #5 2–10 mm	3.04	20.5	59.9	0.32	1.25	1.00	6.55	0.89	5.85	0.29	0.52	0.94
Deponit CAN ABM2 #5 10–20 mm	2.98	20.3	59.8	0.30	1.44	1.06	6.87	0.80	5.80	0.23	0.48	0.95
Deponit CAN ABM2 #5 10–20 mm	2.98	20.3	60.0	0.32	1.45	1.03	6.82	0.81	5.70	0.23	0.46	0.95
Deponit CAN ABM2 #5 20–50 mm	2.91	20.4	60.1	0.25	1.26	1.10	6.80	0.78	5.68	0.24	0.47	0.95
Deponit CAN ABM2 #5 20–50 mm	2.91	20.4	60.1	0.27	1.26	1.09	6.81	0.80	5.68	0.23	0.47	0.96
Deponit CAN ABM2 #5 50–70 mm	2.86	20.4	60.1	0.30	0.96	1.14	6.90	0.87	5.82	0.28	0.48	0.97
Deponit CAN ABM2 #5 50–70 mm	2.86	20.3	60.2	0.31	0.98	1.15	6.85	0.87	5.79	0.27	0.47	0.96
Deponit CAN ABM2 #5 70–100 mm	2.77	20.3	59.9	0.34	1.01	1.15	7.05	0.82	5.86	0.32	0.52	0.97
Deponit CAN ABM2 #5 70–100 mm	2.56	20.2	59.0	0.20	0.75	1.08	7.98	0.71	6.27	0.28	0.49	0.93
DepCAN ABM reference c65d52	3.1	20.3	59.5	0.37	1.3	1.3	6.2	0.9	6.3	0.1	0.6	1.1

#### 6.1.4 IbecoSeal

In the XR-D data of the IbecoSeal samples (Figure 6-13 to Figure 6-14) a illite/mica reflection sometimes could be seen at around 10 deg two theta, however with no trend correlating to the position of the sample in relation to the heater (very similar to what was seen in the ABM2 MX-80 samples). No other significant change could be seen in the low angle region or in the area of the 060 reflection around 75 degrees two theta. XRD of the samples did not show any significant qualitative changes of the clay minerals present. The basal spacing (001 reflection) moved towards lower angles (higher spacings) in the samples from the ABM2 experiment, which is correlating with the higher Ca-content of the samples (Ca-montmorillonite hydrates more easily than Na-montmorillonite at ambient relative humidity).



**Figure 6-13.** XRD patterns of the IbecoSeal block #11 profile of samples. Co K $\alpha$  raditation.

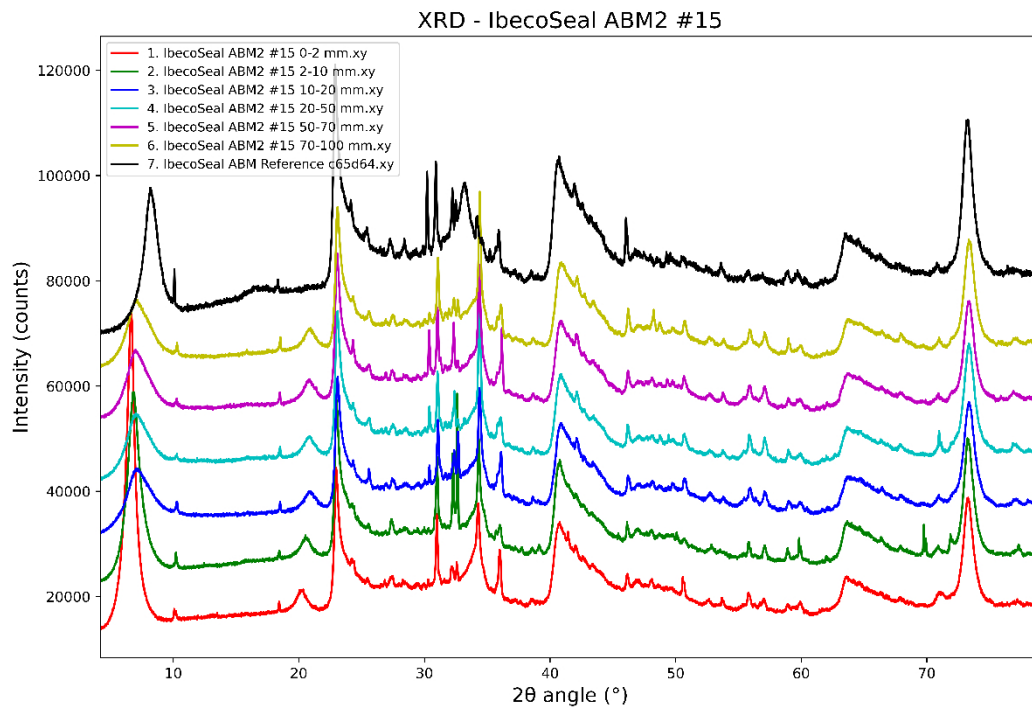


**Figure 6-14.** XRD patterns of the IbecoSeal block #15 profile of samples. Co K $\alpha$  raditation.

Chemical data of the ABM2 IbecoSeal samples is seen in Table 6-6. Mg showed a clear redistribution with minor accumulation towards the heater. Fe typically increased in the samples closest to the heater, due to the corrosion. Cl and Ca generally increased, Na decreased significantly.

**Table 6-6. IbecoSeal ABM2 Chemical composition (XRF).**

Sample	MgO	Al <sub>2</sub> O <sub>3</sub>	SiO <sub>2</sub>	P <sub>2</sub> O <sub>5</sub>	SO <sub>3</sub>	K <sub>2</sub> O	CaO	MnO	Fe <sub>2</sub> O <sub>3</sub>	Cl	Na <sub>2</sub> O	TiO <sub>2</sub>
IbecoSeal ABM reference	4.19	19.67	61.47	0.00	0.83	1.67	4.25	0.08	4.91	0.06	2.39	0.48
IbecoSeal ABM reference	4.08	19.92	62.44	0.04	0.79	1.48	3.26	0.06	4.82	0.03	2.56	0.53
IbecoSeal ABM2 #11 0–2 mm	5.36	19.04	60.79	0.00	0.80	1.28	5.16	0.09	6.25	0.25	0.40	0.57
IbecoSeal ABM2 #11 0–2 mm	5.38	19.95	60.23	0.01	0.83	1.32	4.84	0.09	6.20	0.17	0.39	0.54
IbecoSeal ABM2 #11 0–2 mm	5.27	19.79	60.13	0.02	0.78	1.33	5.11	0.10	6.34	0.16	0.40	0.58
IbecoSeal ABM2 #11 2–10 mm	4.68	19.77	62.10	0.00	0.46	1.43	4.78	0.09	5.25	0.30	0.61	0.54
IbecoSeal ABM2 #11 2–10 mm	4.62	20.57	61.52	0.02	0.51	1.39	4.66	0.08	5.47	0.19	0.43	0.54
IbecoSeal ABM2 #11 2–10 mm	4.57	20.58	61.44	0.02	0.43	1.47	4.79	0.10	5.40	0.17	0.48	0.55
IbecoSeal ABM2 #11 10–20 mm	4.54	19.63	61.80	0.00	0.29	1.46	5.67	0.10	5.03	0.19	0.44	0.49
IbecoSeal ABM2 #11 10–20 mm	4.34	20.45	61.75	0.03	0.28	1.41	5.57	0.11	4.96	0.17	0.40	0.53
IbecoSeal ABM2 #11 10–20 mm	4.35	20.44	61.80	0.03	0.28	1.42	5.54	0.11	4.93	0.17	0.40	0.53
IbecoSeal ABM2 #11 20–50 mm	4.26	19.59	61.61	0.00	0.37	1.44	6.15	0.10	4.99	0.18	0.49	0.50
IbecoSeal ABM2 #11 20–50 mm	4.02	20.32	61.44	0.01	0.34	1.45	6.06	0.11	5.08	0.18	0.44	0.54
IbecoSeal ABM2 #11 20–50 mm	4.04	20.36	61.49	0.02	0.34	1.43	6.02	0.11	5.03	0.17	0.46	0.54
IbecoSeal ABM2 #11 50–70 mm	4.09	19.49	61.79	0.00	0.32	1.45	6.23	0.10	5.03	0.19	0.49	0.50
IbecoSeal ABM2 #11 50–70 mm	3.92	20.37	61.58	0.02	0.31	1.43	6.14	0.11	4.99	0.18	0.42	0.53
IbecoSeal ABM2 #11 50–70 mm	3.93	20.44	61.55	0.02	0.31	1.41	6.10	0.11	4.99	0.18	0.43	0.53
IbecoSeal ABM2 #11 70–100 mm	4.07	19.40	62.31	0.00	0.24	1.41	6.03	0.09	4.89	0.21	0.51	0.49
IbecoSeal ABM2 #11 70–100 mm	3.90	20.35	62.12	0.02	0.23	1.37	5.92	0.10	4.81	0.21	0.45	0.52
IbecoSeal ABM2 #11 70–100 mm	3.92	20.35	62.18	0.02	0.21	1.41	5.86	0.10	4.80	0.23	0.43	0.52
IbecoSeal ABM2 #15 0–2 mm	4.33	19.74	60.07	0.02	0.22	1.30	5.27	0.09	7.58	0.37	0.52	0.49
IbecoSeal ABM2 #15 0–2 mm	4.43	19.78	60.13	0.01	0.28	1.29	4.89	0.09	7.72	0.40	0.49	0.50
IbecoSeal ABM2 #15 2–10 mm	4.02	20.56	61.45	0.02	0.22	1.38	4.96	0.08	5.79	0.42	0.60	0.52
IbecoSeal ABM2 #15 2–10 mm	3.95	20.65	61.81	0.02	0.22	1.40	4.74	0.08	5.60	0.46	0.57	0.50
IbecoSeal ABM2 #15 10–20 mm	3.88	20.29	61.30	0.02	0.23	1.41	6.08	0.10	5.19	0.42	0.54	0.53
IbecoSeal ABM2 #15 10–20 mm	3.92	20.41	61.44	0.02	0.23	1.37	5.95	0.10	5.08	0.42	0.55	0.52
IbecoSeal ABM2 #15 20–50 mm	3.85	20.37	61.32	0.02	0.22	1.38	6.36	0.11	4.86	0.43	0.57	0.52
IbecoSeal ABM2 #15 20–50 mm	3.85	20.34	61.23	0.01	0.23	1.39	6.38	0.11	4.94	0.45	0.55	0.54
IbecoSeal ABM2 #15 50–70 mm	3.82	20.34	61.32	0.02	0.22	1.39	6.39	0.11	4.84	0.45	0.58	0.52
IbecoSeal ABM2 #15 50–70 mm	3.81	20.33	61.32	0.01	0.24	1.39	6.42	0.11	4.82	0.45	0.57	0.53
IbecoSeal ABM2 #15 70–100 mm	3.78	20.26	61.17	0.01	0.23	1.37	6.38	0.10	5.09	0.49	0.59	0.52
IbecoSeal ABM2 #15 70–100 mm	3.75	20.24	61.20	0.01	0.23	1.39	6.38	0.10	5.12	0.49	0.57	0.52

### 6.1.5 Ikosorb

In the XRD data of the Ikosorb samples (Figure 6-15 to Figure 6-16) a minor illite/mica reflection sometimes could be seen at around 10 deg two theta, however with no trend correlating to the position of the sample in relation to the heater. No other significant change could be seen in the low angle region. In the innermost sample closest to the heater the 060 region had a somewhat different pattern, possibly indicating the presence of minor trioctahedral clay minerals (that sample is also higher in Mg; Table 6-7).

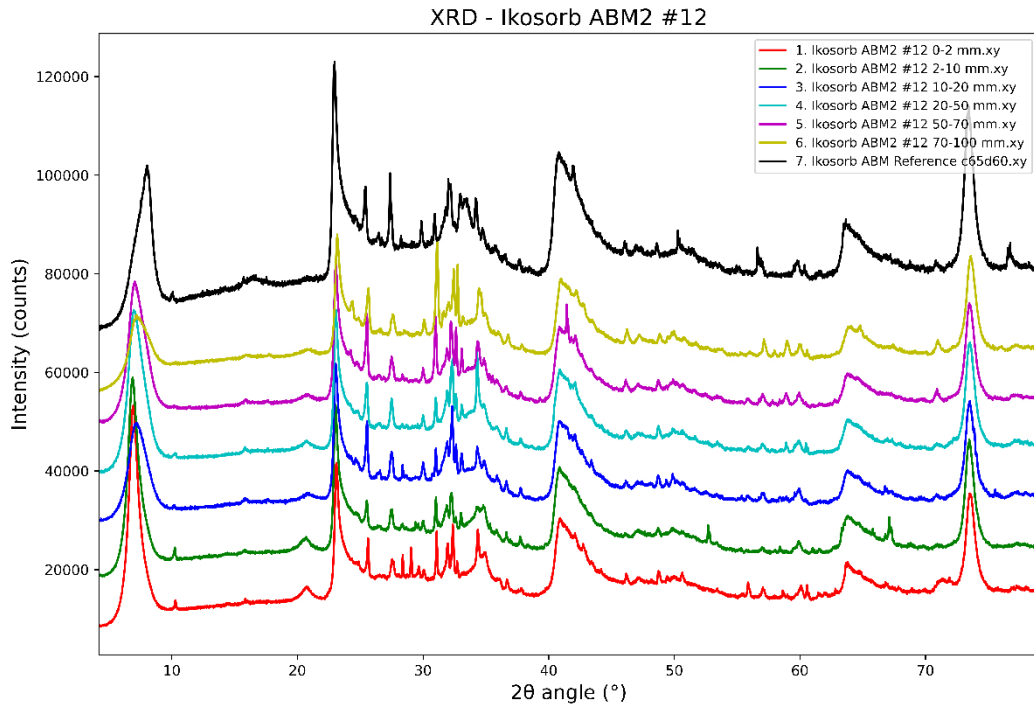


**Figure 6-15.** XRD patterns of the Ikosorb block #12 profile of samples. Co K $\alpha$  raditation.

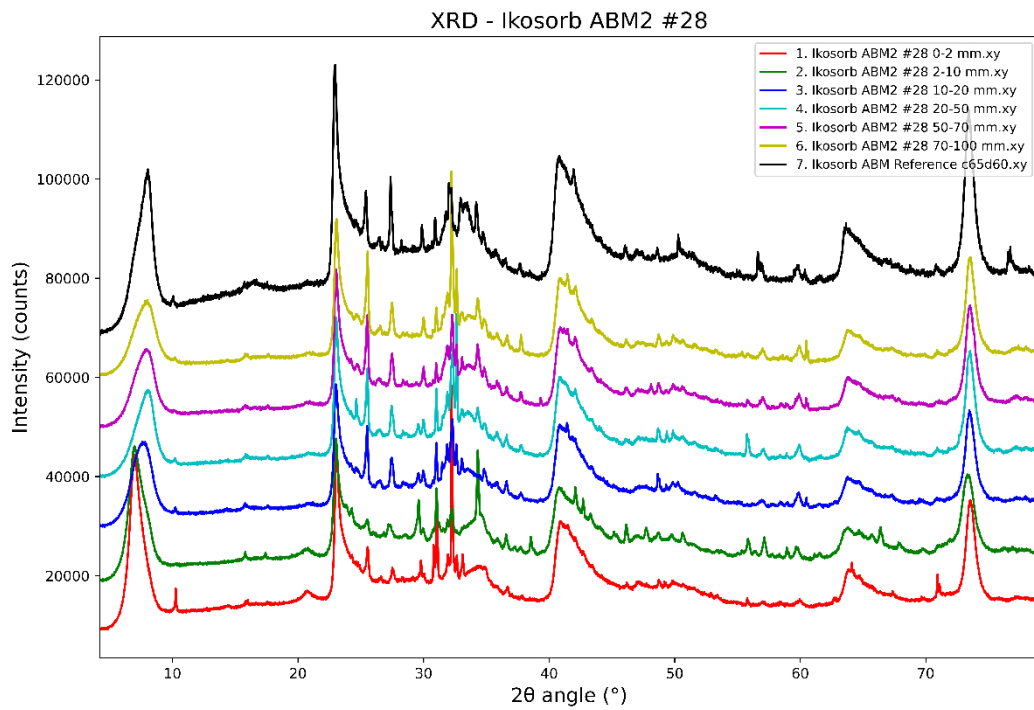


**Figure 6-16.** XRD patterns of the Ikosorb block #28 profile of samples. Co K $\alpha$  raditation.

Chemical data of the ABM2 Ikosorb samples is seen in Table 6-7. Mg showed a clear redistribution with minor accumulation towards the heater. Fe typically increased in the samples closest to the heater, due to the corrosion. Cl and Ca generally increased, Na decreased significantly. There is a strong accumulation of sulfate at 2–10 mm from the heater in block #28, but a general depletion in block #12.

**Table 6-7. Ikosorb ABM2 Chemical composition (XRF).**

Sample	MgO	Al <sub>2</sub> O <sub>3</sub>	SiO <sub>2</sub>	P <sub>2</sub> O <sub>5</sub>	SO <sub>3</sub>	K <sub>2</sub> O	CaO	MnO	Fe <sub>2</sub> O <sub>3</sub>	Cl	Na <sub>2</sub> O	TiO <sub>2</sub>
Ikosorb ABM2 #12 0–2 mm	2.98	24.29	59.27	0.00	0.32	0.84	4.66	0.03	6.49	0.15	0.67	0.32
Ikosorb ABM2 #12 0–2 mm	2.96	24.43	59.48	0.00	0.28	0.86	4.22	0.02	6.62	0.16	0.67	0.30
Ikosorb ABM2 #12 2–10 mm	2.13	25.92	62.06	0.00	0.10	0.96	3.57	0.02	3.96	0.22	0.76	0.32
Ikosorb ABM2 #12 2–10 mm	2.21	26.12	61.79	0.00	0.09	0.92	3.69	0.02	3.84	0.25	0.73	0.35
Ikosorb ABM2 #12 10–20 mm	2.03	26.07	62.42	0.01	0.07	1.11	3.82	0.02	3.21	0.21	0.72	0.33
Ikosorb ABM2 #12 10–20 mm	2.03	26.02	62.31	0.01	0.07	1.10	3.91	0.02	3.26	0.21	0.73	0.33
Ikosorb ABM2 #12 20–50 mm	2.06	26.34	62.19	0.00	0.06	0.98	4.10	0.02	3.03	0.24	0.66	0.32
Ikosorb ABM2 #12 20–50 mm	2.07	26.41	62.19	0.00	0.06	0.95	4.03	0.02	3.02	0.27	0.66	0.31
Ikosorb ABM2 #12 50–70 mm	2.03	25.89	62.70	0.00	0.07	0.99	4.09	0.03	2.95	0.25	0.69	0.32
Ikosorb ABM2 #12 50–70 mm	2.04	25.99	62.63	0.00	0.08	0.95	4.09	0.03	2.94	0.27	0.67	0.32
Ikosorb ABM2 #12 70–100 mm	2.02	25.33	63.14	0.00	0.10	1.03	4.10	0.03	2.96	0.28	0.71	0.32
Ikosorb ABM2 #12 70–100 mm	2.02	25.30	63.24	0.00	0.09	1.03	4.07	0.03	2.94	0.28	0.70	0.31
Ikosorb ABM2 #28 0–2 mm	3.90	25.46	60.18	0.00	0.17	0.70	3.50	0.02	4.77	0.53	0.46	0.31
Ikosorb ABM2 #28 0–2 mm	3.86	25.56	60.26	0.00	0.18	0.66	3.48	0.02	4.67	0.54	0.46	0.30
Ikosorb ABM2 #28 2–10 mm	4.14	20.13	59.20	0.03	1.48	1.02	5.88	0.14	6.06	0.60	0.43	0.90
Ikosorb ABM2 #28 2–10 mm	4.18	20.14	59.20	0.03	1.40	1.04	5.82	0.14	6.09	0.63	0.44	0.90
Ikosorb ABM2 #28 10–20 mm	2.35	25.96	61.74	0.00	0.39	0.99	3.65	0.03	3.51	0.51	0.55	0.34
Ikosorb ABM2 #28 10–20 mm	2.37	25.98	61.68	0.00	0.39	0.99	3.66	0.03	3.52	0.51	0.55	0.34
Ikosorb ABM2 #28 20–50 mm	2.10	25.78	61.71	0.00	0.33	1.07	4.35	0.02	3.10	0.54	0.68	0.32
Ikosorb ABM2 #28 20–50 mm	2.11	25.76	61.64	0.00	0.34	1.12	4.36	0.02	3.15	0.51	0.68	0.32
Ikosorb ABM2 #28 50–70 mm	1.78	25.88	61.81	0.00	0.06	1.12	4.61	0.02	3.02	0.64	0.74	0.33
Ikosorb ABM2 #28 50–70 mm	1.81	25.88	61.72	0.00	0.06	1.14	4.64	0.02	3.07	0.62	0.72	0.33
Ikosorb ABM2 #28 70–100 mm	1.72	25.82	61.89	0.00	0.06	1.16	4.44	0.01	3.11	0.71	0.76	0.32
Ikosorb ABM2 #28 70–100 mm	1.73	25.79	61.88	0.00	0.05	1.15	4.46	0.02	3.10	0.74	0.76	0.32
Ikosorb ABM reference c65d61	2.56	26	61.8	0	0.11	1.3	2.23	0.01	3.2	0.5	2	0.35

### 6.1.6 Kunigel

In the XRD data of the Kunigel samples (Figure 6-17 to Figure 6-18) the most dominant change is the shift in the basal spacing reflections (e.g. 001) towards lower angles due to the ion exchange to more Ca due to the interaction with other bentonites and/or the Äspö groundwater. No other significant change could be seen in the low angle region. In some samples in block #22 a glassy phase was observed (Figure 6-19). This glassy phase was identified as halite (NaCl) using XRD (Figure 6-18). The halite was most likely formed due to enrichment of salt from the groundwater due to local boiling/heavy evaporation. The halite formed a cake with the bentonite in the contact zone with the iron heater, and the rest of the bentonite block was heavily physically affected.

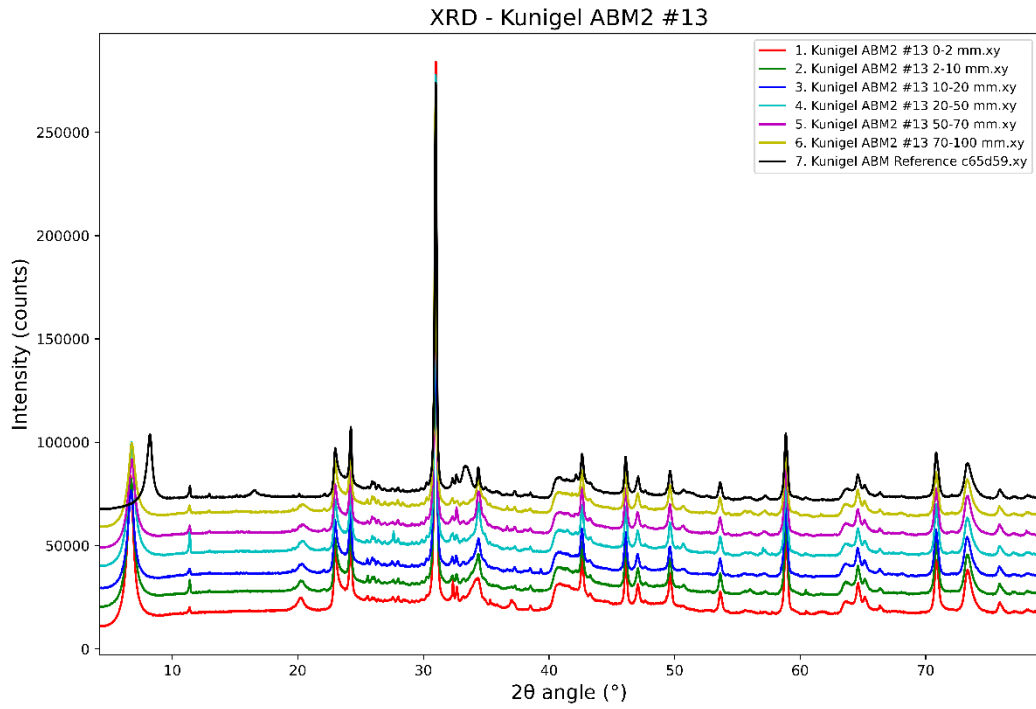


**Figure 6-17.** XRD patterns of the Kunigel block #13 profile of samples. Co K $\alpha$  raditation.

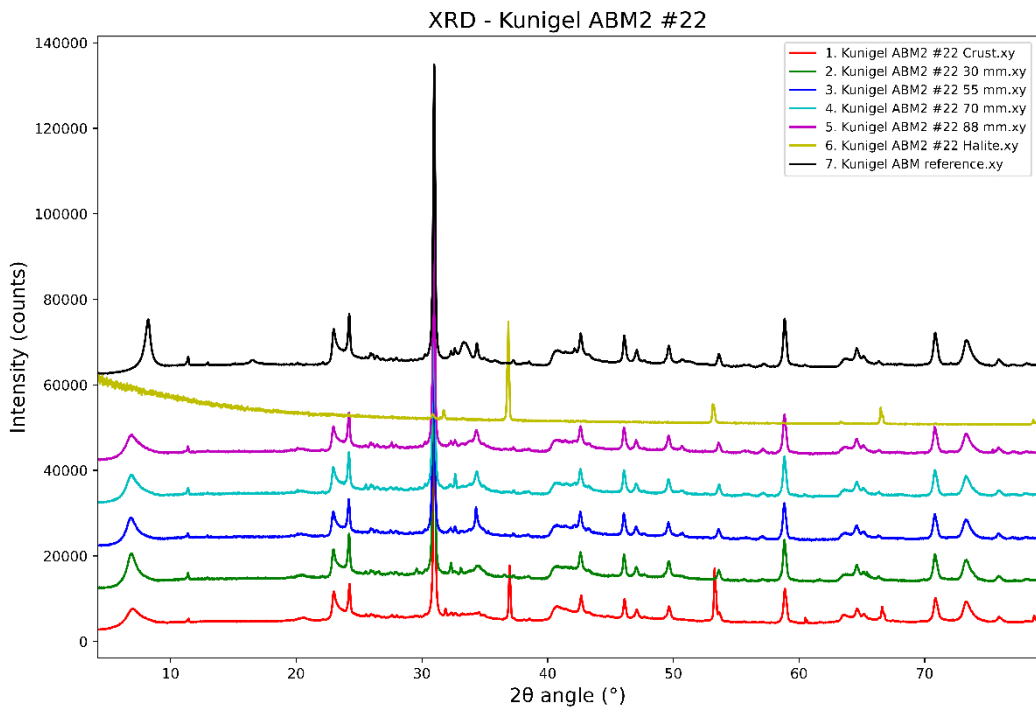


**Figure 6-18.** XRD patterns of the Kunigel block #22 profile of samples. Co K $\alpha$  raditation.



*Figure 6-19. ABM2. A highly glassy halite present in lenses of approximately 8 × 4 mm size (Kunigel #22).*

Chemical data for the ABM2 Kunigel samples can be found in Table 6-8. Mg exhibited a minor possible redistribution with a small possible accumulation towards the heater. Fe content typically increased in the samples closest to the heater due to corrosion. Cl and Ca generally increased, while Na decreased significantly, with the exception of the vicinity to the canister where Na + Cl accumulated in halite. In the 45–60 mm sample, a local accumulation of SO<sub>3</sub> was found, likely in the form of gypsum/anhydrite. The scraping sample was identified as akageneite with XRD.

**Table 6-8. Kunigel ABM2 Chemical composition (XRF).**

Sample	Na <sub>2</sub> O	MgO	Al <sub>2</sub> O <sub>3</sub>	SiO <sub>2</sub>	SO <sub>3</sub>	Cl	K <sub>2</sub> O	CaO	TiO <sub>2</sub>	MnO	Fe <sub>2</sub> O <sub>3</sub>
ABM2 #22 Kunigel Scraping		0.12	0.696	3.12	0.15	6.67	0.09	0.11	0.08	0.037	88.7
ABM2 #22 Kunigel 0–10 mm	2.24	2.66	14.17	63.1	0.72	7.40	0.74	3.63	0.19	0.050	5.12
ABM2 #22 Kunigel 40–45 mm	0.67	3.05	15.71	70.3	0.75	1.82	0.31	3.83	0.28	0.089	3.21
ABM2 #22 Kunigel 45–60 mm	0.66	2.52	15.48	69.3	1.31	1.97	0.33	5.45	0.28	0.085	2.57
ABM2 #22 Kunigel 60–80 mm	0.74	2.31	15.58	69.6	0.74	2.14	0.34	5.50	0.28	0.084	2.59
ABM2 #22 Kunigel 80–100 mm	0.73	2.29	15.45	69.3	0.73	2.38	0.34	5.66	0.27	0.086	2.69
Kunigel ABM reference c65d59	2.05	2.38	16.63	72.6	0.61	0.002	0.36	2.39	0.28	0.076	2.56

### 6.1.7 Febex

In the XRD data of the Febex samples (Figure 6-20 to Figure 6-22), a significant change was observed in block #9 samples towards the iron heater. A new reflection in the 060 region (around 75 degrees two theta) was dominant in these samples. This new reflection indicates the presence of a trioctahedral clay mineral. This change was observed in both the 0–2 mm sample (Figure 6-20) and a scraping sample taken directly from the iron heater (Figure 6-21; Figure 6-23). Additionally, the scraping sample was subjected to magnetic separation, and the magnetic fraction was identified as magnetite (Figure 6-21). Other than these observations, no significant changes were observed in the XRD data of the Febex samples.

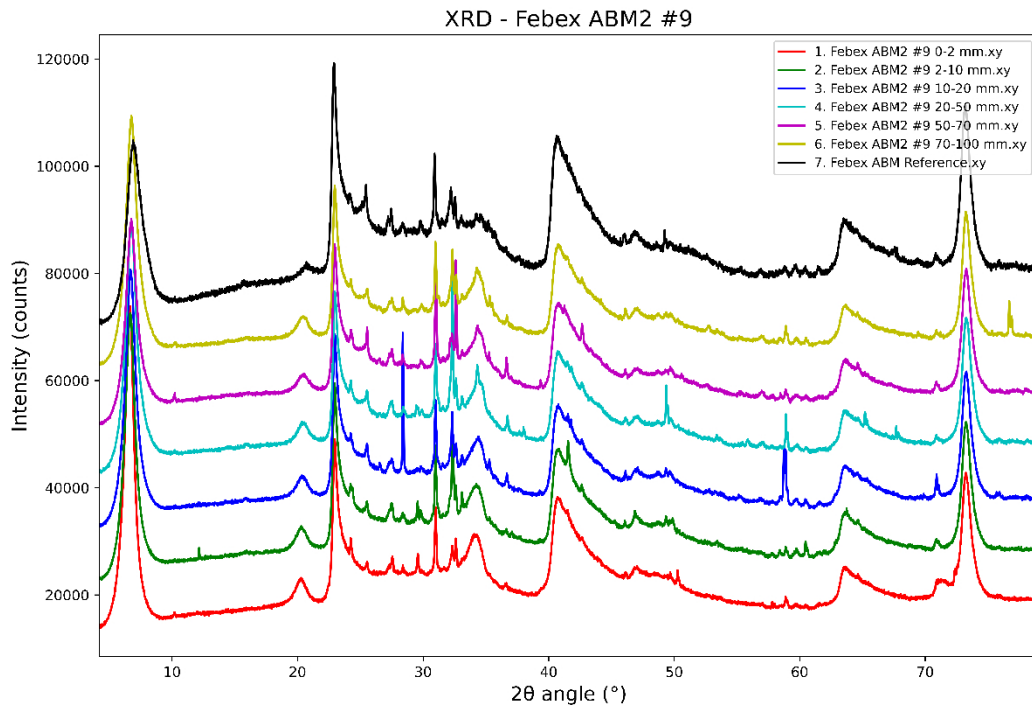


**Figure 6-20.** XRD patterns of the Febex 9 profile of samples. Co K $\alpha$  raditation.

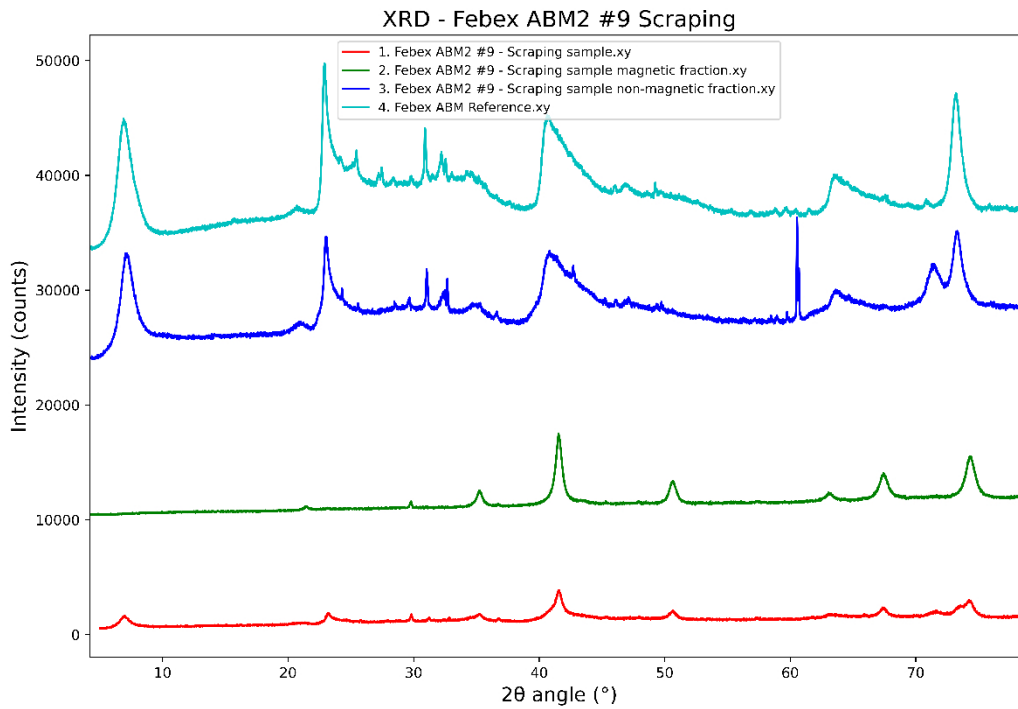


**Figure 6-21.** XRD patterns of the Febex 9 scraping sample, sub sample and reference. Co K $\alpha$  raditation. The two 060 reflections in diffractogram #3 are at 1.50 and 1.53 Å.

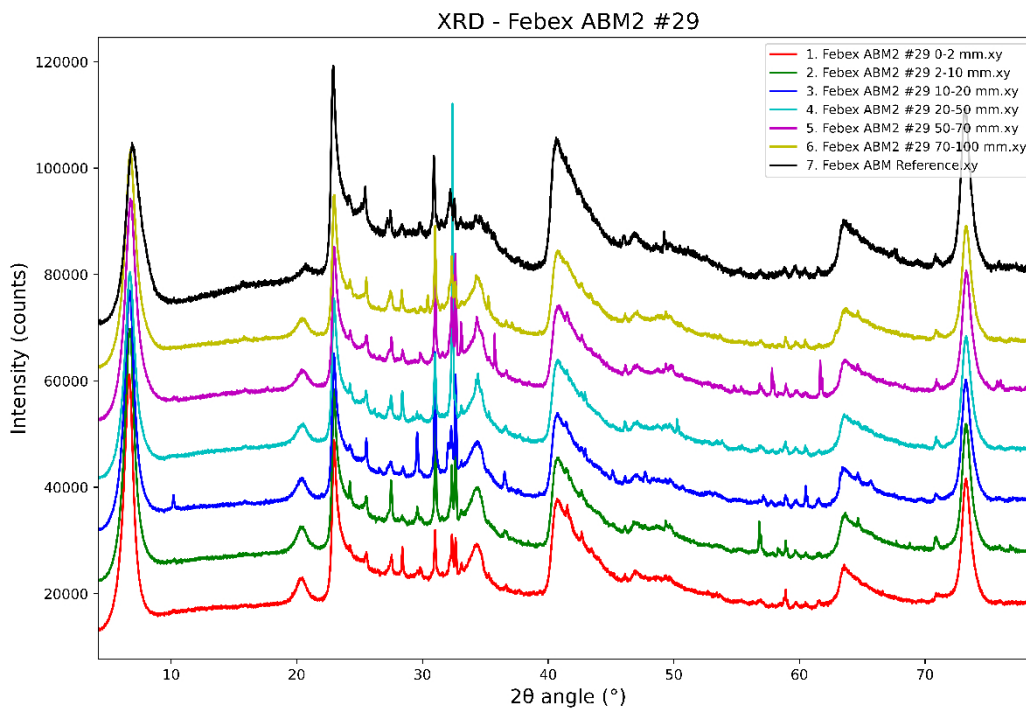


**Figure 6-22.** XRD patterns of the Febex 29 profile of samples. Co K $\alpha$  raditation.

Chemical data for the ABM2 Febex samples can be found in Table 6-9. Mg exhibited clear redistribution with minor accumulation towards the heater. Fe content typically increased in the samples closest to the heater due to corrosion. Cl and Ca generally increased, while Na decreased significantly. In the Febex ABM2 #29 10–20 mm sample, a local accumulation of SO<sub>3</sub> was found, likely in the form of gypsum/anhydrite.

**Table 6-9. Febex ABM2 Chemical composition (XRF).**

Sample	MgO	Al <sub>2</sub> O <sub>3</sub>	SiO <sub>2</sub>	SO <sub>3</sub>	K <sub>2</sub> O	CaO	MnO	Fe <sub>2</sub> O <sub>3</sub>	Cl	Na <sub>2</sub> O	TiO <sub>2</sub>
Febex ABM Reference	4.97	20.57	65.26	0.15	1.37	2.11	0.03	4.28	0.09	0.93	0.23
Febex ABM Reference	5.00	20.69	64.85	0.14	1.35	2.25	0.03	4.36	0.10	0.98	0.26
Febex ABM Reference	5.15	20.78	65.51	0.07	1.21	1.95	0.03	4.07	0.09	0.93	0.21
Febex ABM Reference	4.91	20.39	65.64	0.11	1.31	2.02	0.03	4.32	0.10	0.93	0.25
Febex ABM2 #29 0–2 mm	5.36	19.78	63.38	0.18	1.02	3.62	0.04	5.47	0.51	0.43	0.23
Febex ABM2 #29 0–2 mm	5.38	19.74	63.25	0.19	1.04	3.69	0.05	5.52	0.52	0.39	0.23
Febex ABM2 #29 2–10 mm	4.29	20.27	64.04	0.43	1.11	3.80	0.03	4.75	0.53	0.50	0.25
Febex ABM2 #29 2–10 mm	4.30	20.25	64.14	0.41	1.10	3.80	0.05	4.73	0.55	0.45	0.23
Febex ABM2 #29 10–20 mm	4.23	19.86	62.90	1.56	1.17	4.33	0.03	4.72	0.49	0.47	0.24
Febex ABM2 #29 10–20 mm	4.18	19.84	63.16	1.25	1.14	4.35	0.05	4.82	0.52	0.46	0.24
Febex ABM2 #29 20–50 mm	4.27	20.23	64.46	0.38	1.08	4.06	0.03	4.25	0.51	0.52	0.22
Febex ABM2 #29 20–50 mm	4.27	20.30	64.08	0.39	1.16	4.17	0.05	4.25	0.59	0.51	0.23
Febex ABM2 #29 50–70 mm	4.16	20.29	64.95	0.01	1.11	3.86	0.04	4.17	0.64	0.57	0.23
Febex ABM2 #29 50–70 mm	4.20	20.43	64.75	0.00	1.12	3.88	0.03	4.14	0.58	0.63	0.23
Febex ABM2 #29 70–100 mm	4.24	20.65	64.72	0.02	1.04	3.61	0.03	4.19	0.69	0.63	0.20
Febex ABM2 #29 70–100 mm	4.14	20.42	64.56	0.03	1.09	3.83	0.04	4.31	0.76	0.60	0.24
Febex #9 ABM2 0–2 mm	5.10	19.04	62.37	0.30	0.79	3.17	0.04	8.27	0.20	0.50	0.23
Febex #9 ABM2 2–10 mm	4.42	19.95	64.94	0.13	1.16	3.19	0.04	5.12	0.26	0.56	0.23
Febex #9 ABM2 10–20 mm	4.43	19.70	65.45	0.15	1.18	3.24	0.04	4.72	0.25	0.62	0.24
Febex #9 ABM2 20–50 mm	4.44	19.68	65.71	0.08	1.18	3.40	0.05	4.24	0.39	0.58	0.24
Febex #9 ABM2 50–70 mm	4.41	19.74	65.94	0.01	1.18	3.40	0.04	4.12	0.36	0.57	0.22
Febex #9 ABM2 70–100 mm	4.36	19.75	65.36	0.14	1.05	3.56	0.04	4.46	0.46	0.60	0.23
Febex #9 Scraping	7.54	14.51	54.33		0.73	1.88		20.40		0.12	0.20
Febex #9 Ca-exchanged. Scraping	6.80	15.80	55.20	0.50	0.80	3.50		16.60		0.00	

A significant increase was seen in the MgO content in the non-magnetic fraction (7.5 wt%) compared with the original bentonite (4.9 wt%; Table 6-9). Also, the Fe<sub>2</sub>O<sub>3</sub> content increased from 4.5 % in the original clay to 8.2 % in the sample taken at 0 to 2 mm from the heater, 20.4 % in the scraping sample from the heater (including magnetite) and 16.6 % in the non-magnetic part of the sample (after magnetite removal) and Ca-exchanged fraction. The CaO content in the entire profile in the field test increased, and was interpreted as a result of cation exchange reaction with the Äspö ground water and/or surrounding bentonite blocks. The mineralogical content of the purified sample was estimated by Svensson (2015) with the Rietveld Siroquant software (CSIRO, version 3) using the XRD data. For the smectite, the unit cell, the preferred orientation and the peak shape were refined. The estimated mineralogical content was 91 wt% smectite, 6.5 % albite and 2.5 % quartz.

The scraping sample collected from the surface of the iron heater (Febex block #9; Figure 6-23) was found to be a mixture of magnetite resulting from corrosion, the original bentonite, and a newly formed trioctahedral smectite (shown as a new 060 reflection next to the other one). The two 060 reflections were at 1.50 and 1.53 Å. The sample was dispersed in water, and the magnetite fraction was separated using a magnet. The non-magnetic fraction was then cation-exchanged into the calcium form to eliminate any interlayer magnesium for the calculation of the structural formula. Saturation with ethylene glycol resulted in a basal spacing of approximately 17 Å, and no other reflections corresponding to different clay minerals were observed in the low angle region (Svensson 2015). Due to the limited amount of sample available (~100 mg), only a restricted number of measurements could be performed. The intensity relationship between the 060 reflections in the XRD data allowed for an estimation of the dioctahedral to trioctahedral smectite ratio in the sample, which was approximately 60:40 (this is a rough approximation).

In Svensson (2015) an attempt was made to estimate the chemical content of the new trioctahedral phase. The chemical contribution of the identified accessory minerals and the estimated content of the original dioctahedral smectite (based on the 060-intensity relation) were subtracted from the measured elemental composition of the Ca-exchanged non-magnetic fraction of the scraping sample. The ratio between dioctahedral to trioctahedral was varied slightly in order to obtain an (Mg+Fe)/(Al+Si) ratio close to 0.75, which is the ideal theoretical value for a trioctahedral smectite. This was attained with a 52.5 % dioctahedral smectite and 38.5 % trioctahedral smectite (58:42 ratio, very close to the 60:40 estimated from the 060 intensity relations). The estimated chemical composition of the trioctahedral smectite fitted well with an iron rich saponite with excess Fe that possibly is present as amorphous corrosion products intimately mixed with the smectites.

As a complement to XRD, also FR IR data was collected compared to saponite and ferrosaponite samples from BGR (Figure 6-24). Linear combination of IR data from references support an approximately 60:40 relation between dioctahedral:trioctahedral smectite, based on overall best fit of the OH-strech + H<sub>2</sub>O-bend + OH-bend bands.



**Figure 6-23.** ABM2 Febex block 9. A crust on the surface of the iron heater.

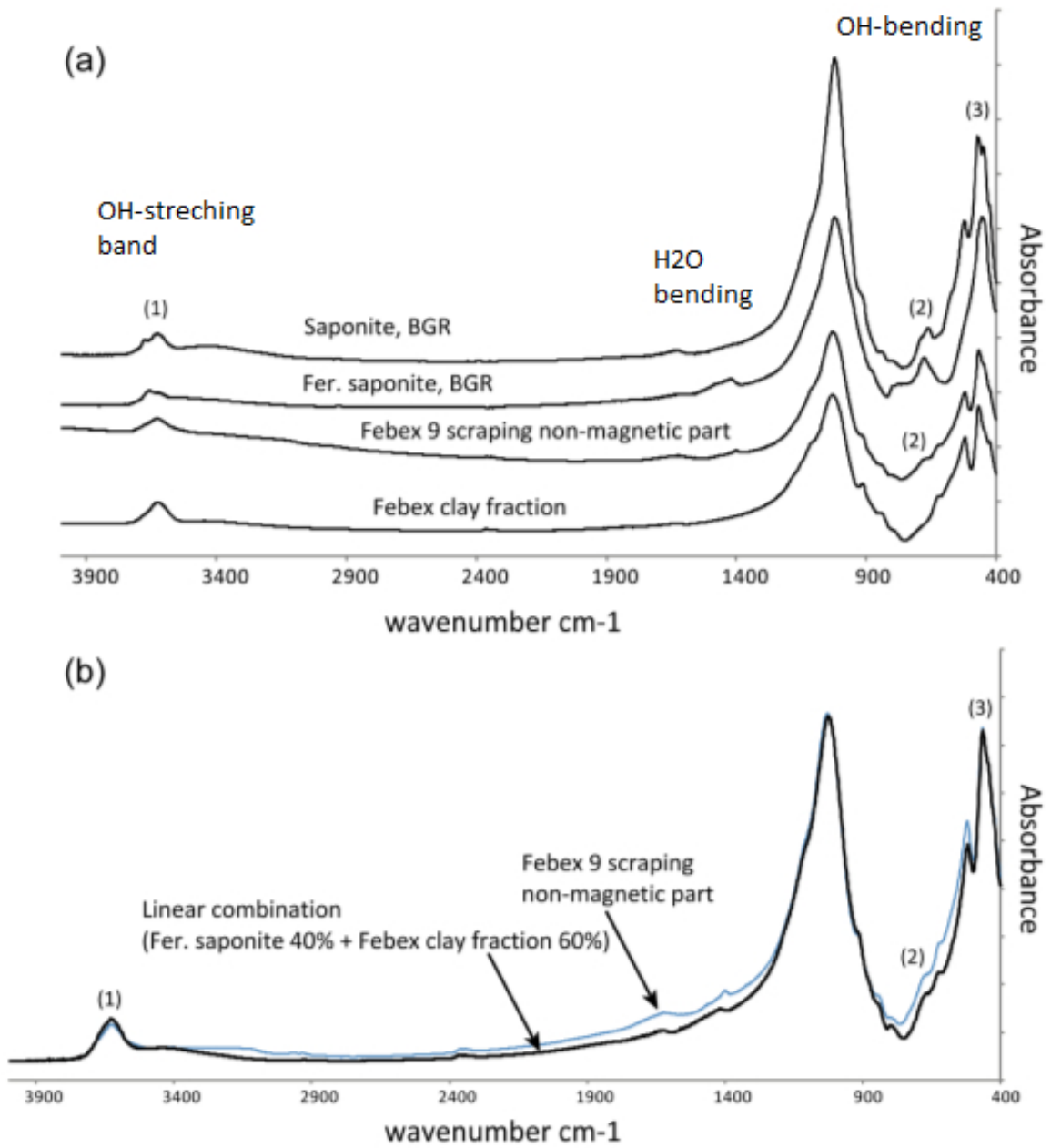


**Figure 6-24.** (a) FT IR dataset of ABM2 Febex block 9. Scraping sample and reference samples. (b) Linear combination of IR data from references support an approximately 60:40 relation between dioctahedral:trioctahedral smetite based on best fit of the OH-strech + H<sub>2</sub>O-bend + OH-bend bands.

### 6.1.8 Rokle

In the XRD data of the Rokle samples (Figure 6-25) very little changed and no significant change was observed. Some variations in 10 Å reflections were observed, interpreted as mica that sometimes gives very strong diffraction reflections based on its orientation.

Chemical data of the ABM2 Rokle samples is seen in Table 6-10. Mg showed a minor redistribution or dilution, with minor depletion towards the rock. Fe increased in the sample closest to the heater, due to the corrosion. Cl and Na generally increased. Ca did not change much, possibly enriched a little towards the heater. No sulfate has entered into the Rokle block neither from the groundwater nor from the surrounding blocks.

**Table 6-10. Rokle ABM2 Chemical composition (XRF).**

Sample	MgO	Al <sub>2</sub> O <sub>3</sub>	SiO <sub>2</sub>	P <sub>2</sub> O <sub>5</sub>	SO <sub>3</sub>	K <sub>2</sub> O	CaO	MnO	Fe <sub>2</sub> O <sub>3</sub>	Cl	Na <sub>2</sub> O	TiO <sub>2</sub>
Rokle Reference	2.3	15.8	48.6	0.7	0.0	1.2	3.4	0.2	22.1	0.0	0.1	5.5
Rokle ABM2 #7 0–2 mm	2.3	16.8	49.5	0.6	0.0	0.9	3.7	0.2	19.8	0.3	0.5	5.3
Rokle ABM2 #7 0–2 mm	2.3	16.9	49.6	0.6	0.0	1.0	3.6	0.2	19.7	0.3	0.5	5.3
Rokle ABM2 #7 2–10 mm	2.2	17.0	49.5	0.7	0.0	1.0	3.6	0.2	19.6	0.3	0.5	5.3
Rokle ABM2 #7 2–10 mm	2.3	17.0	49.4	0.6	0.0	1.0	3.5	0.2	19.6	0.4	0.5	5.3
Rokle ABM2 #7 10–20 mm	2.0	17.0	50.8	0.7	0.0	1.1	3.4	0.1	18.7	0.3	0.5	5.3
Rokle ABM2 #7 10–20 mm	2.0	17.1	50.8	0.7	0.0	1.1	3.4	0.1	18.6	0.3	0.5	5.3
Rokle ABM2 #7 20–50 mm	2.0	17.1	50.7	0.7	0.0	1.1	3.4	0.1	18.8	0.3	0.5	5.3
Rokle ABM2 #7 20–50 mm	2.0	17.1	50.7	0.7	0.0	1.1	3.4	0.1	18.8	0.3	0.5	5.3
Rokle ABM2 #7 50–70 mm	1.9	17.0	50.4	0.7	0.0	1.1	3.4	0.1	19.0	0.3	0.5	5.4
Rokle ABM2 #7 50–70 mm	1.9	17.1	50.6	0.7	0.0	1.1	3.4	0.1	18.9	0.3	0.5	5.4
Rokle ABM2 #7 70–100 mm	1.9	17.0	50.4	0.7	0.0	1.1	3.4	0.1	19.2	0.3	0.5	5.3
Rokle ABM2 #7 70–100 mm	1.9	17.1	50.3	0.7	0.0	1.1	3.4	0.1	19.2	0.3	0.5	5.3

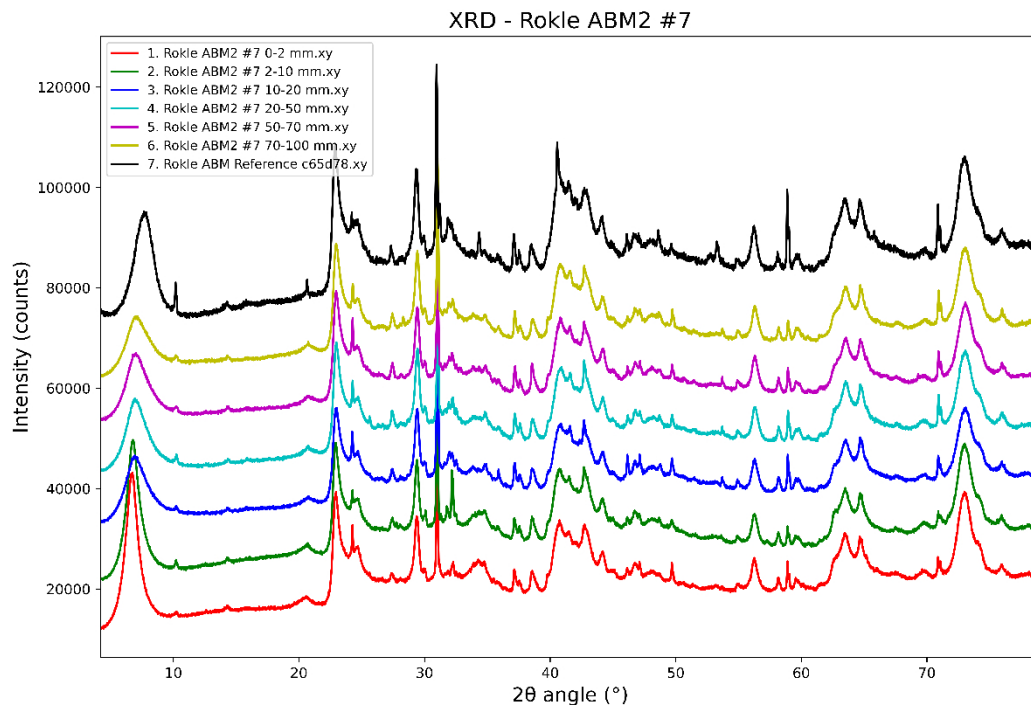


**Figure 6-25.** XRD patterns of the Rokle 7 profile of samples. Co K $\alpha$  radiation.

### 6.1.9 Asha505

In the XRD data of the Asha505 samples (Figure 6-26) very little changed and the only significant change observed was the shift of the 001 basal reflection from around 12 Å to around 15 Å due to ion exchange of the Na-smectite to Ca-smectite during the experiment.

Chemical data of the ABM2 Asha505 samples is seen in Table 6-11. Mg showed a minor increase in all samples, and an accumulation in the sample closest to the heater. Fe increased in the sample closest to the heater, due to the corrosion. Na decreased, while Ca increased. Cl did decrease somewhat, while SO<sub>3</sub> was somewhat accumulated towards the heater.

**Table 6-11. Asha505 ABM2 Chemical composition (XRF).**

Sample	MgO	Al <sub>2</sub> O <sub>3</sub>	SiO <sub>2</sub>	P <sub>2</sub> O <sub>5</sub>	SO <sub>3</sub>	K <sub>2</sub> O	CaO	MnO	Fe <sub>2</sub> O <sub>3</sub>	Cl	Na <sub>2</sub> O	TiO <sub>2</sub>
Asha505 ABM2 #10 0–2 mm	3.45	23.74	49.11	0.00	0.58	0.11	2.40	0.09	18.90	0.21	0.30	1.12
Asha505 ABM2 #10 0–2 mm	3.43	23.79	49.31	0.00	0.63	0.11	2.45	0.10	18.61	0.21	0.30	1.08
Asha505 ABM2 #10 2–10 mm	2.02	25.16	51.85	0.01	0.46	0.11	2.52	0.05	16.04	0.24	0.39	1.14
Asha505 ABM2 #10 2–10 mm	2.07	24.89	52.10	0.01	0.31	0.12	2.51	0.06	16.13	0.24	0.38	1.19
Asha505 ABM2 #10 10–20 mm	1.94	25.31	52.82	0.01	0.29	0.12	2.38	0.05	15.22	0.25	0.41	1.20
Asha505 ABM2 #10 10–20 mm	1.96	25.13	52.91	0.01	0.32	0.10	2.42	0.06	15.24	0.26	0.39	1.20
Asha505 ABM2 #10 20–50 mm	1.98	24.81	52.88	0.00	0.17	0.13	2.40	0.06	15.63	0.25	0.40	1.30
Asha505 ABM2 #10 20–50 mm	2.00	24.78	53.41	0.00	0.17	0.11	2.42	0.07	15.02	0.29	0.40	1.33
Asha505 ABM2 #10 50–70 mm	1.86	25.65	52.67	0.00	0.02	0.13	2.42	0.06	15.35	0.26	0.41	1.19
Asha505 ABM2 #10 50–70 mm	1.90	25.34	52.88	0.01	0.03	0.13	2.37	0.07	15.37	0.30	0.39	1.22
Asha505 ABM2 #10 70–100 mm	2.14	24.89	54.26	0.01	0.03	0.23	2.37	0.05	14.13	0.32	0.45	1.13
Asha505 ABM2 #10 70–100 mm	2.19	24.53	54.56	0.01	0.03	0.21	2.75	0.08	13.66	0.37	0.43	1.19
Asha 505 ABM reference c65d6c	2.0	24.6	52.1	0.02	0.1	0.1	0.8	0.1	16.7	0.5	1.8	1.3

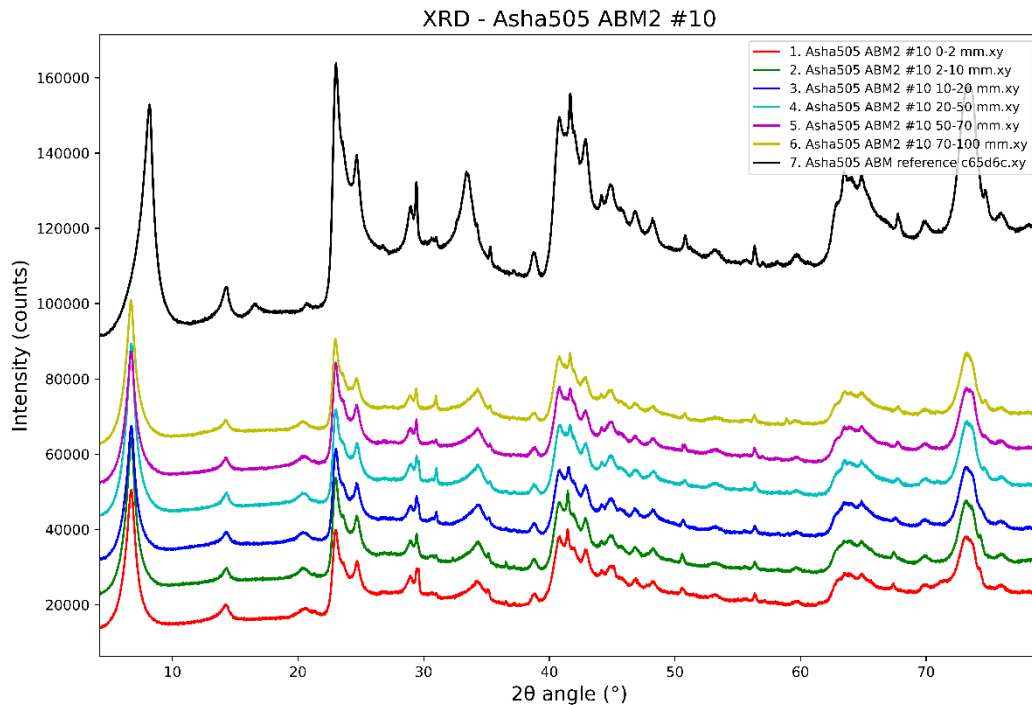


**Figure 6-26.** XRD patterns of the ABM2 Asha505 block 10 profile of samples. Co K $\alpha$  radiation.

## 6.2 Conclusions and discussion ABM2

Based on the CEC results, there was no significant overall change in the smectite content between the reference material and the exposed material. In general, the XRD data did not show significant changes in the mineralogy of the clays, except for a few exceptions: (1) the formation of corrosion products, (2) dissolution-precipitation reactions such as gypsum, halite etc, and (3) changes observed in the 060 region. In one specific case (Febex bentonite block #9), a significant formation of trioctahedral smectite, likely ferrosaponite, was observed. However, this formation was extremely small and has no impact on the buffer performance since the formed mineral is also a swelling clay mineral and the extent of formation is very low.

Similar observations of trioctahedral smectite in ABM2 samples in XRD data was done by Leal Olloqui (2020) and by Kaufhold et al. (2017). However, they only observed smaller changes in the 060 region compared to what was seen in the scraping sample in the Febex block #9.

The chemical data obtained from XRF analysis revealed that in sodium-dominated bentonites, calcium (Ca) typically increased, while the opposite trend was observed in calcium-dominated bentonites. This is expected due to cation exchange reactions between the different clay minerals. This cation exchange is supported also by findings by Dohrmann and Kaufhold (2017), who did a detailed study on the cation exchange reactions in ABM2.

The chloride (Cl) content generally increased in all samples due to interactions with the Äspö groundwater. In Kunigel block #22 the accumulation of halite was extreme as visible lenses of halite was observed, most likely this can be attributed to local boiling or similar accumulation process due to the high temperature.

In the proximity of the iron heater, the clay samples showed an increase in iron (Fe) content. There was also a redistribution and accumulation of magnesium (Mg) towards the iron heater observed in many clays.

Wersin et al. (2021) reported no evidence of smectite alteration in ABM2. However, they observed the presence of corrosion products, primarily ferric (oxyhydr)oxides, which resulted in the introduction of iron into the bentonite at a distance of approximately 5–20 mm from the interface with the metallic heater. Additionally, the authors noted that some of the structural iron in the smectite was partially reduced during the experiment as the redox potential transitioned from oxidizing to reducing over the course of the experiment.

## 7 ABM5 results from analysis

### 7.1 Chemical and mineralogical evolution in ABM5

#### *Mineralogy*

Powder X-ray diffraction (XRD) analysis was conducted to examine the crystalline phase composition of the bentonite clays (Figure 7-1 to Figure 7-4). Overall, very few significant changes were observed in the diffractograms. Minor differences are expected due to natural variations in the content of the bentonites. No significant changes were observed in the 060 region around 73 degrees two theta, indicating the absence of trioctahedral smectite formation. The appearance of the basal spacings sometimes shifted somewhat due to the variations in the smectite hydration and interlayer cation composition. In the Asha505 samples a calcite reflection (approximately 35 deg two theta; 3.03 Å) was present in some of the samples from the field experiment, and at the innermost contact with the heater a small reflection is visible at approximately 15 deg two theta (7.59 Å) of an unidentified phase.

Similar findings were reported by Kaufhold et al. (2021) in their analysis of bentonites from the ABM5 experiment. They also did not observe any changes in the 060 region or additional interstratifications in the smectites, such as illitisation. Their conclusions suggest that the minor changes observed were close to the detection limit and not consistently observed.

In another study by Fernández et al. (2022) focusing on the ABM5 experiment, no significant changes in mineralogy, except for corrosion products and dissolution/precipitation reactions of carbonates, were observed. This further supports the notion that the observed changes in the XRD data of the bentonite clays were minimal.

Additionally, Sudheer Kumar et al. (2021) conducted a Rietveld analysis of XRD data collected from samples in the ABM5 experiment and concluded that no significant loss of smectite was observed.

Taken together, these studies provide consistent evidence that there were no significant changes in the mineralogy of the bentonite clays, including the absence of smectite loss or trioctahedral smectite formation.

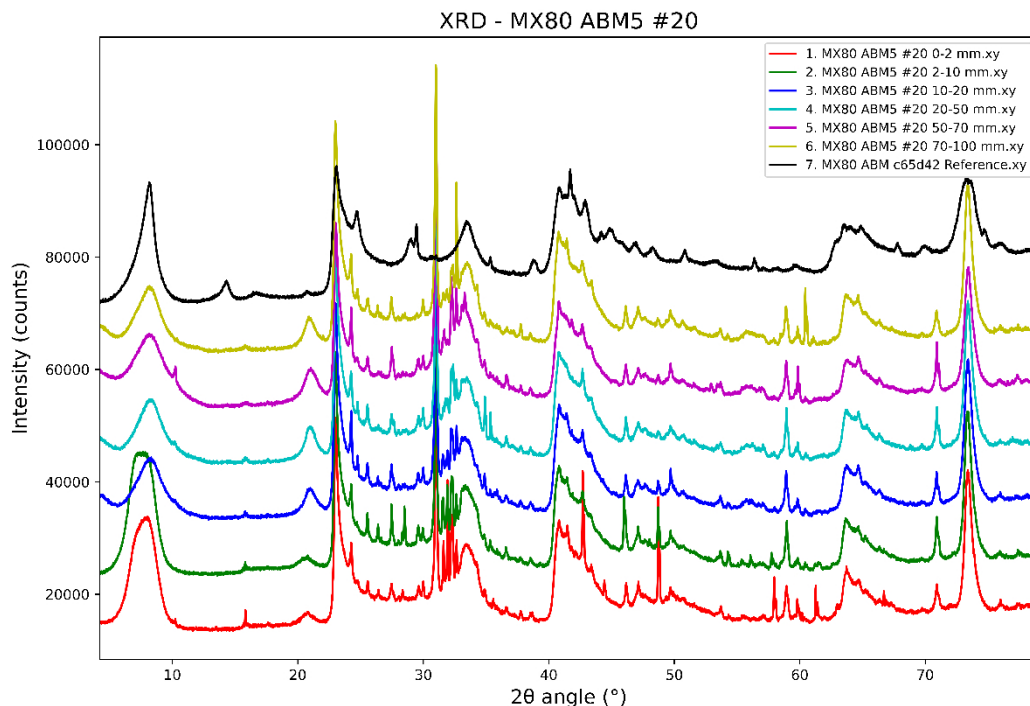


**Figure 7-1.** XRD patterns of the ABM5 MX-80 block 20 profile of samples. Co Ka radiation.

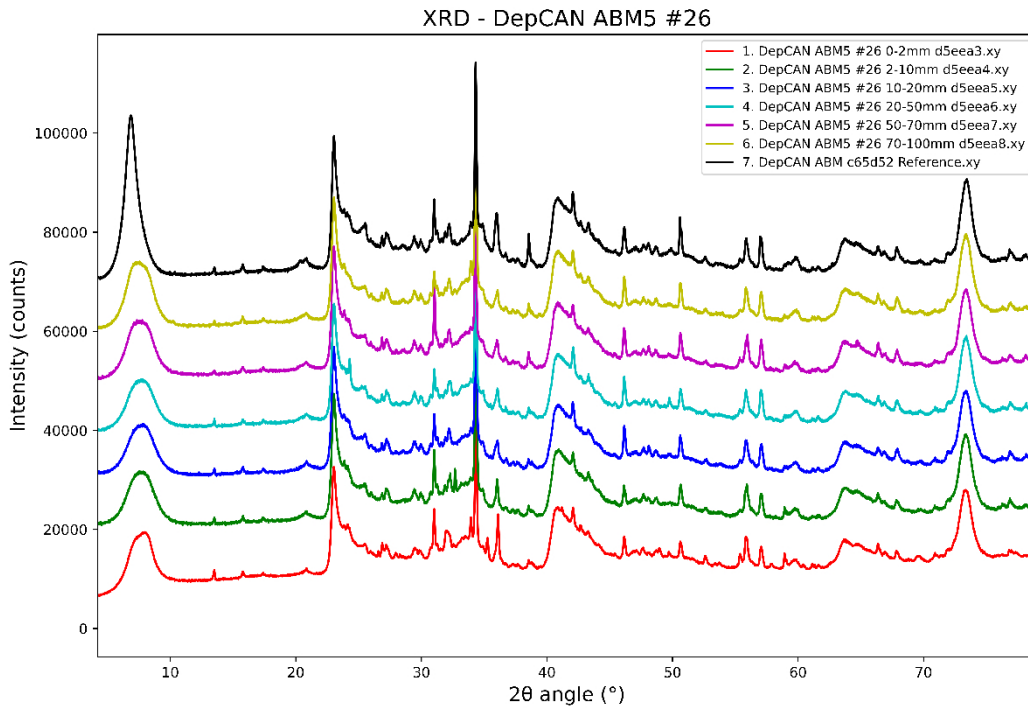


**Figure 7-2.** XRD patterns of the ABM5 DepCAN block 26 profile of samples. Co K $\alpha$  radiation.

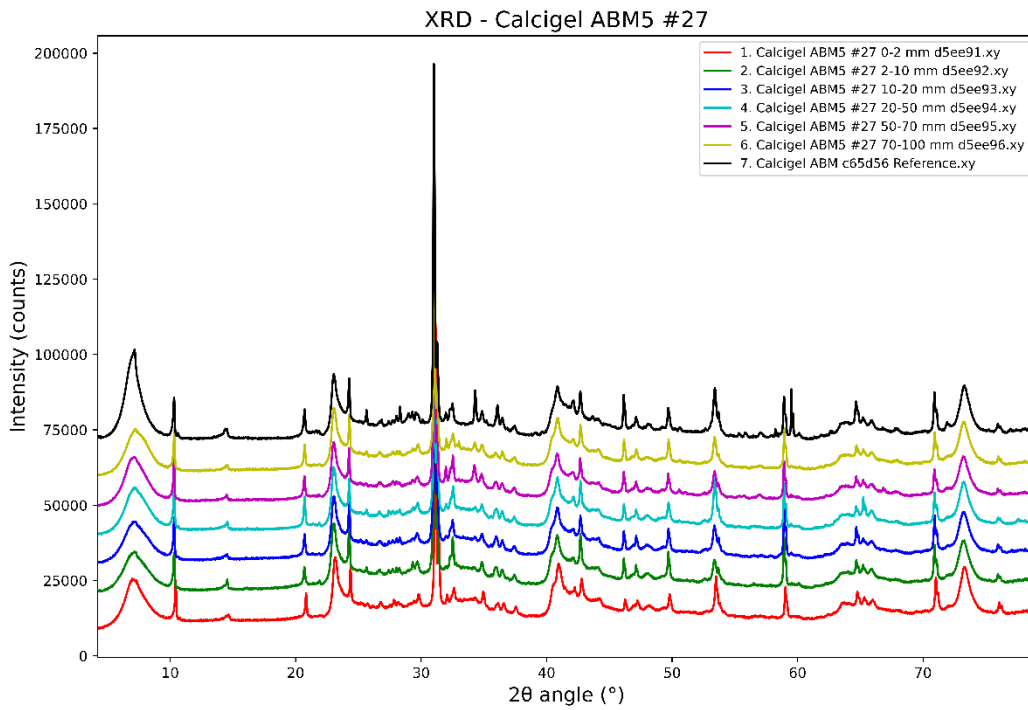


**Figure 7-3.** XRD patterns of the ABM5 Calcigel block 27 profile of samples. Co K $\alpha$  radiation.

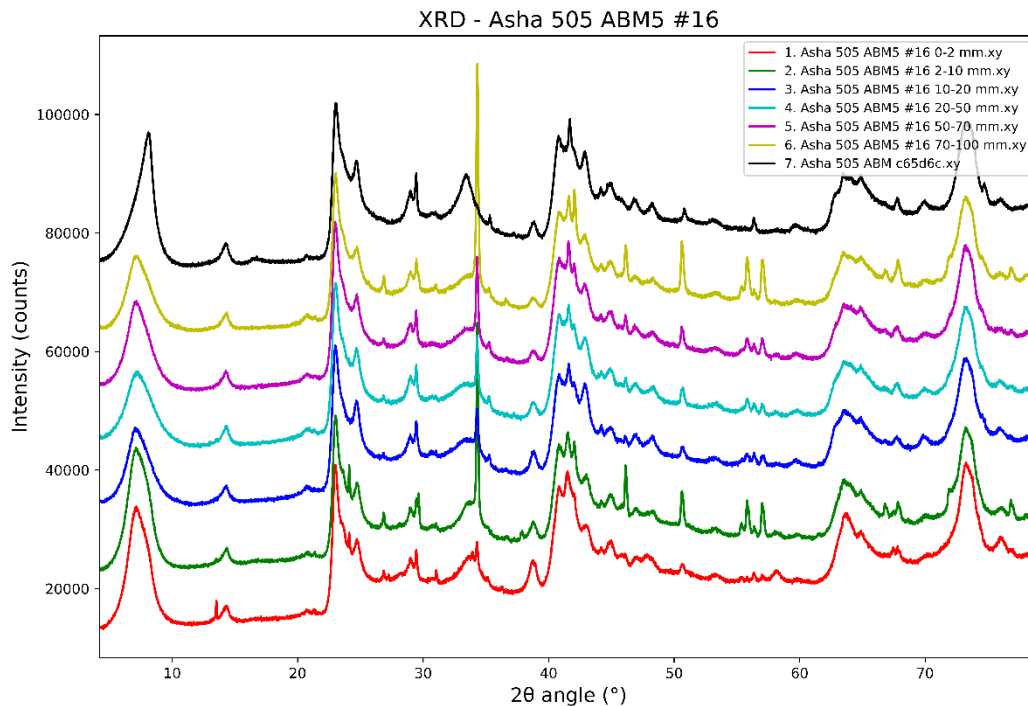


**Figure 7-4.** XRD patterns of the ABM5 Asha505 block 16 profile of samples. Co K $\alpha$  radiation.

### **Cation exchange**

In the sodium bentonites (Asha505 and MX-80), the smectite basal spacings (XRD reflections below 10 degrees two theta) typically increased after the field experiment, indicating the conversion to mixed Na-Ca smectites due to ion exchange with the Äspö water and between different bentonites. This is consistent with observations made by Fernández et al. (2022). On the other hand, in the calcium bentonites (DepCAN and Calcigel), the smectite basal spacings decreased after the experiment. This can be attributed to the lower basal spacings of air-dried sodium smectites compared to calcium smectites. The changes in smectite composition and basal spacings indicate the influence of ion exchange processes.

The total sum of exchangeable cations (total EC) generally increased in the samples from the field experiment, especially in samples closer to the rock (Table 7-1). This increase in total EC suggests the presence of soluble phases in the bentonites. However, the chloride levels were higher near the heater compared to samples closer to the rock, indicating a different trend in soluble phases. Fernández et al. (2022) also noted a salinity gradient across the bentonite blocks, and Kaufhold et al. (2021) suggested that the chloride concentration was influenced by factors such as local inflowing water. The distribution of chloride was found to vary in different parts of the experiment.

In DepCAN, Calcigel, and Asha505, the cation exchange capacity (CEC) of the bulk generally decreased somewhat after the experiment compared to the reference samples. However, in MX-80, the CEC did not show a significant change. In contrast, the CEC of the clay fractions increased somewhat in the samples from the ABM5 experiment compared to the reference samples. Fernández et al. (2022) also observed a drop in CEC in all samples, with the most significant decrease at the heater interface. They also observed a decrease in external surface area and a slight increase in total and tetrahedral surface charge, which is consistent with the increase in CEC observed in the clay fraction by SKB. The change in surface external area is probably also linked to the cation exchange (Kaufhold et al. 2010). There were indications from Sudheer Kumar et al. (2021) that changes in the smectite structural formula occurred in the vicinity of the heater, possibly affecting the layer charge. The corrosion process released Fe, and previous experiments have shown the dissolution of Si minerals such as cristobalite. It is also common for Mg to accumulate towards the heater, which makes precise chemical formula calculations of the smectite challenging. The increase in chloride content was observed, although different trends were reported by different research teams. The decrease in CEC is not easily explained, but it may be correlated with the lower external surface area observed by Fernández et al. (2022), considering that the smectite content remained constant.

**Table 7-1. Exchangeable cations (EC) and cation exchange capacity (CEC) of ABM5 samples. Unit is cmol(+)/kg.**

Sample	Sample id	Ca	K	Mg	Na	$\Sigma_{EC}$	CEC Cu-tri (n = 3; SD)
Asha 505 ABM5 #16 0–2 mm	d5ee9d	45.01	1.27	12.68	32.30	91.26	75.2 (0.2)
Asha 505 ABM5 #16 2–10 mm	d5ee9e	46.39	1.18	12.55	32.54	92.66	78.1 (1.1)
Asha 505 ABM5 #16 10–20 mm	d5ee87	47.31	1.25	15.07	29.15	92.78	74.5 (0.1)
Asha 505 ABM5 #16 20–50 mm	d5ee88	49.54	1.45	15.13	31.73	97.84	81.7 (0.3)
Asha 505 ABM5 #16 50–70 mm	d5ee89	50.80	1.35	15.18	32.08	99.41	82.6 (0.7)
Asha 505 ABM5 #16 70–100 mm	d5ee8a	53.54	1.39	15.19	32.62	102.74	81.2 (0.2)
Asha 505 reference	c65d6c	17.02	0.71	16.25	56.02	90.00	87.6 (0.2)
MX-80 ABM5 #20 0–2 mm	d5ee97	32.09	1.76	8.46	31.56	73.88	84.1 (0.35)
MX-80 ABM5 #20 2–10 mm	d5ee98	36.16	2.42	11.03	34.39	84.00	82.6 (0.7)
MX-80 ABM5 #20 10–20 mm	d5ee99	38.00	2.43	11.50	36.01	87.94	83.0 (0.1)
MX-80 ABM5 #20 20–50 mm	d5ee9a	38.43	2.62	10.63	37.60	89.28	84.4 (0.3)
MX-80 ABM5 #20 50–70 mm	d5ee9b	36.74	2.18	9.85	36.12	84.88	85.3 (0.4)
MX-80 ABM5 #20 70–100 mm	d5ee9c	40.31	2.15	10.37	37.32	90.16	87.7 (0.8)
MX-80 ABM reference	c65d42	16.72	2.34	7.00	51.95	78.01	83.4 (0.4)
Deponit Can ABM5 #26 0–2 mm	d5eea3	65.35	2.84	3.31	26.07	97.58	77.5 (0.7)
Deponit Can ABM5 #26 2–10 mm	d5eea4	64.81	3.55	5.10	27.41	100.87	79.1 (0.8)
Deponit Can ABM5 #26 10–20 mm	d5eea5	64.99	3.36	5.68	26.89	100.91	78.2 (1.3)
Deponit Can ABM5 #26 20–50 mm	d5eea6	66.75	3.25	5.19	27.65	102.85	78.6 (0.6)
Deponit Can ABM5 #26 50–70 mm	d5eea7	71.27	3.01	3.07	27.59	104.93	80.3 (0.3)
Deponit Can ABM5 #26 70–100 mm	d5eea8	69.87	2.92	2.85	28.41	104.05	83.7 (0.7)
Deponit Can reference	c65d52	39.93	2.40	29.22	22.16	93.72	78.9 (1.4)
Calcigel ABM5 #27 0–2 mm	d5ee91	52.15	3.47	1.59	22.19	79.41	63.7 (0.3)
Calcigel ABM5 #27 2–10 mm	d5ee92	44.33	4.38	3.47	21.57	73.74	61.1 (0.8)
Calcigel ABM5 #27 10–20 mm	d5ee93	44.88	4.27	3.28	22.02	74.46	62.4 (0.3)
Calcigel ABM5 #27 20–50 mm	d5ee94	45.26	3.51	1.42	19.77	69.96	62.8 (0.5)
Calcigel ABM5 #27 50–70 mm	d5ee95	57.89	3.29	1.34	20.47	82.98	63.1 (0.5)
Calcigel ABM5 #27 70–100 mm	d5ee96	56.88	3.08	1.33	19.74	81.02	63.7 (0.3)
Calcigel reference	c65d56	53.95	1.92	16.76	2.64	75.28	69.8 (0.6)

### **Chemical content**

The chemical data (XRF) is presented in Table 7-2. In general, there was a small increase in Mg content observed in all bentonites, except for DepCAN. However, there was no clear accumulation of Mg towards the hottest part of the experiment. The increase in Mg content may be attributed to various factors. The accumulation/redistribution of Ca, Na, and Cl content was discussed in the previous section regarding cation exchange.

Fe content showed an overall increase in the vicinity of the corroding heater in all cases, consistent with the observations made by Fernández et al. (2022) and Kaufhold et al. (2021). Fernández et al. (2022) conducted Mössbauer investigations and found that the Fe(II)/Fe(III) ratio increased towards the heater, although Fe(III) dominated in all samples.

To summarize, Fe and Cl content tended to increase towards the heater in many cases, while there was a general increase in Mg content observed overall, without significant accumulation towards the heater.

**Table 7-2. Chemical analysis of ABM5 samples using XRF.**

Ident	Na <sub>2</sub> O	MgO	Al <sub>2</sub> O <sub>3</sub>	SiO <sub>2</sub>	P <sub>2</sub> O <sub>5</sub>	SO <sub>3</sub>	Cl	K <sub>2</sub> O	CaO	TiO <sub>2</sub>	MnO	Fe <sub>2</sub> O <sub>3</sub>
Asha ABM5 #16 0–2 mm d5ee85	0.8	2.7	20.7	47.8	0.00	0.4	0.5	0.1	2.7	1.1	0.1	23.0
Asha ABM5 #16 2–10 mm d5ee86	0.9	2.8	20.8	48.8	0.00	0.2	1.0	0.1	5.7	1.1	0.1	18.5
Asha ABM5 #16 10–20 mm d5ee87	0.9	2.5	22.9	50.3	0.00	0.2	0.3	0.1	2.5	1.1	0.1	19.0
Asha ABM5 #16 20–50 mm d5ee88	0.9	2.6	23.1	51.5	0.00	0.1	0.4	0.1	2.7	1.1	0.1	17.4
Asha ABM5 #16 50–70 mm d5ee89	1.0	2.5	23.3	51.7	0.00	0.1	0.4	0.1	3.2	1.2	0.1	16.4
Asha ABM5 #16 70–100 mm d5ee82	0.9	2.6	22.1	49.6	0.00	0.2	0.4	0.1	6.2	1.2	0.1	16.5
Asha 505 ABM reference c65d6c	1.8	2.0	24.6	52.1	0.02	0.1	0.5	0.1	0.8	1.3	0.1	16.7
MX-80 ABM5 #20 0–2 mm d5ee7f	1.0	2.7	21.9	62.9	0.00	0.5	0.7	0.6	2.2	0.2	0.0	7.2
MX-80 ABM5 #20 2–10 mm d5ee80	1.0	2.7	22.3	63.9	0.00	0.5	0.8	0.6	2.2	0.2	0.0	5.8
MX-80 ABM5 #20 10–20 mm d5ee81	1.2	2.6	22.6	64.8	0.01	0.6	0.2	0.7	2.0	0.2	0.0	5.1
MX-80 ABM5 #20 20–50 mm d5ee82	1.2	2.7	22.6	64.9	0.00	0.6	0.2	0.6	2.2	0.2	0.0	4.9
MX-80 ABM5 #20 50–70 mm d5ee83	1.2	2.6	22.7	64.9	0.01	0.5	0.2	0.6	2.2	0.2	0.0	4.8
MX-80 ABM5 #20 70–100 mm d5ee84	1.2	2.6	22.6	65.1	0.00	0.3	0.3	0.6	2.1	0.2	0.0	4.8
MX-80 ABM reference c65d44	2.2	2.3	21.9	67.2	0.09	0.2	0.0	0.5	0.5	0.2	0.2	5.0
Calcigel ABM5 #27 0–2 mm d5ee91	0.9	3.8	19.9	60.9	0.01	0.2	0.3	2.6	2.9	0.5	0.6	7.9
Calcigel ABM5 #27 2–10 mm d5ee92	0.8	3.7	19.6	61.4	0.05	0.2	0.2	2.1	3.3	0.4	0.5	8.3
Calcigel ABM5 #27 10–20 mm d5ee93	0.9	3.9	20.0	62.0	0.06	0.2	0.3	2.5	2.9	0.5	0.5	6.8
Calcigel ABM5 #27 20–50 mm d5ee94	0.9	3.9	20.0	61.8	0.00	0.4	0.2	2.6	3.2	0.5	0.6	6.9
Calcigel ABM5 #27 50–70 mm d5ee95	0.8	3.6	19.2	61.6	0.00	0.3	0.2	2.6	4.8	0.5	0.6	6.7
Calcigel ABM5 #27 70–100 mm d5ee96	0.7	3.7	19.8	61.6	0.00	0.3	0.2	2.6	3.9	0.5	0.6	6.9
Calcigel ABM reference c65d56	0.9	3.5	20.9	61.4	0.10	0.4	0.1	1.8	4.1	0.5	0.5	7.5
DepCAN ABM5 #26 0–2 mm d5eea3	0.7	3.0	18.9	55.9	0.38	1.7	0.7	1.2	6.9	1.0	0.1	9.7
DepCAN ABM5 #26 2–10 mm d5eea4	0.7	3.1	19.9	58.4	0.38	1.1	0.5	1.2	6.6	1.1	1.0	7.3
DepCAN ABM5 #26 10–20 mm d5eea5	0.7	3.1	19.9	58.4	0.34	1.3	0.5	1.2	6.8	1.1	1.0	6.8
DepCAN ABM5 #26 20–50 mm d5eea6	0.7	3.1	19.9	58.4	0.34	1.3	0.5	1.2	7.0	1.1	1.0	6.5
DepCAN ABM5 #26 50–70 mm d5eea7	0.8	3.0	19.9	58.2	0.31	1.1	0.5	1.3	7.5	1.1	0.1	6.5
DepCAN ABM5 #26 70–100 mm 5eea8	0.7	3.0	19.8	58.4	0.34	1.0	0.5	1.3	7.3	1.1	0.1	6.5
DepCAN ABM reference c65d52	0.6	3.1	20.3	59.5	0.37	1.3	0.1	1.3	6.2	1.1	0.9	6.3

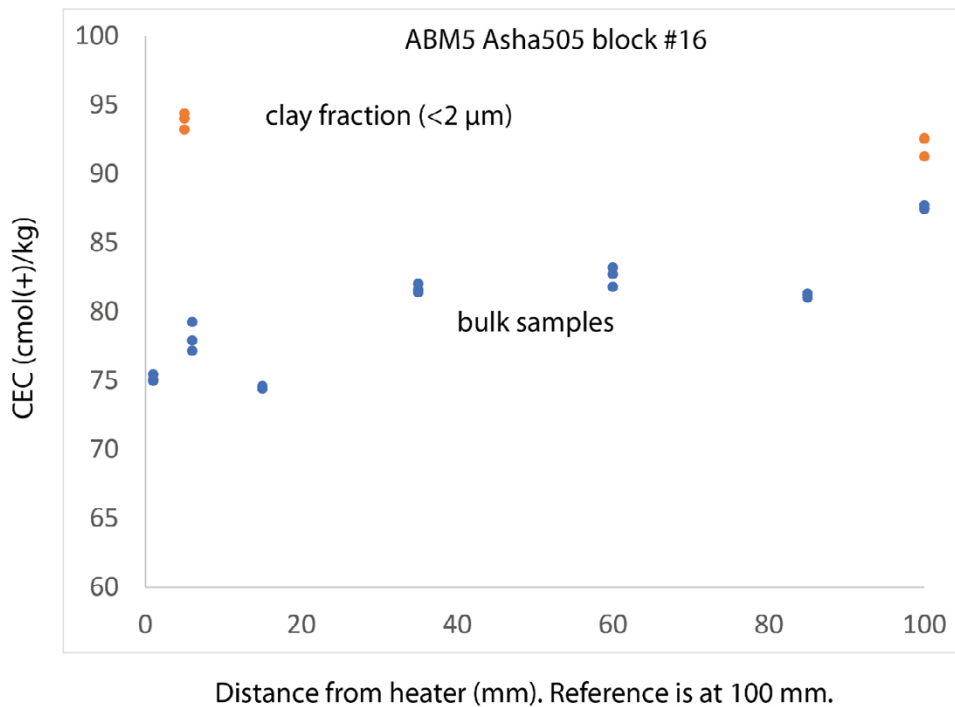


**Figure 7-5. CEC of Asha 505 block 16 profile of samples.**

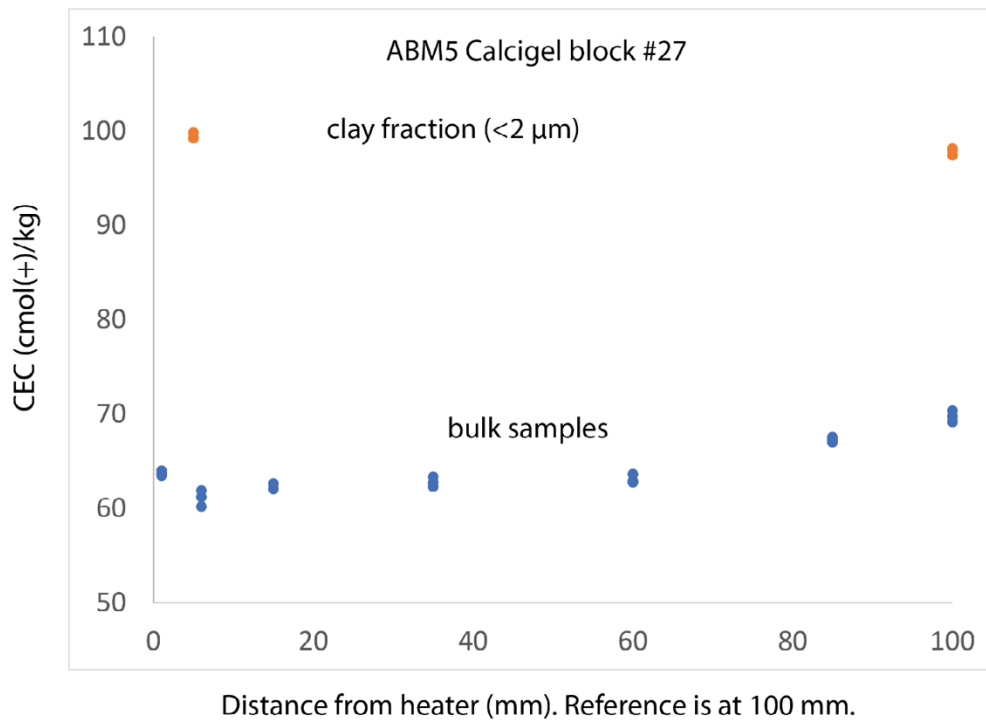


**Figure 7-6.** CEC of Calcigel block 27 profile of samples.

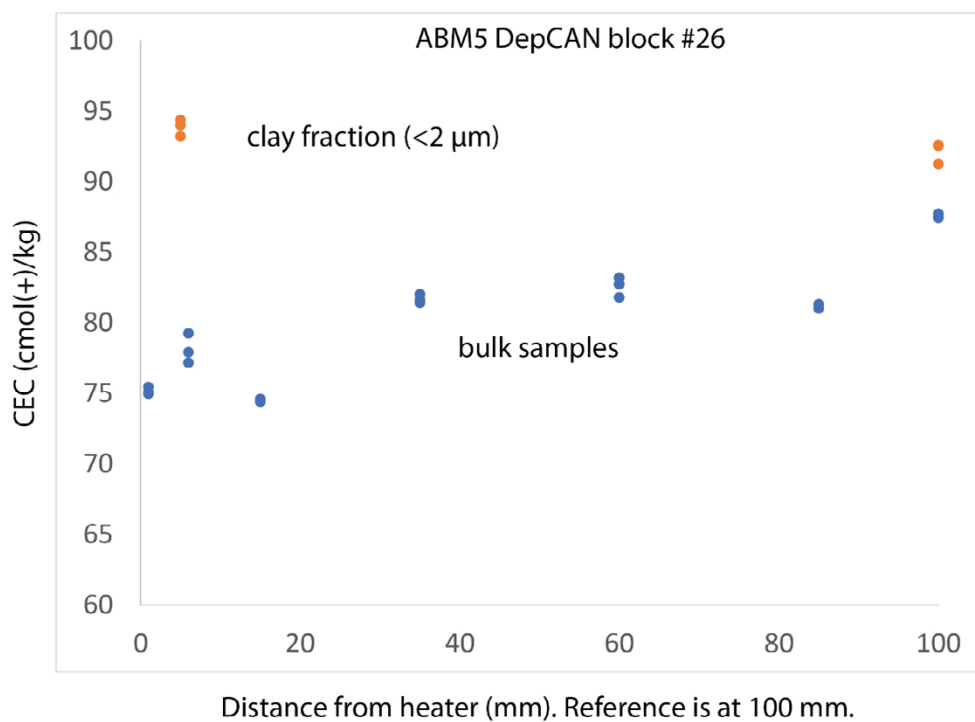


**Figure 7-7.** CEC of DepCAN block 26 profile of samples.

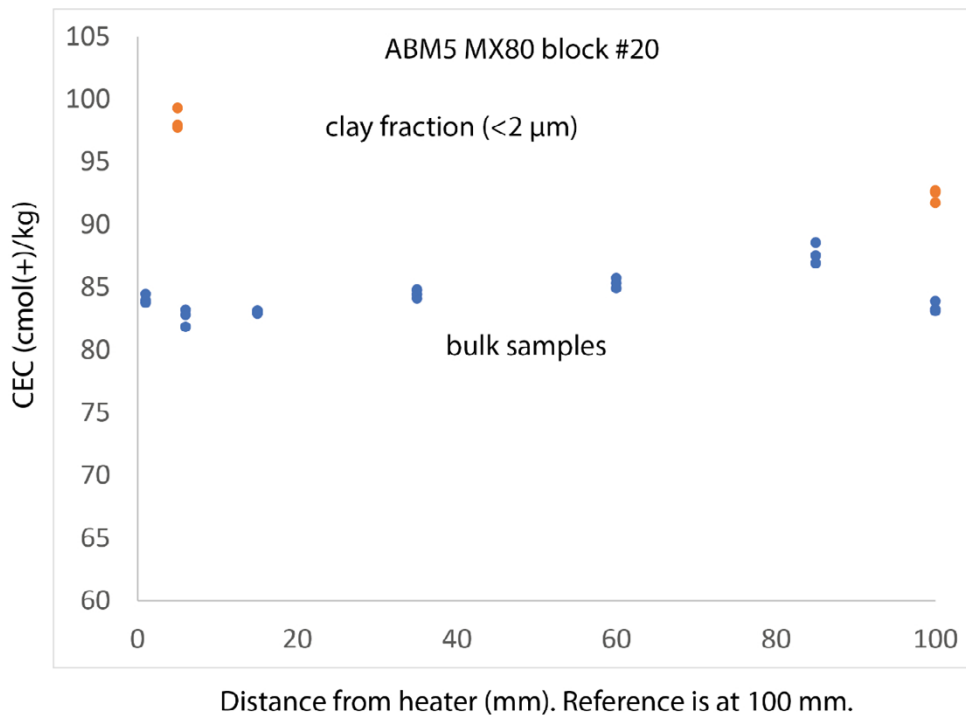


**Figure 7-8.** CEC of MX-80 block 20 profile of samples.

## 7.2 Swelling pressure and hydraulic conductivity in ABM5

The swelling pressure was measured in a series together with hydraulic conductivity in several different chemical conditions. First with deionised water, then with salt solution (1 M CaCl<sub>2</sub>), and then again with deionised water (this is described in much better detail in Chapter 3). By looking on the last step one gets the swelling pressure with deionised water. Hence one can compare the material from the experiment with the reference clay and at the same time excluding effects from cation exchange and salt accumulation which is ideal conditions for finding smectite degradation.

In Calcigel (Figure 7-9) the densities ended up a little bit low for ideal comparison, they suggest a possible small increase in swelling pressure in the samples from ABM5 compared to the reference samples. However, the hydraulic conductivity showed a possible increase. Typically, when the swelling pressure performance increase due to increased smectite content the hydraulic conductivity should decrease. Most likely the explanation for this is that the experimental uncertainties increased at the lower densities used, and the difference in behaviour is far from certain.

In Asha505 (Figure 7-10) the swelling pressure was the same in both ABM5 samples and references. In some samples from the ABM5 experiment at low densities the hydraulic conductivity increased, like in the calcigel case.

In DepCAN (Figure 7-11) and in MX-80 (Figure 7-12) no significant change could be seen between ABM5 samples and reference samples either in swelling pressure or hydraulic conductivity.

**Summary:** At the lowest tested densities possibly there were some changes in performance between samples from ABM5 and reference materials, most likely this was due to the experimental difficulties at the low densities. At the higher densities (the target densities) no change in performance was observed.

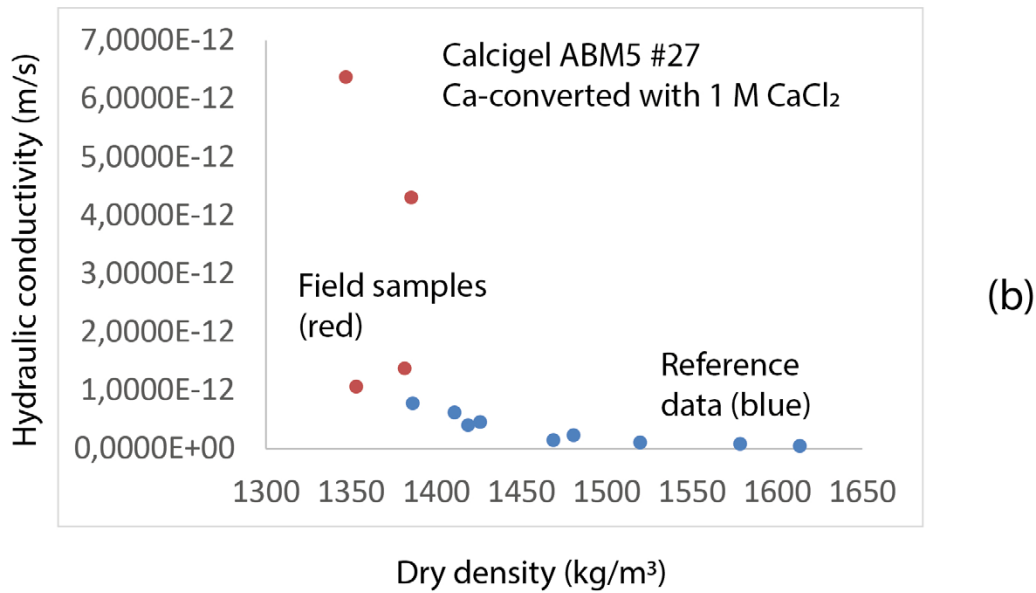
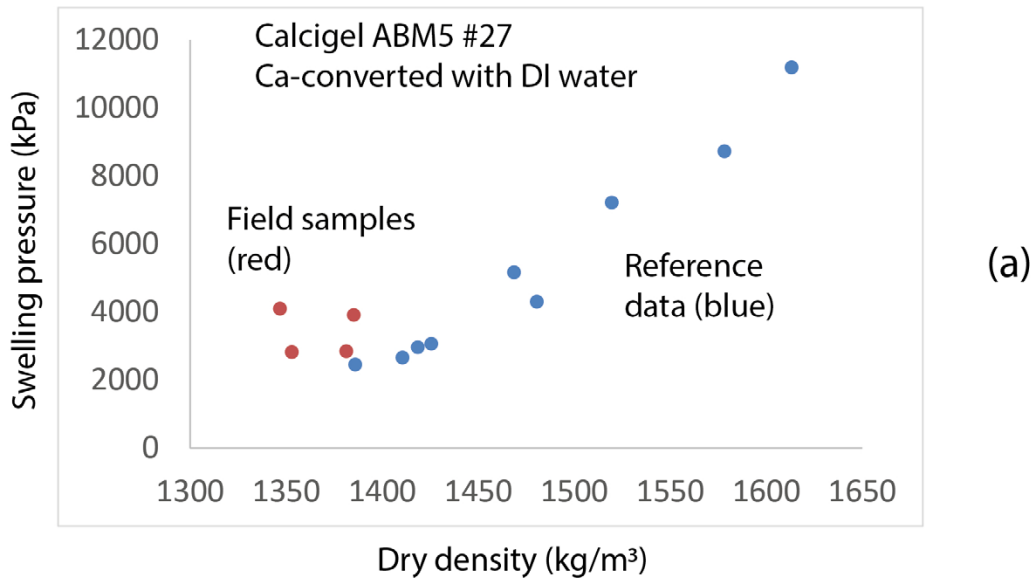


**Figure 7-9.** ABM5 Calcigel #27 samples compared to reference samples. (a) Swelling pressure after Ca-conversion in DI water. (b) Hydraulic conductivity after Ca-conversion in 1 M CaCl<sub>2</sub> solution.

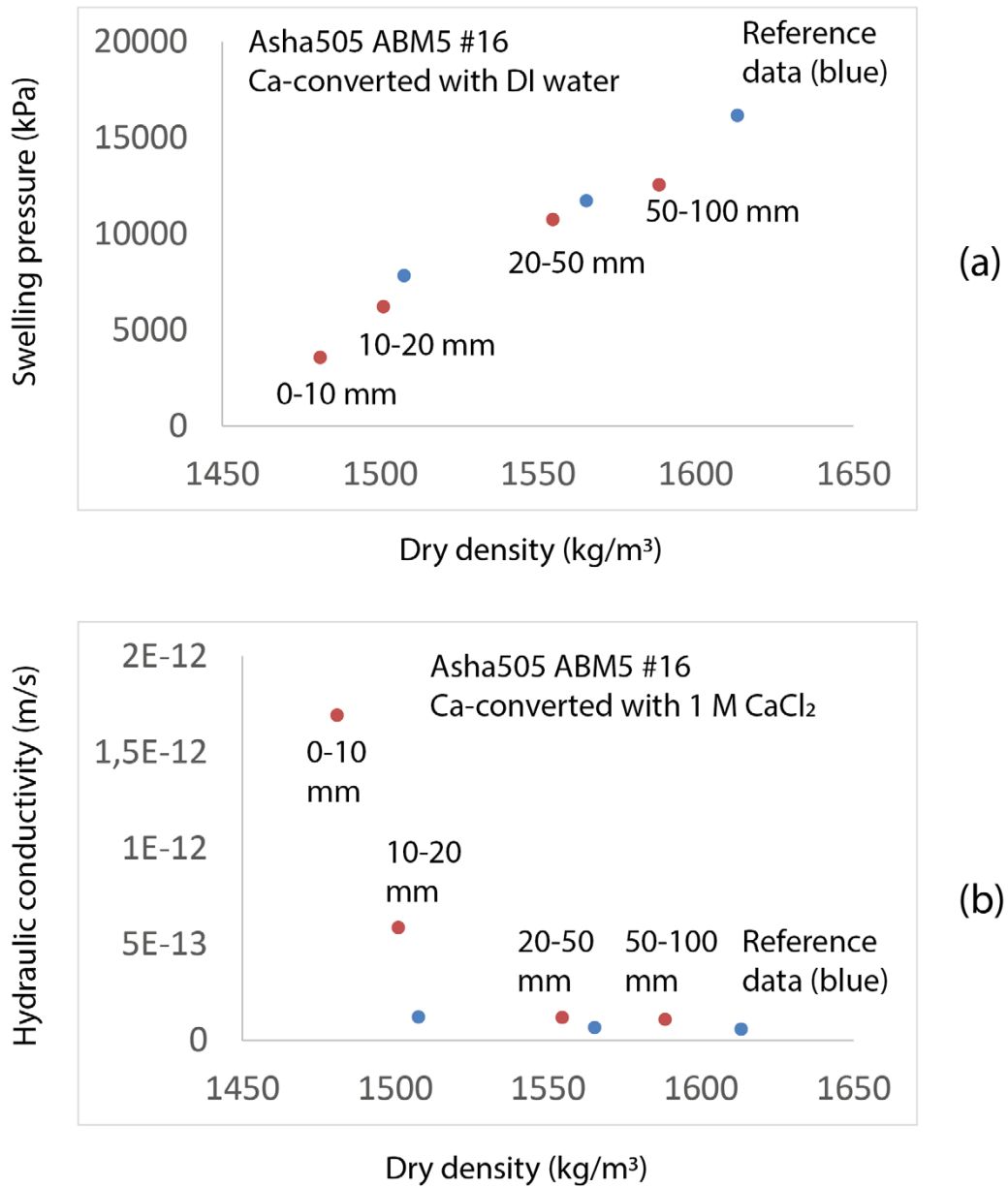


**Figure 7-10.** ABM5 Asha505 #16 samples compared to reference samples. (a) Swelling pressure after Ca-conversion in DI water. (b) Hydraulic conductivity after Ca-conversion in 1 M CaCl<sub>2</sub> solution.

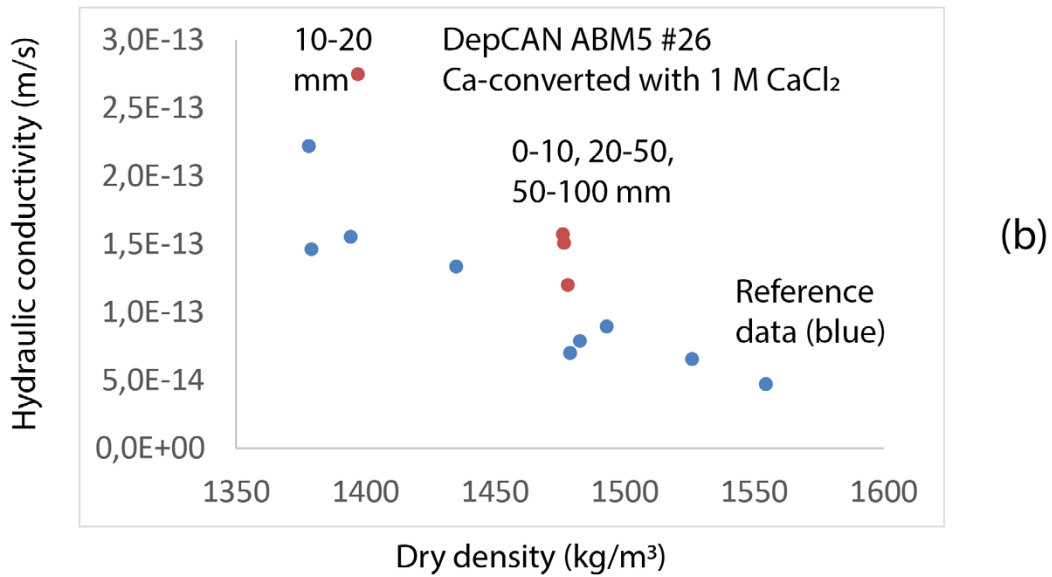
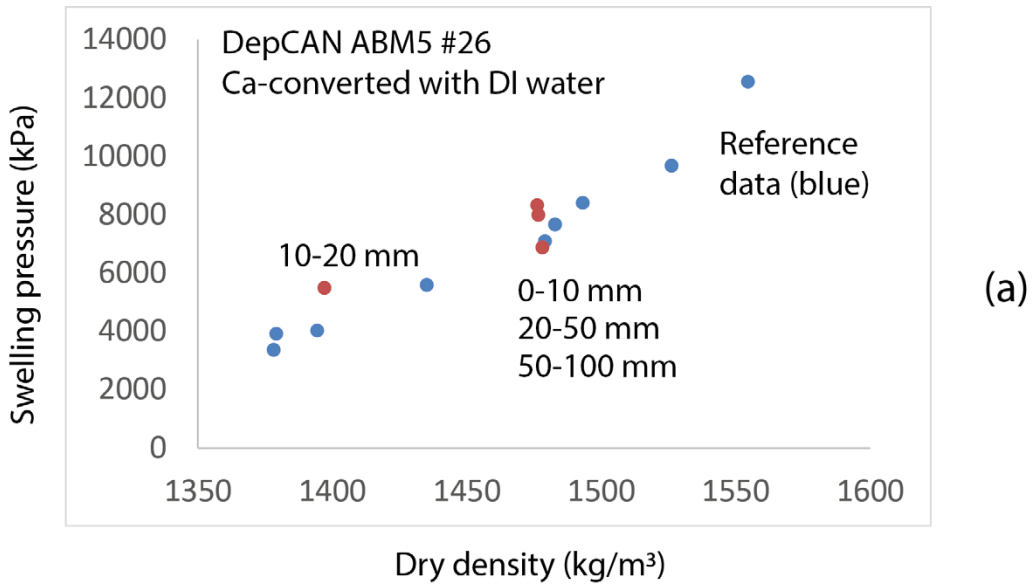


**Figure 7-11.** ABM5 DepCAN #26 samples compared to reference samples. (a) Swelling pressure after Ca-conversion in DI water. (b) Hydraulic conductivity after Ca-conversion in 1 M CaCl<sub>2</sub> solution.

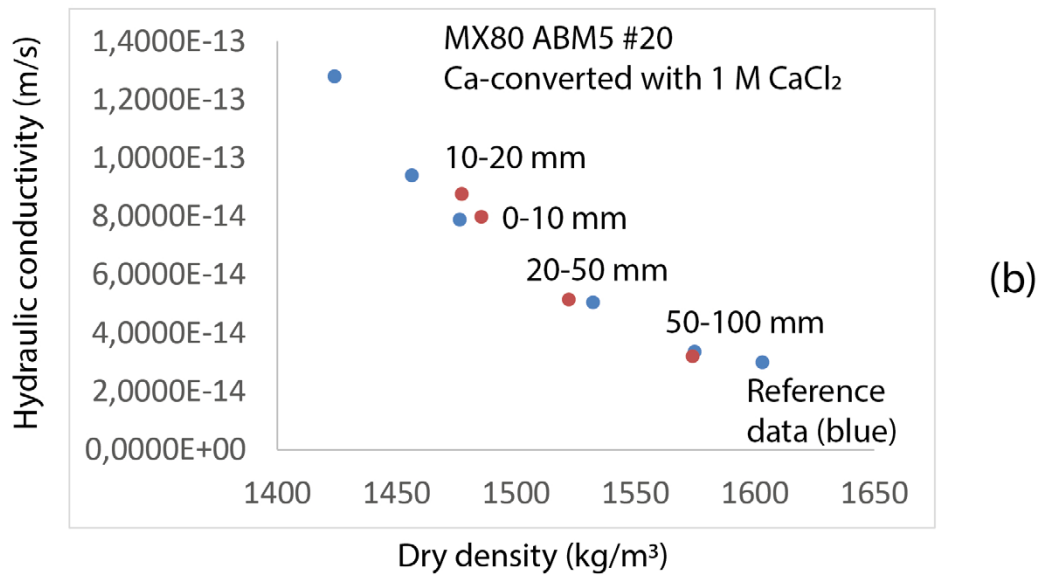
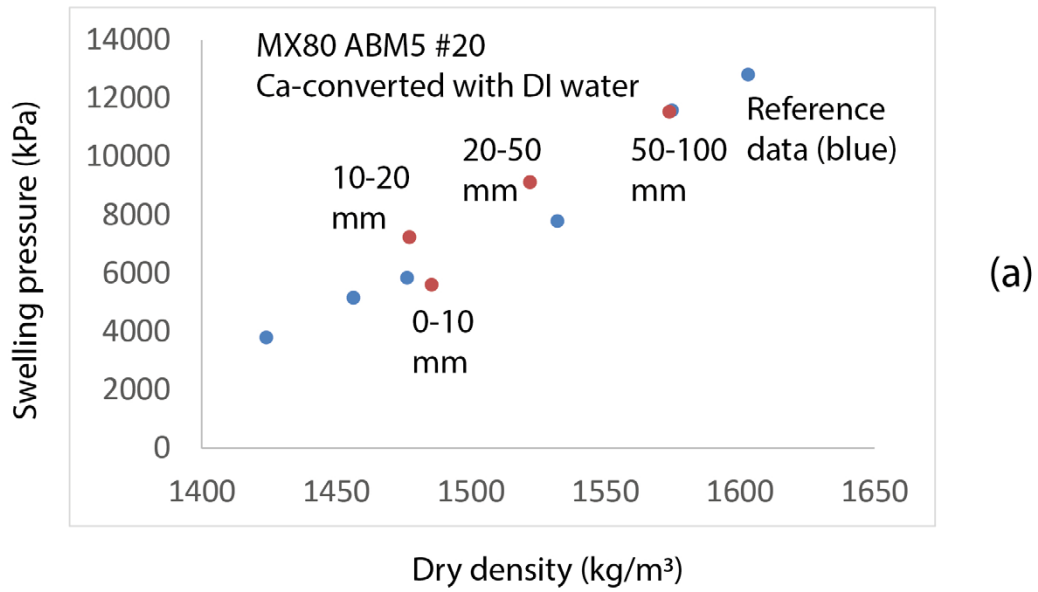


**Figure 7-12.** ABM5 MX-80 #20 samples compared to reference samples. (a) Swelling pressure after Ca-conversion in DI water. (b) Hydraulic conductivity after Ca-conversion in 1 M CaCl<sub>2</sub> solution.

**Table 7-3. Hydraulic conductivity (HC) and swelling pressure (SP) of ABM5 bentonite samples.**

Sample	Dry density (kg/m <sup>3</sup> )	HC DI (m/s)	SP DI (kPa)	HC 1M CaCl <sub>2</sub> (m/s)	SP 1M CaCl <sub>2</sub> (kPa)	SP DI Ca-exch. (kPa)
MX-80 ABM Reference	1456.4	1.27E-13	4765.6	9.41E-14	2990.7	5160.2
MX-80 ABM Reference	1476.4	1.19E-13	5345.9	7.89E-14	3475.2	5838.7
MX-80 ABM Reference	1603.1	7.23E-14	11056.4	3.00E-14	10432.2	12809.0
MX-80 ABM Reference	1424.0	1.39E-13	3701.4	1.28E-13	2129.8	3795.3
MX-80 ABM Reference	1532.2	8.30E-14	7141.5	5.06E-14	5649.7	7789.5
MX-80 ABM Reference	1574.7	4.48E-14	10461.8	3.37E-14	9154.1	11581.7
<b>MX-80 ABM5 #20 0-10 mm</b>	1485.5	1.29E-13	5181.2	7.99E-14	3708.2	5601.8
MX-80 ABM5 #20 10-20 mm	1477.2	1.47E-13	6799.8	8.78E-14	5210.9	7234.1
<b>MX-80 ABM5 #20 20-50 mm</b>	1522.0	1.03E-13	8405.9	5.16E-14	6873.5	9122.1
MX-80 ABM5 #20 50-100 mm	1573.8	8.54E-14	10483.9	3.21E-14	9334.5	11540.2
Deponit CAN Reference	1379.2	2.19E-13	4105.7	1.46E-13	2669.7	3911.6
Deponit CAN Reference	1435.1	1.72E-13	5760.3	1.34E-13	4196.5	5578.6
Deponit CAN Reference	1479.0	1.12E-13	7202.0	7.03E-14	5423.7	7085.8
Deponit CAN Reference	1394.4	2.10E-13	4277.0	1.56E-13	2849.7	4021.9
Deponit CAN Reference	1493.1	9.01E-14	8536.1	8.97E-14	6638.4	8402.7
Deponit CAN Reference	1526.1	5.62E-14	9695.0	6.57E-14	7819.4	9670.6
Deponit CAN Reference	1378.1	2.30E-13	3623.2	2.22E-13	2246.3	3356.2
Deponit CAN Reference	1482.8	8.07E-14	7852.7	7.92E-14	5891.6	7654.3
Deponit CAN Reference	1554.5	6.61E-14	12459.8	4.73E-14	10670.8	12548.8
<b>Deponit CAN ABM5 #26 0-10 mm</b>	1478.1	1.82E-13	6580.8	1.20E-13	5713.4	6866.4
Deponit CAN ABM5 #26 10-20 mm	1397.1	3.70E-13	5294.3	2.75E-13	4524.2	5487.4
<b>Deponit CAN ABM5 #26 20-50 mm</b>	1476.6	2.12E-13	7626.4	1.51E-13	6834.7	7985.7
Deponit CAN ABM5 #26 50-100 mm	1476.2	2.26E-13	7865.7	1.58E-13	7269.6	8318.2
Calcigel ABM Reference	1418.5	4.36E-13	3174.2	4.07E-13	2356.7	2967.5
Calcigel ABM Reference	1468.7	1.74E-13	5359.0	1.52E-13	4053.9	5170.0
Calcigel ABM Reference	1519.6	2.09E-14	7463.8	1.10E-13	5885.1	7215.2
Calcigel ABM Reference	1410.7	6.37E-13	2840.4	6.19E-13	1997.5	2659.4
Calcigel ABM Reference	1386.0	8.72E-13	2711.9	7.80E-13	1818.1	2494.8
Calcigel ABM Reference	1425.7	4.72E-13	3264.9	4.58E-13	2297.1	3064.8
Calcigel ABM Reference	1480.5	2.55E-13	4493.8	2.31E-13	3414.8	4304.3
Calcigel ABM Reference	1578.3	9.81E-14	8954.4	8.21E-14	7467.0	8722.2
Calcigel ABM Reference	1613.2	7.17E-14	11393.0	4.61E-14	9772.3	11188.7
<b>Calcigel ABM5 #27 0-10 mm</b>	1381.4	5.90E-12	2649.4	1.47E-12	2278.2	2844.5
Calcigel ABM5 #27 10-20 mm	1353.0	4.57E-12	2638.9	1.14E-12	2321.0	2819.5
Calcigel ABM5 #27 20-50 mm	1385.3	1.90E-11	3649.1	4.69E-12	3372.7	3915.5
<b>Calcigel ABM5 #27 50-100 mm</b>	1346.8	2.89E-11	4140.2	6.92E-12	3740.2	4272.2
Calcigel ABM5 #27 10-20 mm	1506.5	9.62E-13	7640.5	5.86E-13	7581.7	8328.5
<b>Calcigel ABM5 #27 20-50 mm</b>	1477.2	3.49E-12	7743.1	2.69E-12	7640.0	8228.4
Calcigel ABM5 #27 50-100 mm	1503.1	2.67E-12	9797.9	1.93E-12	9673.0	10404.5
Asha505 ABM Reference	1507.6	1.65E-13	7554.5	1.23E-13	7020.9	7834.2
Asha505 ABM Reference	1565.3	1.04E-13	10989.2	6.70E-14	10883.0	11728.5
Asha505 ABM Reference	1613.2	8.02E-14	14816.2	5.87E-14	15443.9	16158.8
<b>Asha505 ABM5 #16 0-10 mm</b>	1481.0	1.37E-12	3644.9	1.69E-12	2587.9	3565.0
Asha505 ABM5 #16 10-20 mm	1501.1	7.43E-13	5552.7	5.87E-13	5361.1	6221.2
<b>Asha505 ABM5 #16 20-50 mm</b>	1554.7	1.90E-13	9892.2	1.19E-13	9897.8	10756.6
Asha505 ABM5 #16 50-100 mm	1588.4	1.87E-13	11571.5	1.09E-13	11624.5	12555.2

## 8 ABM5 external results

### 8.1 Unconfined compression tests on bentonites from test package 5

#### 8.1.1 General

This chapter presents results of mechanical analyses of bentonite buffer from the field experiment test series ABM45 test package 5 (ABM 5). The effects of repository-like conditions on the bentonite were investigated by comparing the properties of the exposed bentonite with those of the reference material.

The material from the field experiment was analysed by unconfined compression tests. The specimens from the field experiment were crushed, ground and re-compacted, and for the reference tests compacted material from the installation of test series ABM45 was used. The test types were chosen to follow the program previously used after dismantling of large-scale field tests at Äspö HRL in Sweden including test package 1 (ABM 1) in the test series ABM 1–3. The analyses were performed at Clay Technology on material delivered from SKB 2021-06-30.

#### *Test plan for the hydro-mechanical analyses*

In this study, samples from four blocks from ABM 5 were analysed together with samples from the reference material. The reference material was taken from ABM45 reference material which was saved from the manufacturing of blocks 2012. Unconfined compressive strength was determined on crushed and re-compacted specimens from the field experiment and on compacted specimens from the reference material. The testing programme and the dimensions of the specimens were decided together with SKB. The number of tests and the type of preparation for the tests are summarized in Table 8-1. Photos of the samples are provided in Appendix 1.

**Table 8-1. The number of unconfined compression tests on each of the four materials. The materials are given with block numbers together with positions of the specimens and the types of preparation. The height of the specimens was 20 mm and the diameter 20 mm. The positions were measured from the inner mantle surface.**

Material	Block no.	Position	Preparation	Number of specimens	
				only saturated	ion-exchanged
Asha505	16	20, 40, 80	crushed/recompacted	6	4
MX-80	20	20, 40, 80	crushed/recompacted	6	4
DepCaN	26	mixed	crushed/recompacted	6	4
Calcigel	27	mixed	crushed/recompacted	6	4
Asha505	reference		compacted	4	3
MX-80	reference		compacted	4	3
DepCaN	reference		compacted	4	2
Calcigel	reference		compacted	4	2
<b>Sum</b>				<b>40</b>	<b>26</b>

#### *Denomination of specimens*

Each test has a unique Test ID. The denomination of the material from the field experiment consists of the test package and block number followed by the radial distance in mm from the inner mantle surface. For example, the material AB5-20-20 refers to test series ABM 45 package ABM 5 and block number 20 where the sample was taken 20 mm from the inner mantle surface.

Two of the delivered materials were in pieces at the delivery and material from different distances was mixed to represent the whole profile, denominated AB5-26-50 and AB5-27-50. The reference material used, from the installation of test series ABM 45, was denominated with the test package and the block number, e.g. AB5-27 Ref.

### **Type of water**

The water used for the saturation before the unconfined compression tests was the formation water also used for the specimens analysed after dismantling of ABM 1 (i.e. from borehole KA2598A). The solution used had a concentration of 0.1 M Na and 0.06 M Ca.

ABM 5 was probably saturated with formation water shortly after installation. When the heating started the profile dried out due to leakage and the degree of saturation was between 60 and 92 % in the actual materials at the dismantling.

### **Determination of water content and density**

The base variables water content  $w$  (%), dry density  $\rho_d$  ( $\text{kg/m}^3$ ) and degree of saturation  $S_r$  (%) or determination of degree of saturation, the particle densities from Table 8-2 were used together with the water density  $\rho_w = 1000 \text{ kg/m}^3$ .

**Table 8-2. Particle density of the materials used (Table 4-2).**

<b>Material</b>	<b>Block no.</b>	<b>Particle density <math>\text{kg/m}^3</math></b>
Asha505	16	2869
MX-80	20	2780
Deponit CA-N	26	2750
Calcigel	27	2695

## **8.1.2 Unconfined compression tests**

### **General**

The unconfined compression test is an experimentally simple method where a cylindrical specimen is compressed axially with a constant rate of displacement with no radial confinement or external radial stress. With the test the unconfined compressive strength or the maximum deviator stress of the specimen is determined. The strength is commonly determined on specimens having the height equal to double the size of the diameter to allow the failure surface to fully develop. In this study the height was equal to the diameter to keep the time to saturation as low as possible. To minimize the end effect on these short specimens, lubrication of the end surfaces was made. Short specimens have previously been used and further commented in the CRT and TBT projects (Dueck et al. 2011 and Åkesson et al. 2012).

Four different materials from four blocks, see Table 8-1, were tested. All samples from the field experiment were ground and re-compacted to predetermined densities and the reference material was compacted to densities of the same range. The specimens were saturated before the unconfined compression tests which was done by two different methods, described below.

### **Test equipment**

The saturation was done in specially designed saturation devices for 10 or 6 specimens at a time. During the compression test the specimens were placed in a mechanical press according to Figure 8-1 where a constant rate of displacement was applied. The end surfaces were lubricated to minimize the end effects. During the tests the displacement and the applied force were measured by means of a deformation transducer and a load cell. All transducers were calibrated prior to the shearing of one series and checked afterwards.

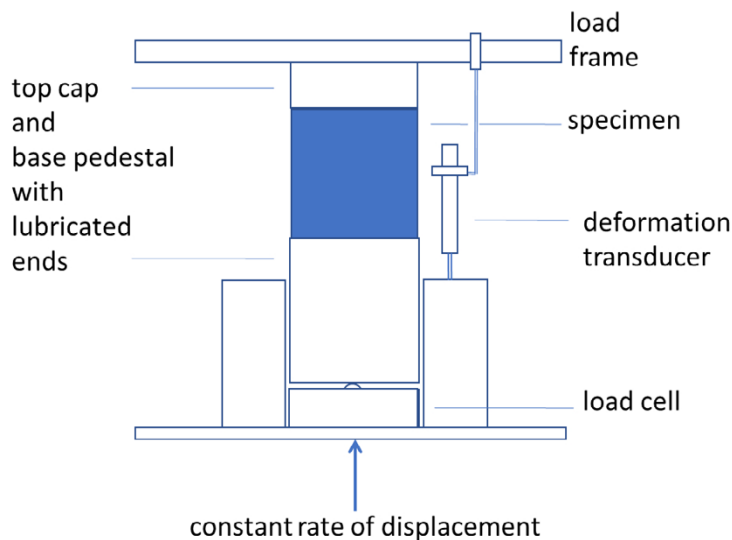


**Figure 8-1.** Set-up for the unconfined compression test.

### **Preparation of specimen and test procedure**

Tests were made on material both from the field experiment and from the reference material. The specimens were prepared in two different ways:

- ground to a grain size less than 1.5 mm and then re-compacted.
- compacted from powder samples.

The material from the field experiment was prepared by the first method and the dry density aim of the re-compacted specimens was between 1 480 and 1 520 kg/m<sup>3</sup>. The reference material was prepared by the second method in the bullet list above aiming at dry densities between 1 420 and 1 580 kg/m<sup>3</sup>.

The diameter of all specimens was 20 mm and the final height was 20 mm. All specimens were prepared in a saturation device before the tests. Two different types of preparation were used for the specimens; they were either saturated with ABM-water or ion-exchanged with 1M CaCl<sub>2</sub>. The ABM-water used is defined in Section 8.1.1.

The specimens saturated with ABM-water were exposed to circulating ABM-water, above and under the specimens, over a short period of time but as stagnant water during the main part of the time. The time used for the saturation was 27–34 days. The specimens, ion-exchanged with 1M CaCl<sub>2</sub>, were prepared for 77–93 days according to the following steps:

1. Saturation by stagnant ABM-water and circulation during shorter time periods, to remove air trapped in the filters, for approximately 5 days.
2. Ion-exchange to be calcium-dominated by continuous circulation of 1M CaCl<sub>2</sub> for approximately 40 days.
3. Removing excess salt by continuous circulation of de-ionized water (DI-water) for 30–50 days until low electrical conductivity.
4. End of test and dismantling for the unconfined compression test.

The time used for the ion-exchange was calculated to correspond approximately to get 80 % ion-exchange in the central part of the specimens. The time used for the circulation of DI-water, to remove excess salt, was chosen to get low electrical conductivity, less than 0.1 mS/cm. After the preparation, all specimens were removed from the saturation device at least 12 h before the shearing to homogenize while protected from evaporation.

The specimens were placed in a mechanical press and the compression was run at a constant deformation rate of 0.16 mm/min which corresponds to a strain rate of 0.8 %/min. The specimens were placed between lubricated end plates and were surrounded by a thin plastic film to minimize evaporation during shearing. After failure the water content and density were determined on all specimens.

The specimens were undrained during shearing and no volume change was taken into account. The deviator stress  $q$  (kPa) and the strain  $\varepsilon$  (%) were derived according to:

$$q = \frac{F}{A_0} \cdot \left( \frac{l_0 - \Delta l}{l_0} \right) \quad \text{(Equation 8-1)}$$

$$\varepsilon = \frac{\Delta l}{l_0} \quad \text{(Equation 8-2)}$$

where  $F$  is the applied vertical load (kN),  $A_0$  is the original cross section area (m<sup>2</sup>),  $l_0$  is the original length (m) and  $\Delta l$  is the change in length (m). The results were corrected for initial problems with the contact surface by decreasing the strain with the intercept on the x-axis of the tangent to the stress-strain curve taken at a stress of 500 kPa.

### 8.1.3 Results

#### **General**

Unconfined compression tests on specimens of Asha505, MX-80, Deponit CA-N and Calcigel were run. The corresponding blocks are 16, 20, 26 and 27, see Table 8-1. The specimens were prepared in two different ways according to Section 8.1.2. They were either saturated with ABM-water or they were saturated with ABM-water and subsequently ion-exchanged to be calcium dominated.

Below results are presented in tables and diagrams. The tables show the maximum deviator stress and the corresponding strain for each specimen together with the dry density, water content and degree of saturation. Each test is presented with a Test ID and the type of material used for the test, see Section 8.1.1. The materials from the field experiment are given with the distance from the heater. In addition, the type of preparation and type of water used are also given. Additional results can be found in Appendix 2.

In the diagrams, different colours (green, blue, red, orange) are used for the different materials (Asha505, MX-80, Deponit CA-N, Calcigel) and the markers (circles, diamonds) show the type of material (material from the field experiment, reference material).

#### **Results of specimens saturated with ABM-water**

The results are given in Table 8-3 with the maximum deviator stress and the corresponding strain for each specimen presented with the dry density, water content and degree of saturation. The results are also shown in Figure 8-2 to Figure 8-5 where the different colours are used for the different materials and the markers circles and diamonds show specimens from the field experiment and from the reference material, respectively.

**Table 8-3. Maximum deviator stress and corresponding strain resulting from unconfined compression tests. All specimens had a height equal to the diameter. For each specimen the Test ID and material are given together with dry density and water content after dismantling. The positions of the specimens from the field experiment are given with block number and radial distance.**

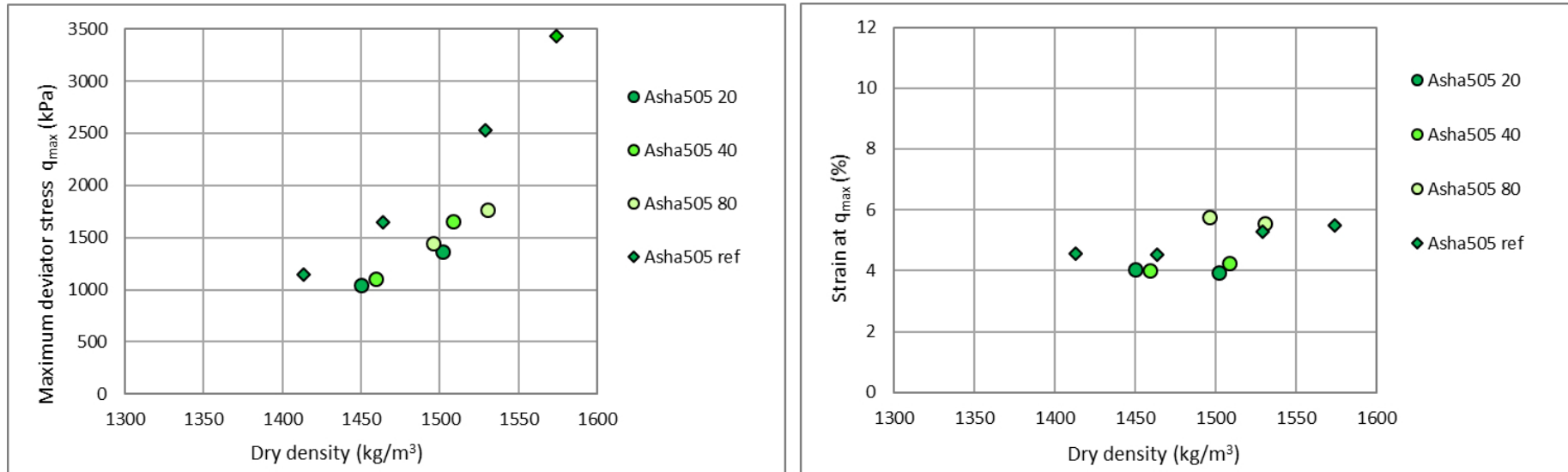
Test ID	Type of material	Material	Block	Radial distance mm	Preparation	Saturation fluid	Dry density kg/m <sup>3</sup>	Water content %	Deg of saturation %	Max deviator stress kPa	Corresponding strain %
UC5-1	Asha505	AB5-16-20	16	20	ground/recomp	ABM-water	1450	31.3	92	1050	4.0
UC5-2	Asha505	AB5-16-20	16	20	ground/recomp	ABM-water	1500	30.4	96	1370	4.0
UC5-3	Asha505	AB5-16-40	16	40	ground/recomp	ABM-water	1460	32.0	95	1110	4.0
UC5-4	Asha505	AB5-16-40	16	40	ground/recomp	ABM-water	1510	30.1	96	1660	4.3
UC5-5	Asha505	AB5-16-80	16	80	ground/recomp	ABM-water	1500	29.9	94	1440	5.8
UC5-6	Asha505	AB5-16-80	16	80	ground/recomp	ABM-water	1530	29.4	97	1760	5.5
UC5-7	Asha505	AB5-16 Ref			comp	ABM-water	1410	34.8	97	1140	4.6
UC5-8	Asha505	AB5-16 Ref			comp	ABM-water	1460	32.6	97	1650	4.5
UC5-9	Asha505	AB5-16 Ref			comp	ABM-water	1530	29.9	98	2530	5.3
UC5-10	Asha505	AB5-16 Ref			comp	ABM-water	1570	28.0	98	3430	5.5
UC4-1	MX-80	AB5-20-20	20	20	ground/recomp	ABM-water	1470	31.9	100	1290	8.2
UC4-2	MX-80	AB5-20-20	20	20	ground/recomp	ABM-water	1510	29.9	98	1550	8.0
UC4-3	MX-80	AB5-20-40	20	40	ground/recomp	ABM-water	1460	32.2	99	1320	8.1
UC4-4	MX-80	AB5-20-40	20	40	ground/recomp	ABM-water	1510	29.6	98	1680	8.0
UC4-5	MX-80	AB5-20-80	20	80	ground/recomp	ABM-water	1490	31.1	100	1460	9.8
UC4-6	MX-80	AB5-20-80	20	80	ground/recomp	ABM-water	1530	28.9	98	1840	9.6
UC4-7	MX-80	AB5-20 Ref			comp	ABM-water	1420	34.1	99	1100	8.2
UC4-8	MX-80	AB5-20 Ref			comp	ABM-water	1460	31.6	97	1460	8.2
UC4-9	MX-80	AB5-20 Ref			comp	ABM-water	1530	28.8	99	1970	7.9
UC4-10	MX-80	AB5-20 Ref			comp	ABM-water	1560	27.9	99	2310	7.7
UC6-1	DepCAN	AB5-26-50	26	0–100 <sup>1</sup>	ground/recomp	ABM-water	1400	34.6	99	1150	4.9
UC6-2	DepCAN	AB5-26-50	26	0–100 <sup>1</sup>	ground/recomp	ABM-water	1430	33.0	98	1420	4.8
UC6-3	DepCAN	AB5-26-50	26	0–100 <sup>1</sup>	ground/recomp	ABM-water	1470	31.5	100	1890	5.4
UC6-4	DepCAN	AB5-26-50	26	0–100 <sup>1</sup>	ground/recomp	ABM-water	1480	30.3	96	2040	5.1
UC6-5	DepCAN	AB5-26-50	26	0–100 <sup>1</sup>	ground/recomp	ABM-water	1520	28.7	97	2470	4.8
UC6-6	DepCAN	AB5-26-50	26	0–100 <sup>1</sup>	ground/recomp	ABM-water	1530	28.8	100	2520 <sup>2</sup>	3.6 <sup>2</sup>
UC6-7	DepCAN	AB5-26 Ref			comp	ABM-water	1410	34.9	100	1510	8.5
UC6-8	DepCAN	AB5-26 Ref			comp	ABM-water	1450	33.1	101	1950	8.4
UC6-9	DepCAN	AB5-26 Ref			comp	ABM-water	1510	29.9	100	2790	8.5
UC6-10	DepCAN	AB5-26 Ref			comp	ABM-water	1540	28.4	100	3390	8.5
UC7-1	Calcigel	AB5-27-50	27	0–100 <sup>1</sup>	ground/recomp	ABM-water	1400	32.1	94	460	5.3

Table 8-3. Continued.

Test ID	Type of material	Material	Block	Radial distance mm	Preparation	Saturation fluid	Dry density kg/m <sup>3</sup>	Water content %	Deg of saturation %	Max deviator stress kPa	Corresponding strain %
UC7-2	Calcigel	AB5-27-50	27	0–100 <sup>1</sup>	ground/recomp	ABM-water	1440	31.1	97	630	4.0
UC7-3	Calcigel	AB5-27-50	27	0–100 <sup>1</sup>	ground/recomp	ABM-water	1450	30.2	95	590	4.1
UC7-4	Calcigel	AB5-27-50	27	0–100 <sup>1</sup>	ground/recomp	ABM-water	1460	29.5	95	750	4.5
UC7-5	Calcigel	AB5-27-50	27	0–100 <sup>1</sup>	ground/recomp	ABM-water	1490	28.4	96	860	3.0
UC7-6	Calcigel	AB5-27-50	27	0–100 <sup>1</sup>	ground/recomp	ABM-water	1520	26.9	94	1280	3.3
UC7-7	Calcigel	AB5-27 Ref			comp	ABM-water	1360	33.2	92	980	4.5
UC7-8	Calcigel	AB5-27 Ref			comp	ABM-water	1420	30.4	91	1210	3.5
UC7-9	Calcigel	AB5-27 Ref			comp	ABM-water	1480	28.6	94	1580	3.6
UC7-10	Calcigel	AB5-27 Ref			comp	ABM-water	1530	26.7	95	2060	3.0

<sup>1</sup> A mixture of material from the distances 0–100 mm was used for the tests.

<sup>2</sup> Uncertain value, small damage at dismantling from saturation device.



**Figure 8-2.** Maximum deviator stress and corresponding strain from unconfined compression tests on specimens of Asha505 from block 16 and from the reference material. In the labels the distance from the heater is given in mm. The specimens were saturated with ABM-water.

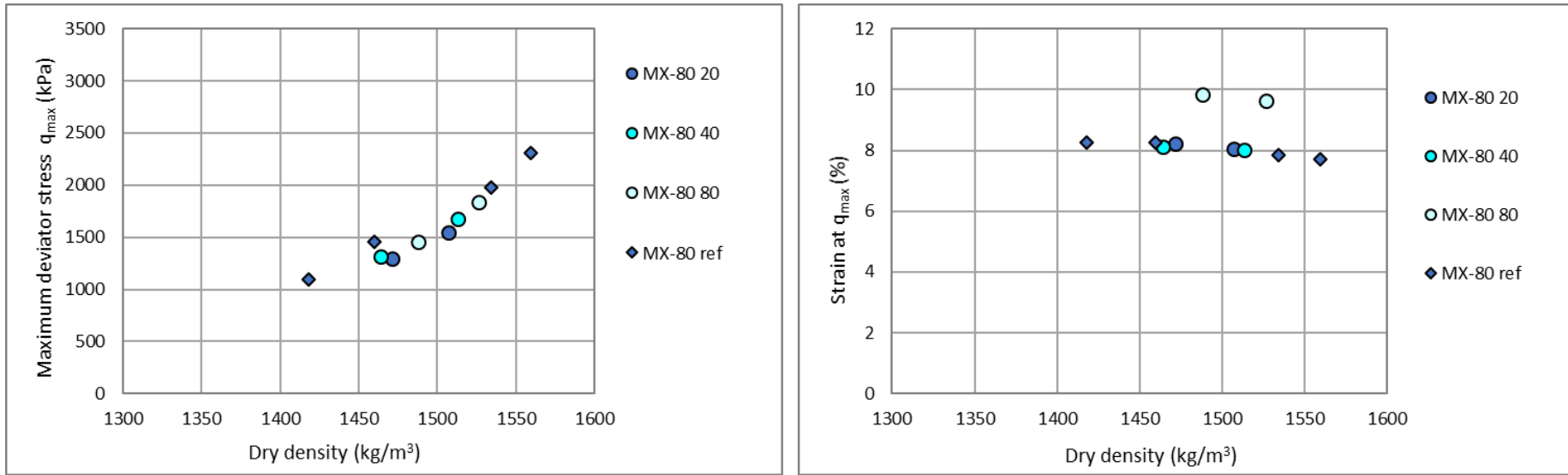


Figure 8-3. Maximum deviator stress and corresponding strain from unconfined compression tests on specimens of MX-80 from block 20 and from the reference material. In the labels the distance from the heater is given in mm. The specimens were saturated with ABM-water.

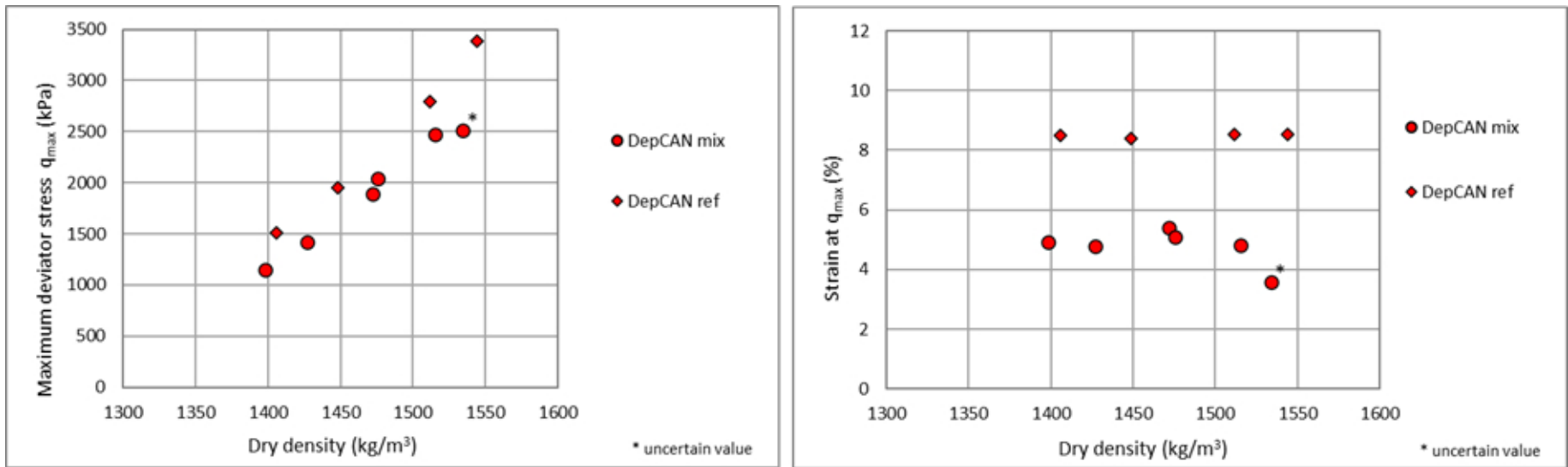
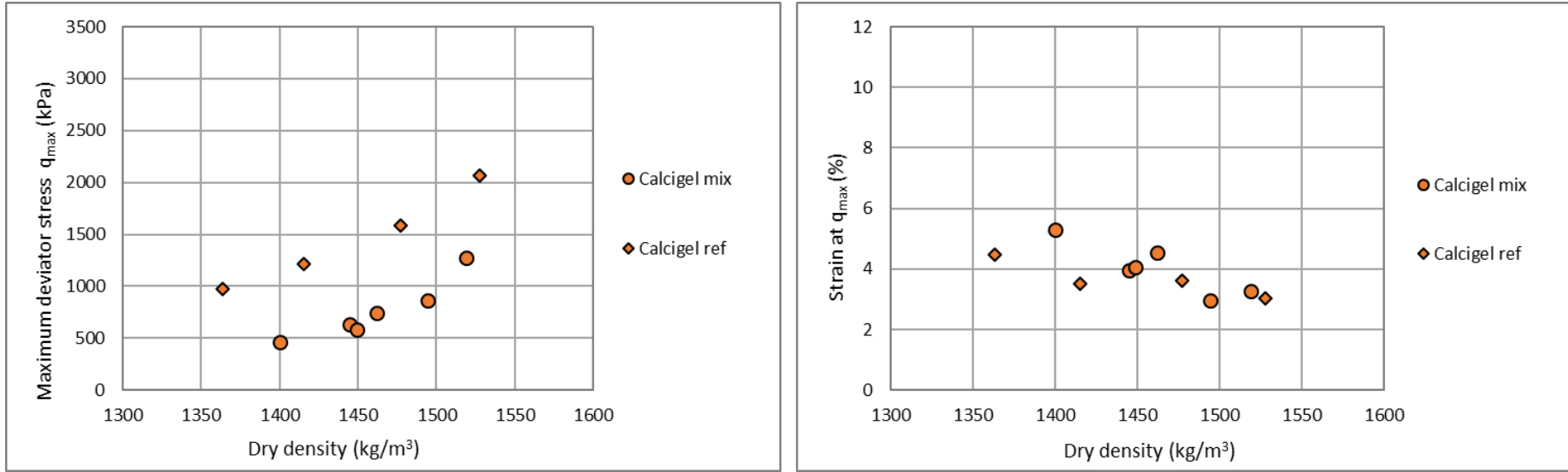


Figure 8-4. Maximum deviator stress and corresponding strain from unconfined compression tests on specimens of Deponit CA-N from block 26 and from the reference material. The specimens were saturated with ABM-water.



**Figure 8-5.** Maximum deviator stress and corresponding strain from unconfined compression tests on specimens of Calcigel from block 27 and from the reference material. The specimens were saturated with ABM-water.

Compared to the references equal or lower maximum deviator stress was seen in all materials. The corresponding strain was approximately the same as the references with the exception of Deponit CA-N where the corresponding strain was clearly lower than the references.

Compared to the references the maximum deviator stress and the corresponding strain differed in the following ways for the different materials:

- In Asha505 specimens the deviator stress was lower, and the corresponding strain approximately the same.
- In MX-80 specimens the deviator stress was somewhat lower, and the corresponding strain was the same or higher.
- In Deponit CA-N specimens the deviator stress was somewhat lower, and the corresponding strain clearly lower.
- In Calcigel specimens the deviator stress was clearly lower, but the correspond strain was approximately the same.

In specimens of Asha505 and MX-80 the influence of position could be evaluated and while no influence was seen on the deviator stress the corresponding strain was higher at the outermost position (at 80 mm) of these two materials.

### ***Results of ion-exchanged specimens***

The results are given in Table 8-4 with the maximum deviator stress and the corresponding strain for each specimen presented with the dry density, water content and degree of saturation. The results are also shown in Figure 8-6 to Figure 8-9 where the different colours are used for the different materials and the markers circles and diamonds show specimens from the field experiment and from the reference material, respectively. The abbreviation ie used in the table and diagrams denote that the specimen was ion-exchanged to be calcium dominated.

**Table 8-4. Maximum deviator stress and corresponding strain resulting from unconfined compression tests. All specimens had a height equal to the diameter. For each specimen the Test ID and material are given together with dry density and water content after dismantling. The specimens were ion-exchanged to be calcium dominated which is denoted by the abbreviation ie. The positions of the specimens from the field experiment are given with block number and radial distance.**

Test ID	Type of material	Material	Block	Radial distance mm	Preparation	Saturation fluid <sup>1</sup>	Dry density kg/m <sup>3</sup>	Water content %	Deg of saturation %	Max deviator stress kPa	Corresponding strain %
UC1-6	Asha505 ie	AB5-16-20	16	20	ground/recomp	ABM-water/CaCl <sub>2</sub> /DI-water	1440	31.6	94	960	8.8
UC1-7	Asha505 ie	AB5-16-20	16	20	ground/recomp	ABM-water/CaCl <sub>2</sub> /DI-water	1480	31.2	95	1320	8.3
UC1-8	Asha505 ie	AB5-16-40	16	40	ground/recomp	ABM-water/CaCl <sub>2</sub> /DI-water	1430	32.9	94	910	6.4
UC1-9	Asha505 ie	AB5-16-40	16	40	ground/recomp	ABM-water/CaCl <sub>2</sub> /DI-water	1480	31.0	94	1270	6.3
UC1-10	Asha505 ie	AB5-16 Ref			comp	ABM-water/CaCl <sub>2</sub> /DI-water	1420	33.6	94	1220	5.8
UC3-2	Asha505 ie	AB5-16 Ref			comp	ABM-water/CaCl <sub>2</sub> /DI-water	1550	29.0	97	3100	6.4
UC3-6	Asha505 ie	AB5-16 Ref			comp	ABM-water/CaCl <sub>2</sub> /DI-water	1440	33.0	96	1520	5.7
UC1-1	MX-80 ie	AB5-20-20	20	20	ground/recomp	ABM-water/CaCl <sub>2</sub> /DI-water	1470	31.7	99	1380	11.3
UC1-2	MX-80 ie	AB5-20-20	20	20	ground/recomp	ABM-water/CaCl <sub>2</sub> /DI-water	1510	29.7	101	1660	7.2
UC1-3	MX-80 ie	AB5-20-40	20	40	ground/recomp	ABM-water/CaCl <sub>2</sub> /DI-water	1460	31.9	100	1380	8.4
UC1-4	MX-80 ie	AB5-20-40	20	40	ground/recomp	ABM-water/CaCl <sub>2</sub> /DI-water	1490	29.0	97	1660	8.7
UC1-5	MX-80 ie	AB5-20 Ref			comp	ABM-water/CaCl <sub>2</sub> /DI-water	1460	30.7	96	1560	8.8
UC3-1	MX-80 ie	AB5-20 Ref			comp	ABM-water/CaCl <sub>2</sub> /DI-water	1580	26.4	97	2970	7.4
UC3-5	MX-80 ie	AB5-20 Ref			comp	ABM-water/CaCl <sub>2</sub> /DI-water	1490	30.5	98	1920	8.6
UC2-1	DepCAN ie	AB5-26-50	26	0–100 <sup>3</sup>	ground/recomp	ABM-water/CaCl <sub>2</sub> /DI-water	1470	31.6	99	1720	6.6
UC2-2	DepCAN ie	AB5-26-50	26	0–100 <sup>3</sup>	ground/recomp	ABM-water/CaCl <sub>2</sub> /DI-water	1500	29.9	100	1410	4.8
UC2-3	DepCAN ie	AB5-26-50	26	0–100 <sup>3</sup>	ground/recomp	ABM-water/CaCl <sub>2</sub> /DI-water	1450	31.0	97	1580	7.3
UC2-4	DepCAN ie	AB5-26-50	26	0–100 <sup>3</sup>	ground/recomp	ABM-water/CaCl <sub>2</sub> /DI-water	1490	30.3	101	2010	6.7
UC2-5	DepCAN ie	AB5-26 Ref			comp	ABM-water/CaCl <sub>2</sub> /DI-water	1470	30.7	99	2240 <sup>4</sup>	8.0 <sup>4</sup>
UC3-3	DepCAN ie	AB5-26 Ref			comp	ABM-water/CaCl <sub>2</sub> /DI-water	1540	28.6	100	3320	9.0
UC2-6 <sup>5</sup>	Calcigel ie	AB5-27-50	27	0–100 <sup>3</sup>	ground/recomp	ABM-water/CaCl <sub>2</sub> /DI-water	1470	30.1	99	690	3.9
UC2-7	Calcigel ie	AB5-27-50	27	0–100 <sup>3</sup>	ground/recomp	ABM-water/CaCl <sub>2</sub> /DI-water	1450	29.4	92	640	5.0
UC2-8 <sup>2</sup>	Calcigel ie	AB5-27-50	27	0–100 <sup>3</sup>	ground/recomp	ABM-water/CaCl <sub>2</sub> /DI-water	1410	31.4	93		
UC2-9 <sup>2</sup>	Calcigel ie	AB5-27-50	27	0–100 <sup>3</sup>	ground/recomp	ABM-water/CaCl <sub>2</sub> /DI-water	1470	30.0	98		
UC2-10	Calcigel ie	AB5-27 Ref			comp	ABM-water/CaCl <sub>2</sub> /DI-water	1410	31.5	93	1240	3.4
UC3-4	Calcigel ie	AB5-27 Ref			comp	ABM-water/CaCl <sub>2</sub> /DI-water	1480	28.1	92	2060	4.5

<sup>1</sup> The specimens were saturated with ABM-water, ion-exchanged with 1M CaCl<sub>2</sub> and excess salt was washed out with de-ionized water, see Section 8.1.2.

<sup>2</sup> No test results. specimens in pieces before the test. <sup>3</sup> A mixture of material from the distances 0–100 mm was used for the tests.

<sup>4</sup> Uncertain data, the specimen was tested twice. <sup>5</sup> Problem with data acquisition for this specimen.

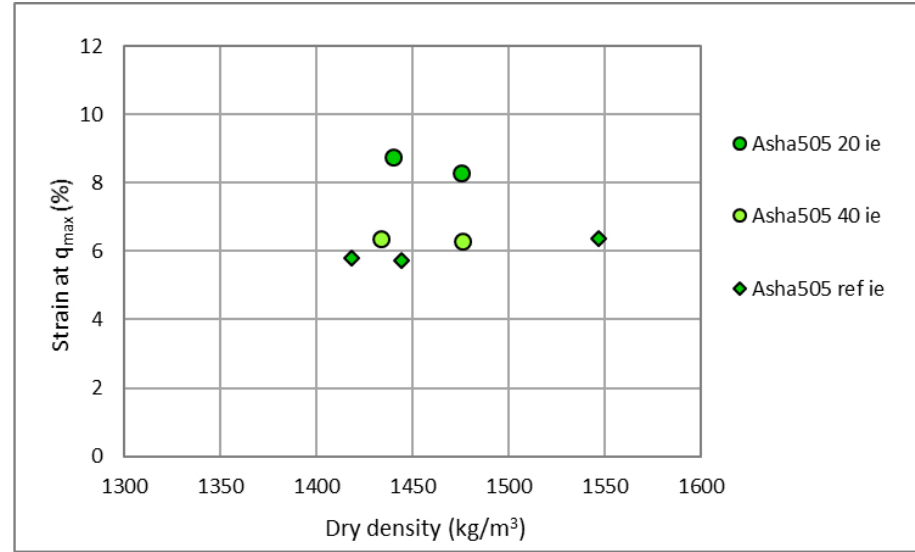
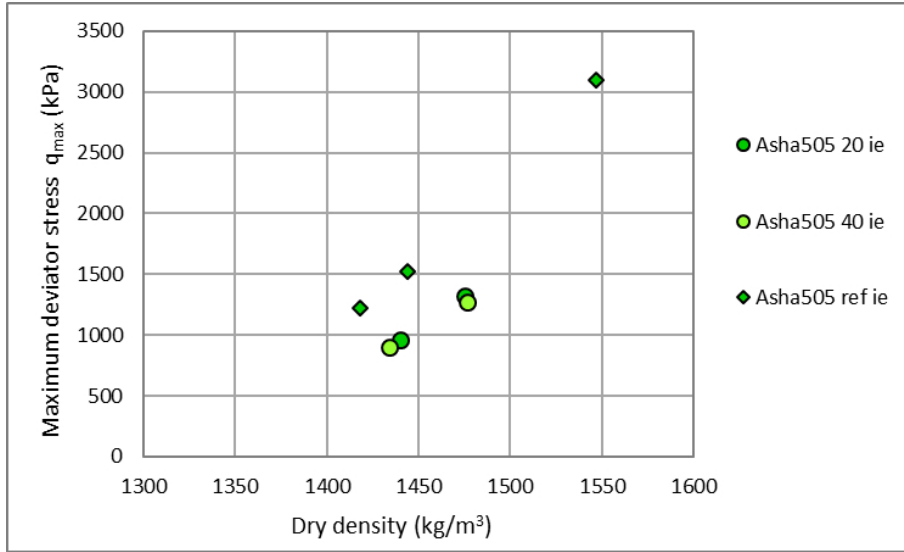


**Figure 8-6.** Maximum deviator stress and corresponding strain from unconfined compression tests on specimens of Asha505 from block 16 and from the reference material. In the labels the distance from the heater is given in mm and ie denotes that the specimens were ion-exchanged to be calcium dominated.

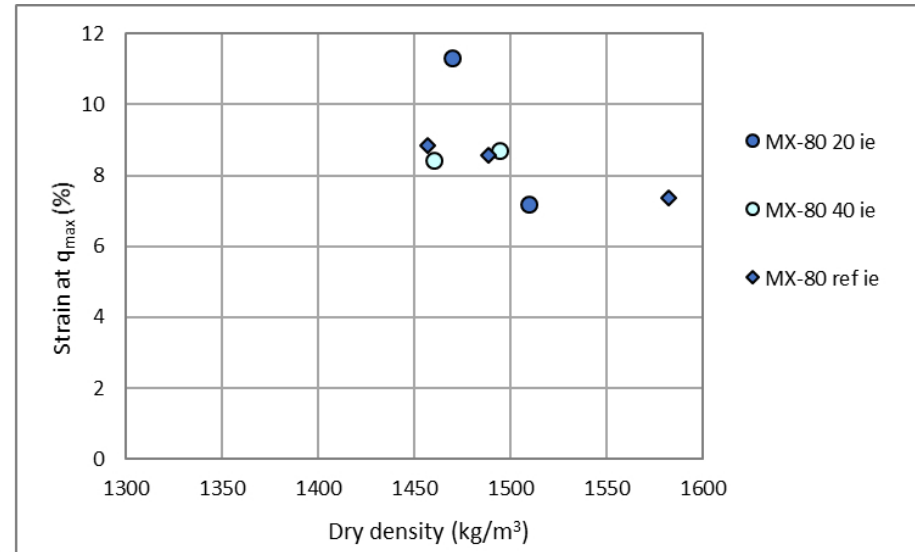
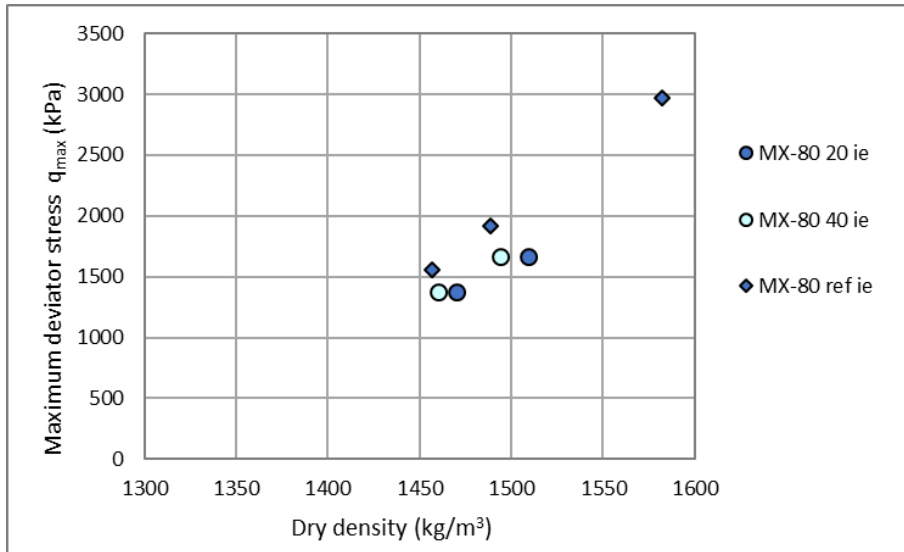


**Figure 8-7.** Maximum deviator stress and corresponding strain from unconfined compression tests on specimens of MX-80 from block 20 and from the reference material. In the labels the distance from the heater is given in mm and ie denotes that the specimens were ion-exchanged to be calcium dominated.

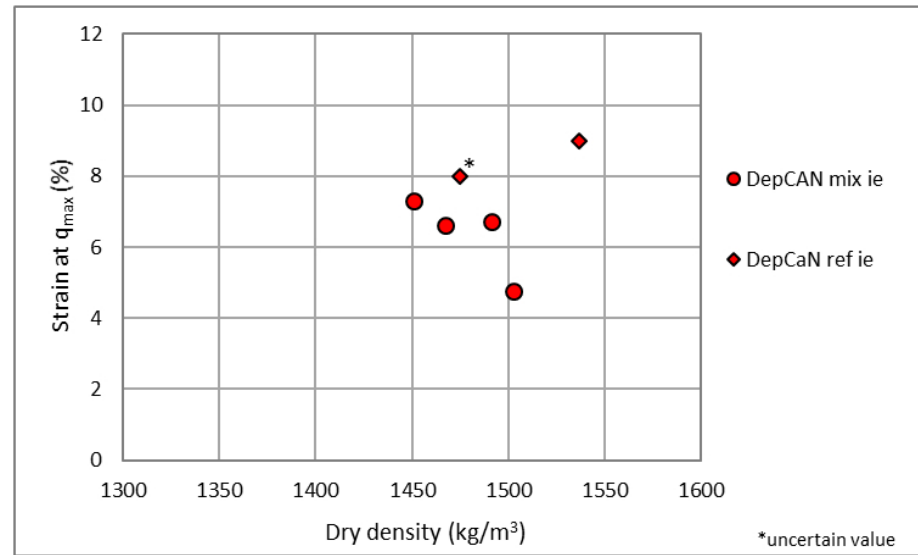
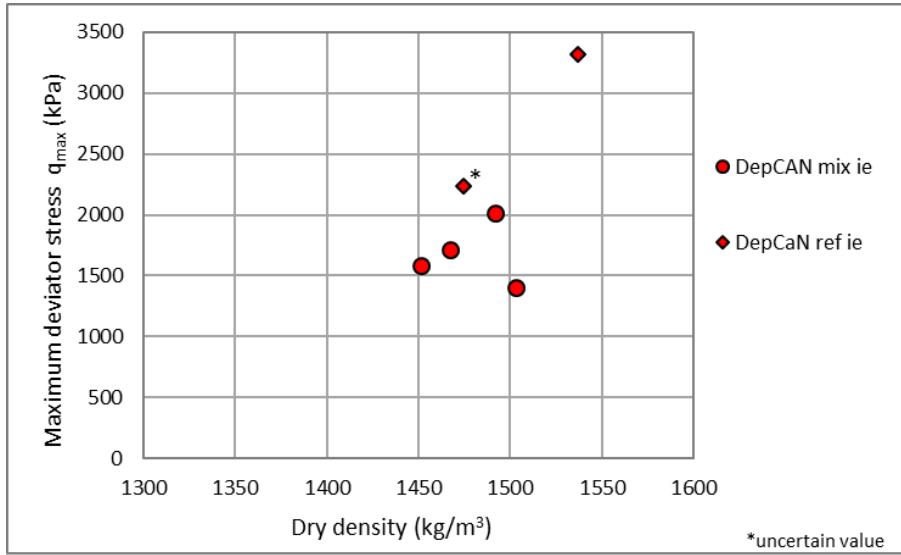


**Figure 8-8.** Maximum deviator stress and corresponding strain from unconfined compression tests on specimens of Deponit CA-N from block 26 and from the reference material. The specimens were ion-exchanged to be calcium dominated (ie).

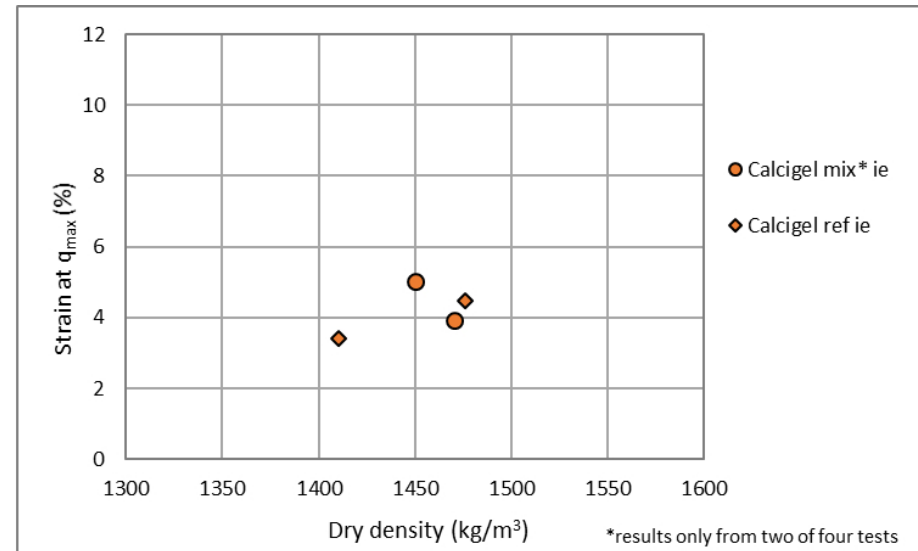
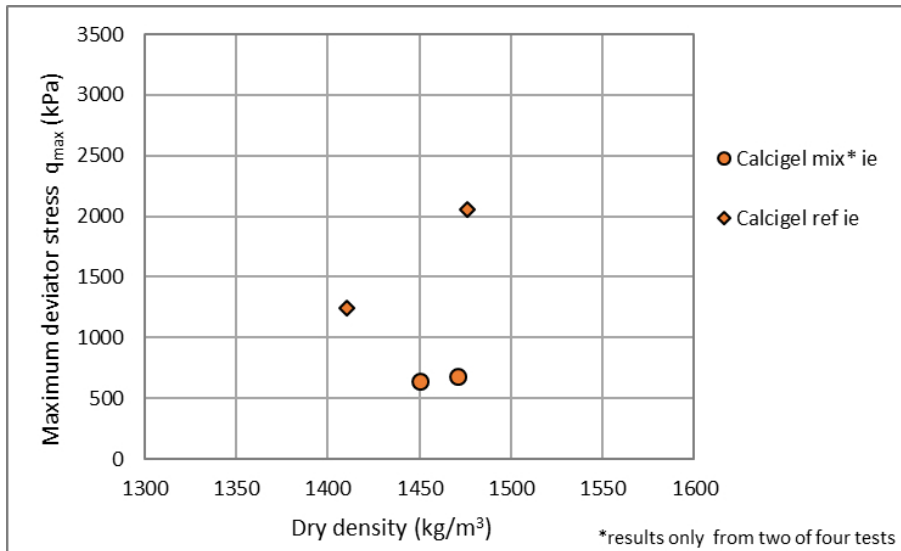


**Figure 8-9.** Maximum deviator stress and corresponding strain from unconfined compression tests on specimens of Calcigel from block 27 and from the reference material. The specimens were ion-exchanged to be calcium dominated (ie).

The specimens of Calcigel were brittle to handle and only two out of four specimens could be tested since they fell apart at dismantling.

Compared to the references lower maximum deviator stress was seen in all materials. No large differences in the corresponding strain compared to the references, however with a large scatter, and examples of higher strain (Asha505) and lower strain (Deponit CA-N).

### ***Discussion***

In Figure 8-10 to Figure 8-13 the results from specimens saturated with ABM-water (markers with black marker lines) are plotted together with the results from ion exchanged specimens (markers without marker lines). All results were shown above. The colours and markers used are the same as in the previous sections where different colours are used for the different materials and the markers circles and diamonds show specimens from the field experiment and from the reference material, respectively.

The deviator stress seemed to be independent of which method was used for the preparation, i.e. if ion-exchange was made or not. This was seen both in the references and in the specimens from the field experiment. In general and compared to the references equal or lower maximum deviator stress was seen in all materials.

The corresponding strain of the reference specimens seemed also to be independent of whether ion-exchange was made or not. However, the corresponding strain of specimens from the field experiment showed somewhat higher values in specimens of Asha505, MX-80 and Deponit CA-N when ion-exchanged while no difference between ion-exchanged and not ion-exchanged specimens was seen in the results of Calcigel. In general and compared to the references a scatter was seen in the corresponding strain and the most clear trend was seen in the results from Deponit CA-N with lower strain.

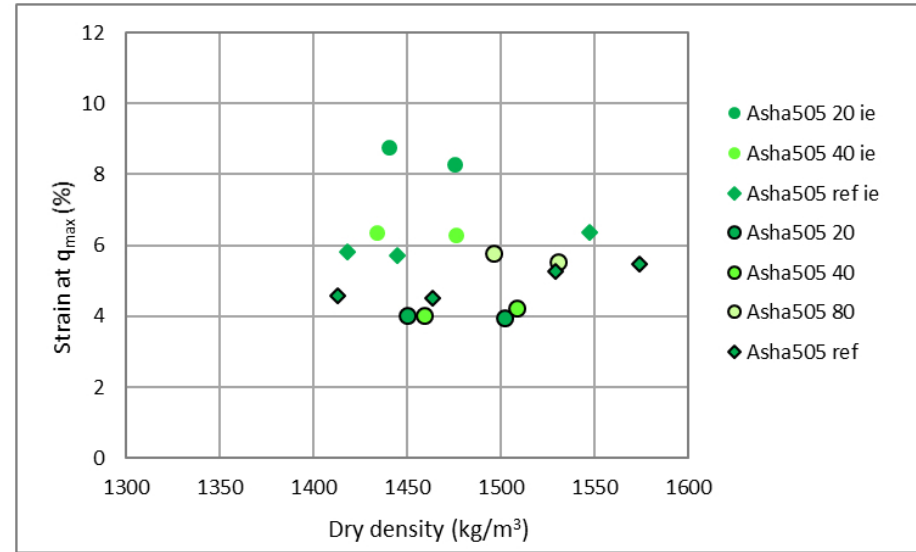
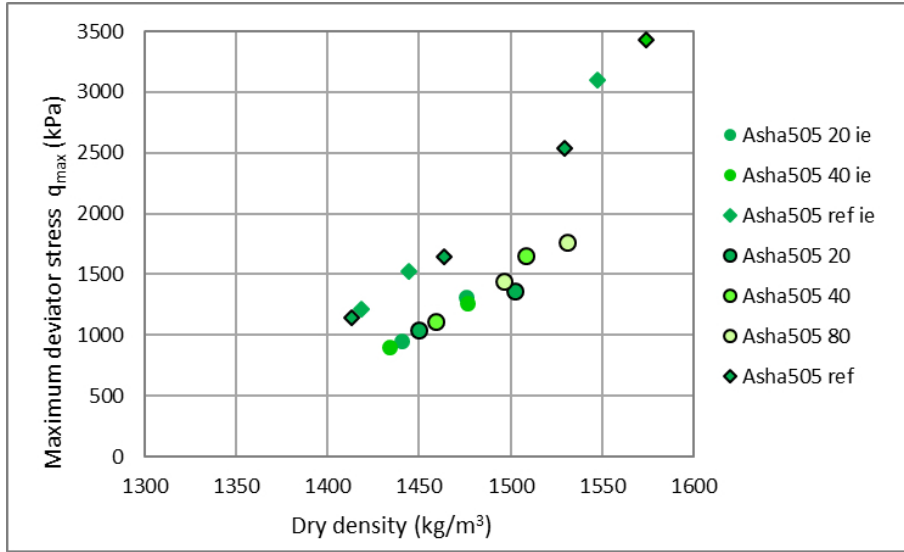


**Figure 8-10.** Maximum deviator stress and corresponding strain from unconfined compression tests on specimens of Asha505 from Figure 8-2 (black marker lines) and Figure 8-6 (no marker lines).

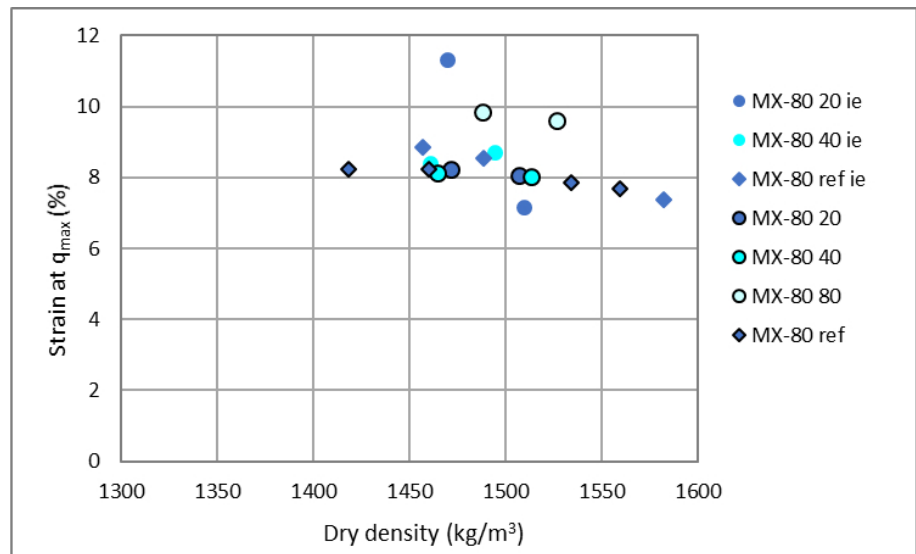
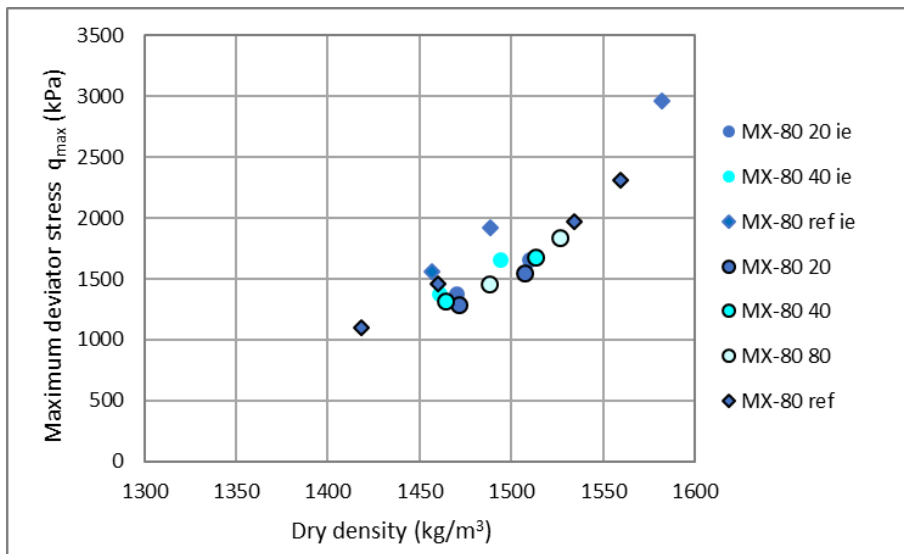


**Figure 8-11.** Maximum deviator stress and corresponding strain from unconfined compression tests on specimens of MX-80 from Figure 8-3 (black marker lines) and Figure 8-7 (no marker lines).

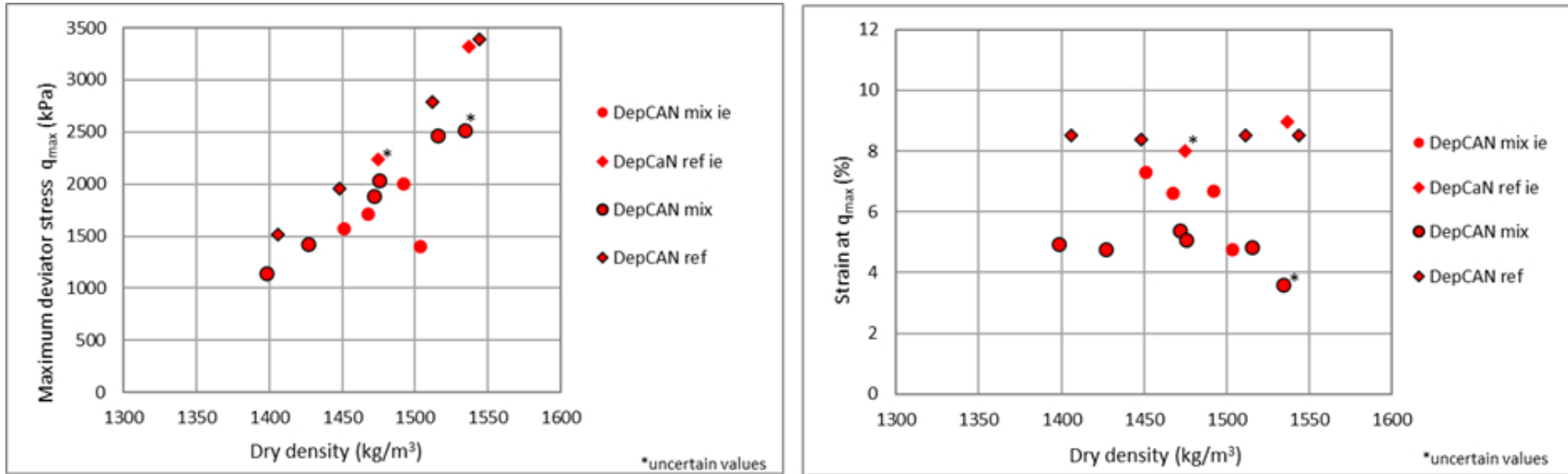


Figure 8-12. Maximum deviator stress and corresponding strain from unconfined compression tests on specimens of Deponit CA-N from Figure 8-4 (black marker lines) and Figure 8-8 (no marker lines).

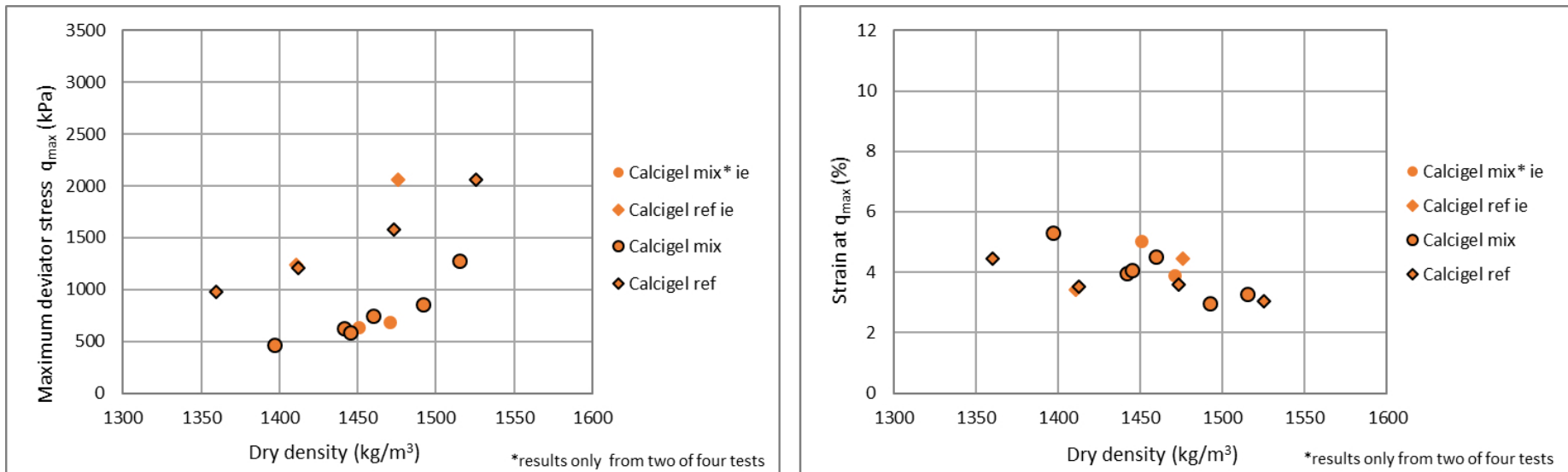
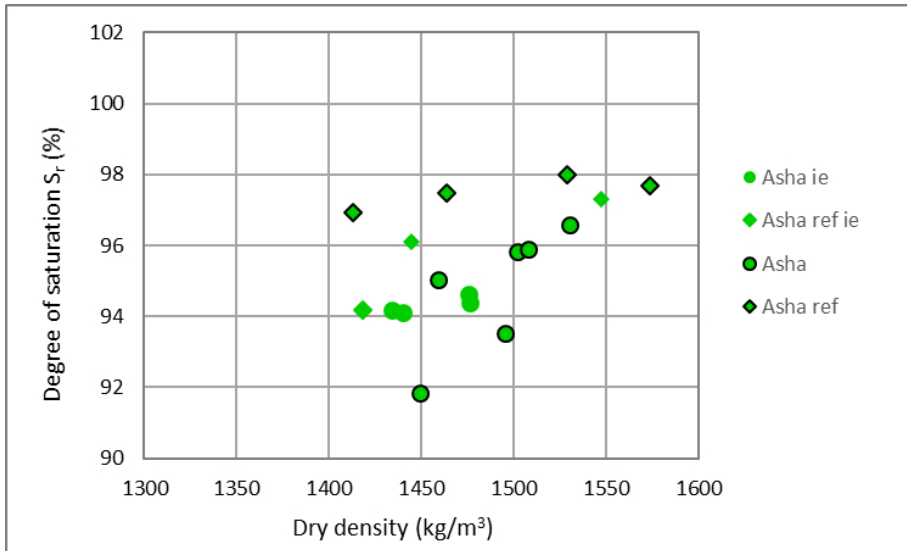


Figure 8-13. Maximum deviator stress and corresponding strain from unconfined compression tests on specimens of Calcigel from Figure 8-5 (black marker lines) and Figure 8-9 (no marker lines).

All specimens were considered to be saturated at shearing. The specimens saturated with ABM-water were prepared for 26–34 days while the ion-exchanged specimens were prepared for 77–93 days. The degree of saturation of all specimens are shown in Figure 8-14 to Figure 8-17 where the same colours, markers and marker lines as in Figure 8-10 to Figure 8-13 are used. From the diagrams below it can be seen that the degree of saturation was low in especially the specimens of Asha505 and Calcigel, which was unexpected.

The influence of degree of saturation on the results from the unconfined compression tests was studied in the report by Dueck (2010). No influence of degree of saturation on the deviator stress was seen on specimens of MX-80 but lower corresponding strain was observed at lower degree of saturation, approximately 2 % lower at a degree of saturation of 90 %.



**Figure 8-14.** Degree of saturation of all specimens of Asha505. Both specimens saturated with ABM-water (black marker lines) and those ion-exchanged (no marker lines) are shown, and both specimens from the field experiment (circles) and references (diamonds) are shown.

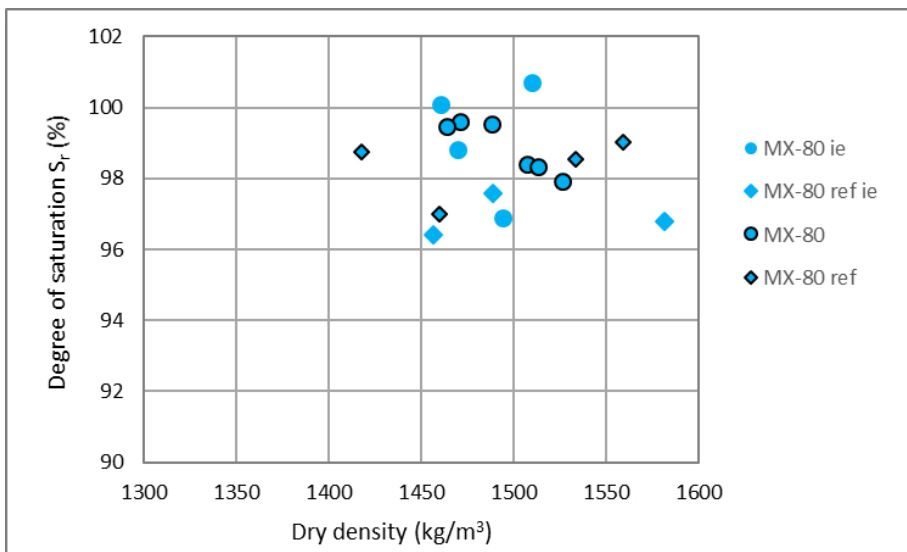


**Figure 8-15.** Degree of saturation of all specimens of MX-80. Both specimens saturated with ABM-water (black marker lines) and those ion-exchanged (no marker lines) are shown, and both specimens from the field experiment (circles) and references (diamonds) are shown.

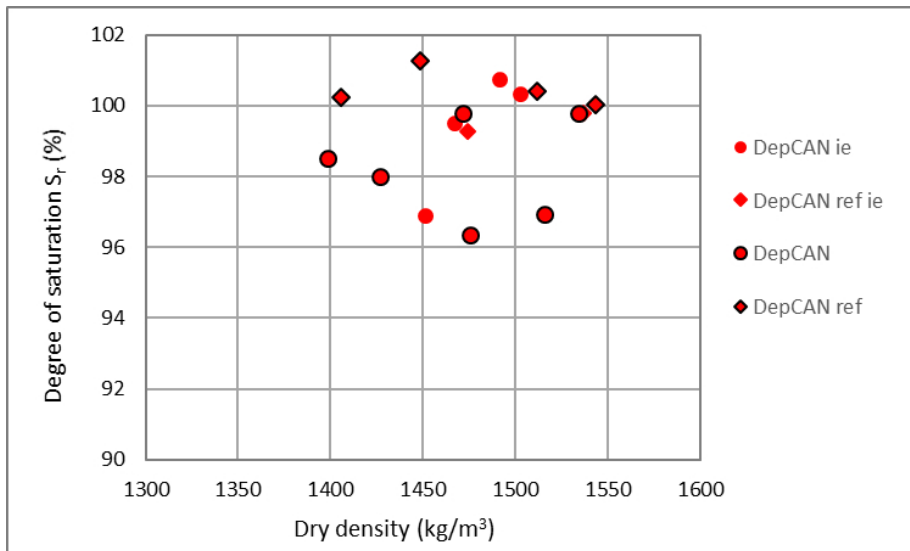


**Figure 8-16.** Degree of saturation of all specimens of Deponit CA-N. Both specimens saturated with ABM-water (black marker lines) and those ion-exchanged (no marker lines) are shown, and both specimens from the field experiment (circles) and references (diamonds) are shown.

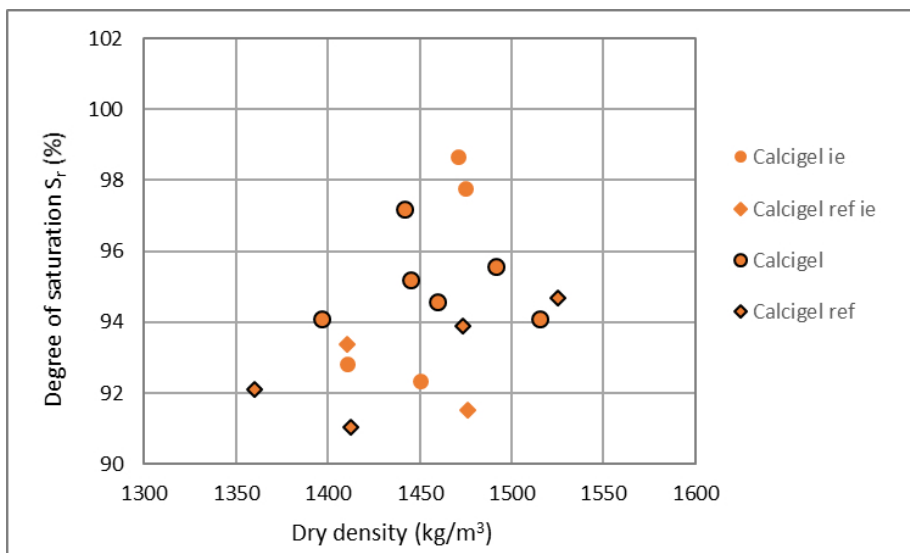


**Figure 8-17.** Degree of saturation of all specimens of Calcigel. Both specimens saturated with ABM-water (black marker lines) and those ion-exchanged (no marker lines) are shown, and both specimens from the field experiment (circles) and references (diamonds) are shown.

### **Comparison with ABM 1**

The package ABM 5 was installed in November 2012 and terminated after 4.5 years. The package was exposed to a maximum temperature of 250 °C and no artificial wetting was used. The package ABM 1, part of test series ABM 1–3, was retrieved 2009 after 2.5 years, exposed to a maximum temperature of 130 °C and artificially wetted (Svensson et al. 2011). In this section the results from re-compacted specimens from ABM 5 are compared to results from re-compacted specimens from ABM 1.

In the tests on material from ABM 1 unconfined compression tests were run on ground and re-compacted specimens of MX-80, Asha505 and Deponit CA-N, and ABM-water was used for the saturation. In Figure 8-18 to Figure 8-20 the results from Figure 8-2 to Figure 8-4 are shown together with the results from ABM 1 (Svensson et al. 2011).

The maximum deviator stress was approximately the same in specimens of MX-80 and Deponit CA-N from ABM 1 and ABM 5 but lower in specimens of Asha505 from ABM 5. The corresponding strain was approximately the same in specimens of Asha505 from the two packages but slightly lower in specimens of MX-80 and clearly lower in specimens of Deponit CA-N when the results from ABM 5 were compared to those from ABM 1.

The references from the two test packages ABM 5 and ABM 1 agree well for all materials which was expected since the same methodology and reference material were used.

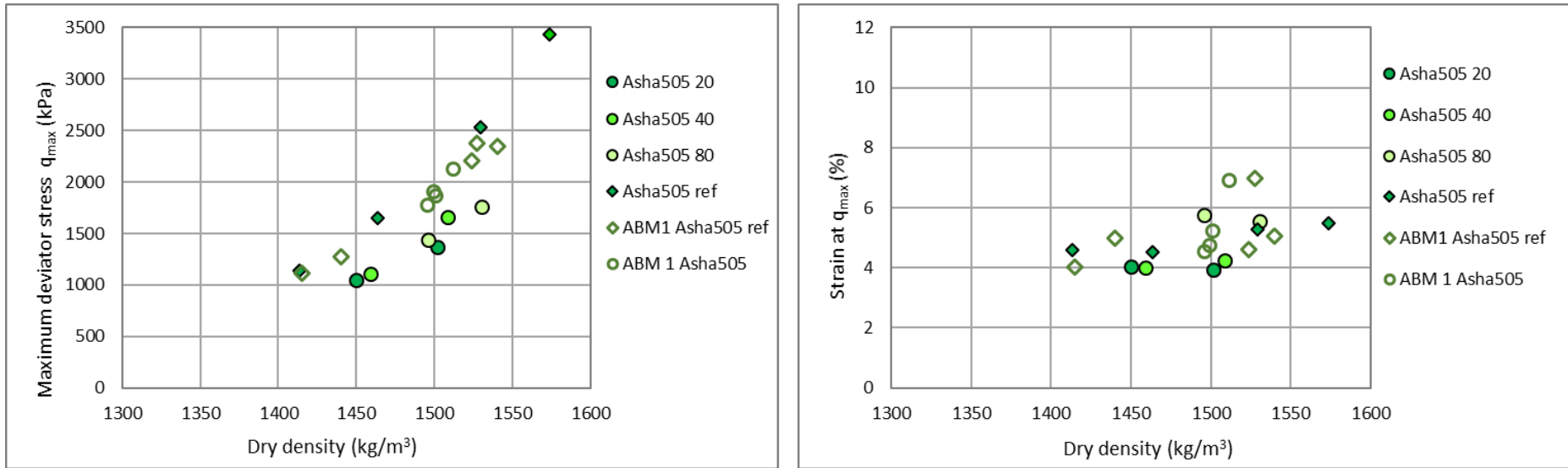


Figure 8-18. Results from Figure 8-2 together with corresponding results from ABM 1 (Svensson et al. 2011) marked with open symbols.

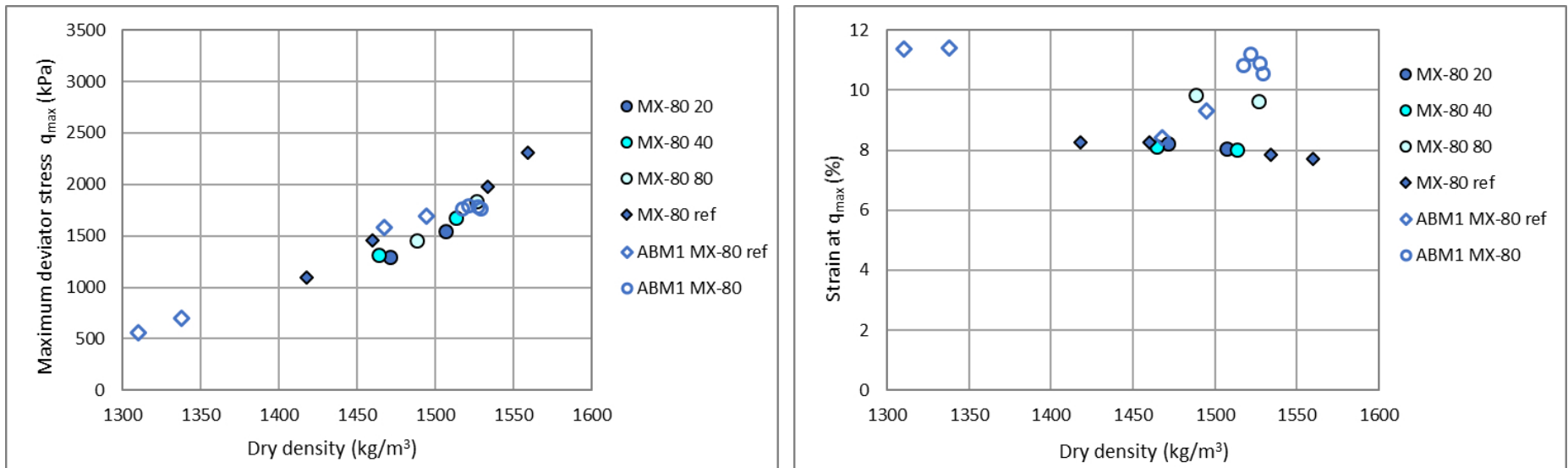


Figure 8-19. Results from Figure 8-3 together with corresponding results from ABM 1 (Svensson et al. 2011) marked with open symbols.

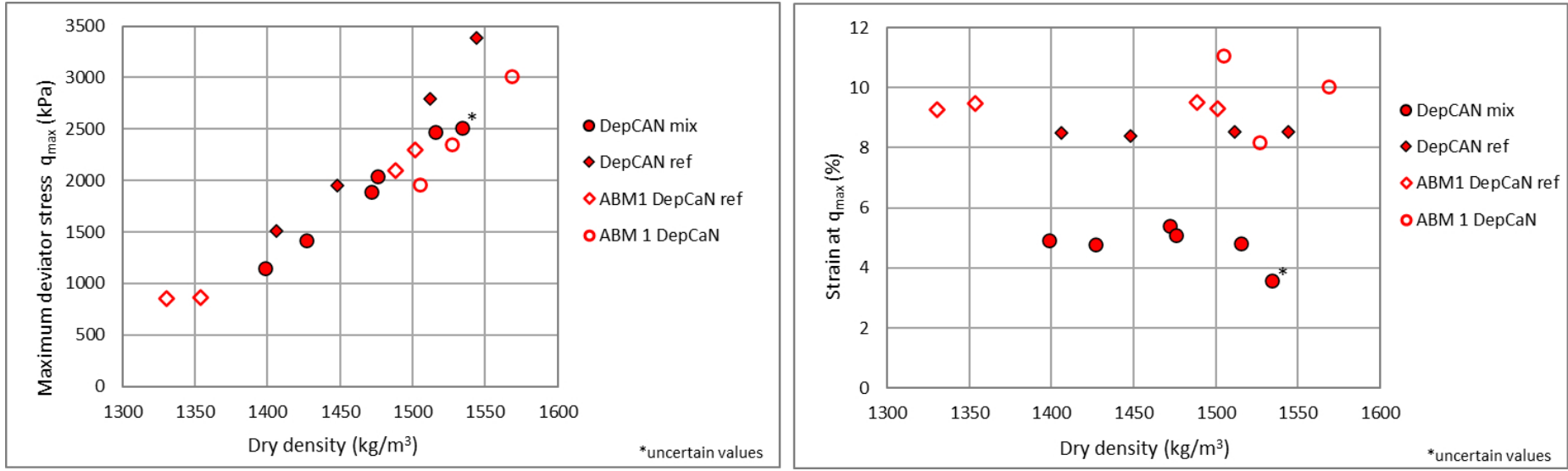


Figure 8-20. Results from Figure 8-4 together with corresponding results from ABM 1 (Svensson et al. 2011) marked with open symbols.

#### 8.1.4 Concluding remarks

Material from the field experiment ABM 45 test package 5 (ABM 5) was analysed by unconfined compression tests on ground and re-compacted specimens. Compared to the references the maximum deviator stress and the corresponding strain differed in the following ways for the different materials when saturated with ABM-water:

- Reduced maximum deviator stress was observed in the specimens of Asha505 and Calcigel.
- Somewhat reduced maximum deviator stress was observed in the specimens of MX-80 and Deponite CaN.
- Significantly reduced strain was observed in specimens of Deponit CA-N.
- The same or slightly higher strain was seen in specimens of MX-80.
- In specimens of Asha505 and MX-80 the influence of position was evaluated and while no influence was seen in the deviator stress the corresponding strain was higher at the outermost position.

Tests were also run on specimens ion-exchanged to be calcium dominated. The deviator stress seemed to be independent on whether ion-exchange was made or not. This was seen both in the references and in the material from the field experiment. The corresponding strain of the reference specimens seemed also to be independent on the ion-exchange. However, the corresponding strain of specimens from the field experiment showed larger values in specimens of Asha505, MX-80 and Deponit CA-N when ion-exchanged while no difference between ion-exchanged and not ion-exchanged specimens was seen in the results from Calcigel.

The specimens were considered to be water saturated at shearing. However, although prepared for four weeks or longer the degree of saturation was relatively low especially in specimens of Asha505 and Calcigel, which was unexpected. No large influence on the maximum deviator stress but somewhat lower corresponding strain could be expected at the actual degree of saturation of these specimens.

The results from the re-compacted specimens from ABM 5 were compared to results from re-compacted specimens from ABM 1. The maximum deviator stress was approximately the same in the specimens of MX-80 and Deponit CA-N from the two packages but lower in the specimens of Asha505 from ABM 5 compared to those from ABM 1. The corresponding strain was approximately the same in the specimens of Asha505 from the two packages but slightly lower in the specimens of MX-80 and clearly lower in the specimens of Deponit CA-N when the results from ABM 5 were compared to those from ABM 1. This is not expected to have any negative impact on the buffer performance.



## 9 Conclusions

Experiments such as ABM2 and ABM5 can be studied in so much detail and from so many perspectives, but due to the complexity and high number of different clays the scope of the investigations needs to be limited and well balanced even though many different groups have been working with the experiments for a long time period.

Based on the findings presented in this report and the collaborative research efforts with multiple groups and publications, the following conclusions can be drawn:

1. No general significant alteration of smectite in the bentonite was observed in either ABM2 or ABM5.
2. Minor changes were detected in the cation exchange capacity (CEC). However, these changes do not seem to be correlated with smectite transformation or any significant impact on important properties of the bentonite, such as swelling pressure and hydraulic conductivity.
3. The crucial properties of swelling pressure and hydraulic conductivity were largely unaffected by the extremely high temperatures in the ABM5 experiment.
4. Minor formation of trioctahedral smectite, most likely ferrosaponite, was observed in ABM2. However, the extent of formation was minimal and is not expected to affect the performance of the bentonite. It is important to note that this reaction has not been observed in experiments using copper heaters, which are the actual canister material in the SKB KBS-3 design.
5. Corrosion products were formed in both ABM2 and ABM5 (at the iron heater interface), as well as dissolution-precipitation and cation exchange reactions.
6. Magnesium redistribution was occasionally observed, and in some cases, it correlated with the formation of trioctahedral smectite and changes in the 060 region of the XRD patterns. Similar magnesium redistribution and accumulation towards the heater have also been observed in experiments with copper heaters to a minor extent, although the underlying mechanisms are not yet fully understood.
7. Unexpected accumulation of halite was observed in the Kunigel block #22 of ABM2 and is attributed to the high temperature, possibly coupled with a pressure drop resulting from a local fracture.
8. Unexpected physical breakdown of some of the bentonite blocks were observed in ABM5 and is attributed to the extremely high temperature conditions during the experiment.

The ABM3, ABM4, and ABM6 are ongoing experiments and are anticipated to be excavated in the near future. The excavation of these experiments will provide an opportunity to further investigate and continue the studies in this field. The data and insights gained from these experiments will continue to contribute to the ongoing research efforts and enhance our understanding of the long-term performance and behavior of the engineered barriers under relevant conditions.



## References

SKB's (Svensk Kärnbränslehantering AB) publications can be found at [www.skb.com/publications](http://www.skb.com/publications).

**Ammann L, Bergaya F, Lagaly G, 2005.** Determination of the cation exchange capacity of clays with copper complexes revisited. *Clay Minerals* 40, 441–453.

**Belyayeva N I, 1967.** Rapid method for the simultaneous determination of the exchange capacity and content of the exchange capacity and content of exchangeable cations in solonchic soils. *Soviet Soil Science* 1409–1413.

**Caballero E, Jiménez de Cisneros C, Huertas F J, Huertas F, Pozzuoli A, Linares J, 2005.**

**Bentonites from Cabo de Gata, Almería, Spain: a mineralogical and geochemical overview.** *Clay Minerals* 40, 463–480.

**Carlson L, Karnland O, Oversby V M, Rance A, Smart N, Snellman M, Vähänen M, Werme L O, 2007.** *Physics and Chemistry of the Earth* 32, 334–345.

**Chen Y G, Liu X M, Mu X, Ye W M, Cui Y J, Chen B, Wu D W, 2018.** Thermal Conductivity of Compacted GO-GMZ Bentonite Used as Buffer Material for a High-Level Radioactive Waste Repository. *Advances in Civil Engineering*, Article ID 9530813.

**Christidis G E, Scott P W, Marcopoulos T, 1995.** Origin of the bentonite deposits of Eastern Milos. Aegean. Greece: geological, mineralogical and geochemical evidence. *Clays and Clay Minerals* 43, 63–77.

**Claret F, Sakharov B A, Drits V A, Velde B, Meunier A, Griffault L, Lanson B, 2004.** Clay minerals in the Meuse-Haute Marne underground laboratory (France): possible influence of organic matter on clay mineral evolution. *Clays and Clay Minerals* 52, 515–532.

**Decher A, Bechtel A, Echle W, Friedrich G, Hoernes S, 1996.** Stable isotope geochemistry of the bentonites from the island of Milos (Greece). *Chemical Geology* 129, 101–113.

**Dueck A, 2010.** Thermo-mechanical cementation effects in bentonite investigated by unconfined compression tests. SKB TR-10-41, Svensk Kärnbränslehantering AB.

**Dueck A, Johannesson L-E, Kristensson O, Olsson S, 2011.** Report on hydro-mechanical and chemical-mineralogical analyses of the bentonite buffer in Canister Retrieval Test. SKB TR-11-07. Svensk Kärnbränslehantering AB.

**Dohrmann R, Kaufhold S, 2017.** Characterization of the Second Package of the Alternative Buffer Material (ABM) Experiment – II Exchangeable Cation Population Rearrangement. *Clays Clay Minerals*, 65, 104–121.

**Elzea J M, Murray H H, 1989.** Trace element composition of the Cretaceous Clay Spur bentonite and implications for its alteration history. Abstract of the 9th International Clay Conference, Strasbourg, 28 August – 2 September 1989, 132.

**Eng A, Nilsson U, Svensson D, 2007.** Alternative Buffer Material. Installation report. SKB report. IPR-07-15, Svensk Kärnbränslehantering AB.

**Elzea J M, Murray H H, 1990.** Variation in the mineralogical, chemical and physical properties of the Cretaceous Clay Spur bentonite in Wyoming and Montana (U.S.A). *Applied Clay Science* 5, 229–248.

**Engineering ToolBox, 2021.** [https://www.engineeringtoolbox.com/mineral-density-d\\_1555.html](https://www.engineeringtoolbox.com/mineral-density-d_1555.html) [21 August 2021]

**ENRESA, 1998.** Bentonite: origin and properties. In FEBEX – Full-scale Engineered Barriers Experiment in crystalline host rock. ENRESA Publication Technica 01/98, 13–30, Spain.

**Fernández A M, Marco, J F, Nieto P, León F J, Robredo L M, Clavero M Á, Cardona, A I, Fernández S, Svensson D, Sellin P, 2022.** Characterization of Bentonites from the In Situ ABM5 Heater Experiment at Äspö Hard Rock Laboratory, Sweden. *Minerals* 12, 471.

- Grim R E, Güven N (eds), 1978.** Bentonites – geology. mineralogy and uses. Developments in Sedimentology 24. Amsterdam. Elsevier
- Karnland O, Olsson S, Nilsson U, 2006.** Mineralogy and sealing properties of various bentonites and smectite-rich clay materials. SKB TR-06-30, Svensk Kärnbränslehantering AB.
- Karnland O, Olsson S, Dueck A, Birgersson B, Nilsson U, Hernan-Håkansson T, Pedersen K, Nilsson S, Eriksen T E, Rosborg B, 2009.** Long term test of buffer material at the Äspö Hard Rock Laboratory, LOT project. Final report on the A2 test parcel. SKB TR-09-29, Svensk Kärnbränslehantering AB.
- Kaufhold, S, Dohrmann R, Klinkenberg M, Siegesmund S, Ufer K, 2010.** N<sub>2</sub>-BET specific surface area of bentonites. Journal of Colloid and Interface Science 349, 275–282.
- Kaufhold S, Dohrmann R, Sandén T, Sellin P, Svensson D, 2013.** Mineralogical investigations of the alternative buffer material test – I. Alteration of bentonites. Clay Minerals 48, 199–213.
- Kaufhold S, Dohrmann R, Götze N, Svensson D, 2017.** Characterization of the second parcel of the alternative buffer material (ABM) Experiment—I mineralogical reactions. Clays Clay Miner 65, 27–41.
- Kaufhold S, Chryssikos G D, Kacandes G, Gionis V, Ufer K, Dohrmann R, 2019.** Geochemical and mineralogical characterization of smectites from the Ventzia basin, western Macedonia, Greece. Clay Minerals, 54, 95–107.
- Kaufhold S, Dohrmann R, Ufer K, Svensson D, Sellin P, 2021.** Mineralogical Analysis of Bentonite from the ABM5 Heater Experiment at Äspö Hard Rock Laboratory, Sweden. Minerals 11, 669.
- Kelepertsis A E, 1989.** Formation of sulfates at the Thiaphes area of Milos Island: possible precursors of kaolinite mineralization. Canadian Mineralogist 27, 241–245.
- Khaled E M, Stucki J W, 1991.** Effects of iron oxidation state on cation fixation in smectites. Soil Science Society of America Journal 50, 550–554.
- Konta J, 1986.** Textural variation and composition of bentonite derived from basaltic ash. Clays and Clay Minerals 34, 257–265.
- Kumpulainen S, Kiviranta L, Carlsson T, Muurinen A, Svensson D, Sasamoto H, Wersin P, 2010.** Long-term alteration of bentonite in the presence of metallic iron. SKB R-10-52, Svensk Kärnbränslehantering AB.
- Lantenois S, Lanson B, Muller F, Bauer A, Jullien M, Plancon A, 2005.** Experimental study of smectite interaction with metal Fe at low temperature: 1. Smectite destabilization. Clays and Clay Minerals 53, 597–612.
- Leal Olloqui M, 2020.** A study of alteration processes in bentonite. PhD thesis, University of Bristol, UK.
- Liu Y M, Chen Z R, 2001.** Bentonite from Gaomiaozhi, Inner Mongolia as an ideal buffer/backfilling material in handling highly radioactive wastes—a feasibility study. Acta Mineralogica Sinica 21:3, 541–543 (in Chinese with English abstract).
- Martin Vivaldi J L, 1962.** The Bentonites of Cabo de Gata (Southeast Spain) and of Guelaya Volcanic Province (North Morocco). Clays and Clay Minerals 11, 327–357.
- Meier L P, Kahr G, 1999.** Determination of the cation exchange capacity (CEC) of clay minerals using the complexes of copper(II) ion with triethylenetetramine and tetraethylenepentamine. Clays and Clay Minerals 47, 386–388.
- Olsson S, Jensen V, Johansson L E, Hansen E, Karnland O, Kumpulainen S, Kirivanta L, Svensson D, Hansen S, Lindén J, 2013.** Prototype Repository – Hydromechanical, chemical and mineralogical characterization of the buffer and backfill material from the outer section of the Prototype Repository. SKB TR-13-21, Svensk Kärnbränslehantering AB.
- Sandén T, Nilsson U, 2020.** Installation. monitoring. dismantling and initial analyses of material from LOT test package S2 and A3. Results from field test. SKB TR-20-11, Svensk Kärnbränslehantering AB.

- Sandén T, Olsson S, Andersson L, Dueck A, Jensen V, Hansen E, Johnsson A, 2014.** Investigation of backfill candidate materials. SKB R-13-08, Svensk Kärnbränslehantering AB.
- Sandén T, Nilsson U, Andersson L, Svensson D, 2018.** ABM 45 experiment at Äspö Hard Rock Laboratory. Installation report. SKB P-18-20, Svensk Kärnbränslehantering AB.
- Shah N R, 1997.** Indian bentonite: focus on the Kutch region. *Industrial Minerals* 359, 43–47.
- Slaughter M, Earley J W, 1965.** Mineralogy and geological significance of the Mowry bentonites. Wyoming. New York: Geological Society of America. Wyoming, NY. (Geological Society of America Special Paper 83)
- Svensson D, 2015.** The bentonite barrier: swelling properties. redox chemistry and mineral evolution. PhD thesis. Lund University, Sweden.
- Svensson D, Hansen S, 2013.** Redox chemistry in two iron-bentonite field experiments at Äspö Hard Rock Laboratory, Sweden: An XRD and Fe K-edge XANES study. *Clays and Clay Minerals* 61, 566–579.
- Svensson D, Dueck A, Nilsson U, Sandén T, Lydmark S, Jägerwall S, Pedersen K, Hansen S, 2011.** Alternative buffer material. Status of ongoing laboratory investigation of reference material and test package 1. SKB TR-11-06, Svensk Kärnbränslehantering AB.
- Svensson D, Lundgren C, Johannesson L-E, Norrfors K, 2017.** Developing strategies for acquisition and control of bentonite for a high level radioactive waste repository. SKB TR-16-14, Svensk Kärnbränslehantering AB.
- Svensson D, Eriksson P, Johannesson L-E, Lundgren C, Bladström T, 2019.** Development and testing of methods suitable for quality control of bentonite as KBS-3 buffer and backfill. SKB TR-19-25, Svensk Kärnbränslehantering AB.
- Sudheer Kumar R, Podlech C, Grathoff G, Warr L N, Svensson D, 2021.** Thermally Induced Bentonite Alterations in the SKB ABM5 Hot Bentonite Experiment. *Minerals* 11:1017.
- Sun D, Sun W, Fang L, 2014.** Swelling characteristics of Gaomiaozi bentonite and its prediction. *Journal of Rock Mechanics and Geotechnical Engineering* 6:2, 113–118.
- Süd-Chemie AG, 2011.** Zusammensetzung und Vorkommen von Bentoniten. Munich: Süd-Chemie Agrimont.
- Takagi T, 2005.** Bentonite in Japan – Geology and industries. Umezono, Japan. (Open file report of Geological Survey of Japan, no. 425)
- Wersin P, Hadi J, Jenni A, Svensson D, Grenèche J-M, Sellin P, Leupin O X, 2021.** Interaction of Corroding Iron with Eight Bentonites in the Alternative Buffer Materials Field Experiment (ABM2). *Minerals* 11:907.
- Åkesson M, Olsson S, Dueck A, Nilsson U, Karnland O, Kiviranta L, Kumpulainen S, Lindén J, 2012.** Temperature buffer test. Hydro-mechanical and chemical/mineralogical characterizations. SKB P-12-06, Svensk Kärnbränslehantering AB.



**Photos of sampling for unconfined compression tests**

Samples from different parts of ABM 5 were taken for the actual analyses. Four different materials (MX-80, Asha505, Calcigel, Deponit CA-N) were used and photos from the sampling are shown below.



*Figure A1-1. MX-80 samples from ABM 5 used for the analyses. Samples were taken from block number 20.*



*Figure A1-2. Asha505 samples from ABM 5 used for the analyses. Samples were taken from block number 16.*



**Figure A1-3.** Samples from ABM 5 for the analyses; Deponit CA-N (to the left) and Calcigel (to the right). The samples were taken from block number 26 and 27, respectively.

## Results from unconfined compression tests

In the diagrams below the results from all unconfined compression tests are presented as deviator stress as a function of strain, see Section 8.1.3. The different materials (Asha505, MX-80, Deponit CA-N, Calcigel) are marked with different colours (green, blue, red, orange) as in the section mentioned above and the references are marked with black lines. The labels contain the Test ID, according to Table 8-3 and Table 8-4, and the dry density of the specimens.

In Figure A2-1 to Figure A2-4 results from specimens saturated with ABM-water are shown. In Figure A2-5 to Figure A2-8 the results from specimens saturated with ABM-water and subsequently ion-exchanged to be calcium dominated are shown.

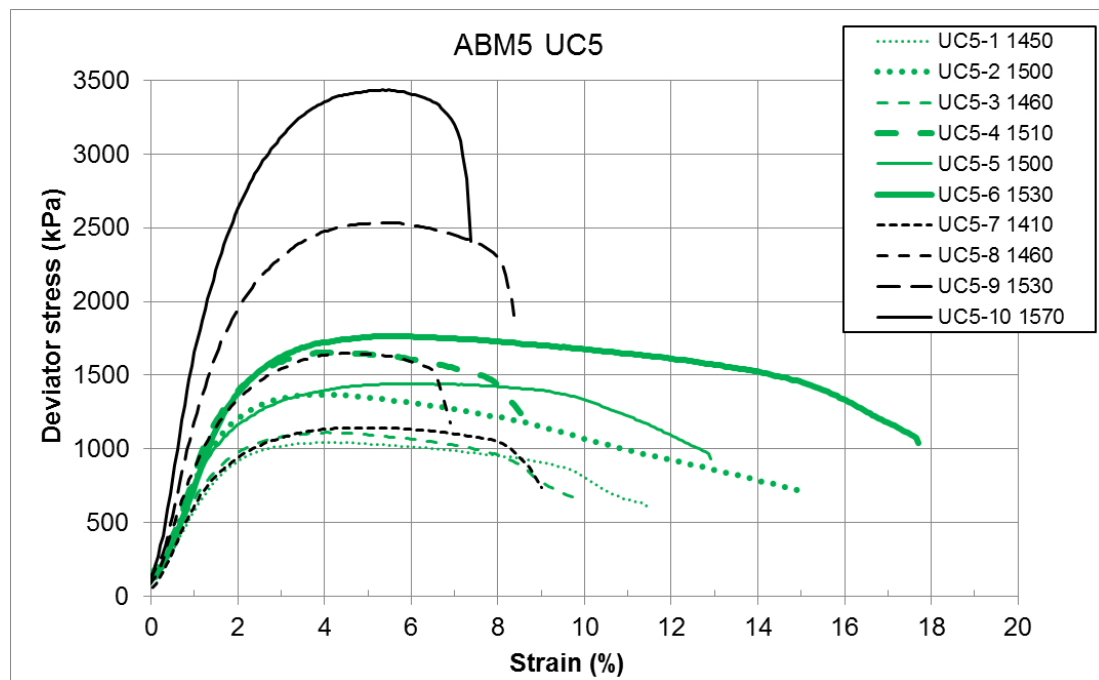


**Figure A2-1.** Evolution of deviator stress as a function of strain of Asha505 specimens saturated with ABM-water. The colours green and black denote specimens from block 16 and reference material, respectively. The labels contain Test ID and dry density ( $\text{kg/m}^3$ ).

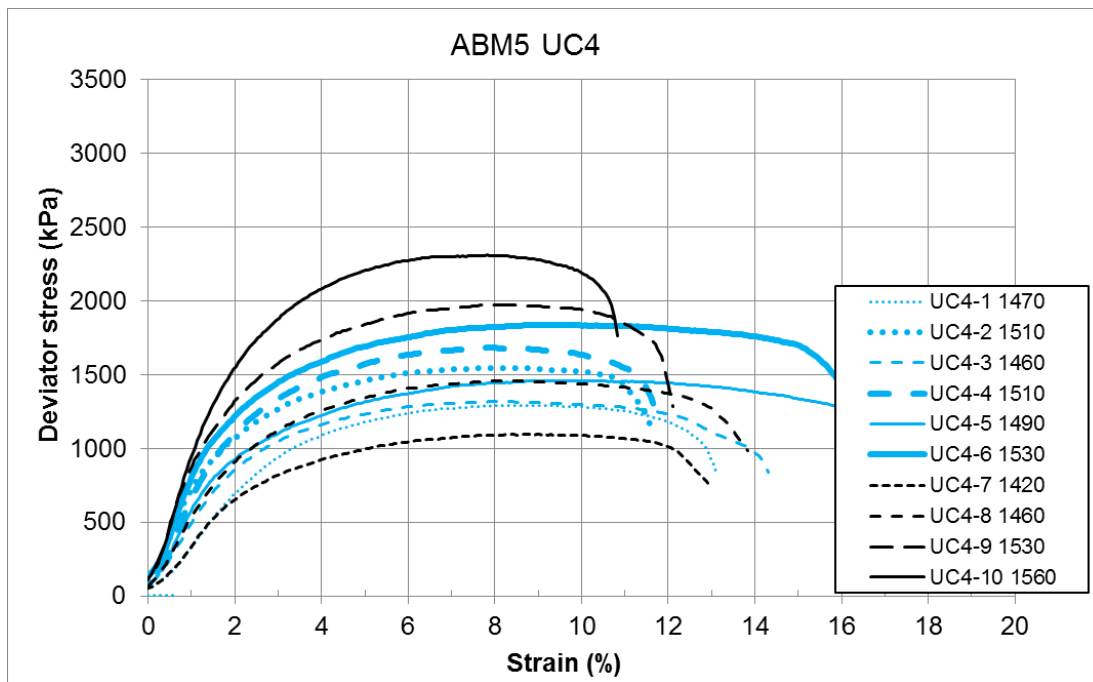


**Figure A2-2.** Evolution of deviator stress as a function of strain of MX-80 specimens saturated with ABM-water. The colours blue and black denote specimens from block 20 and reference material, respectively. The labels contain Test ID and dry density ( $\text{kg/m}^3$ ).

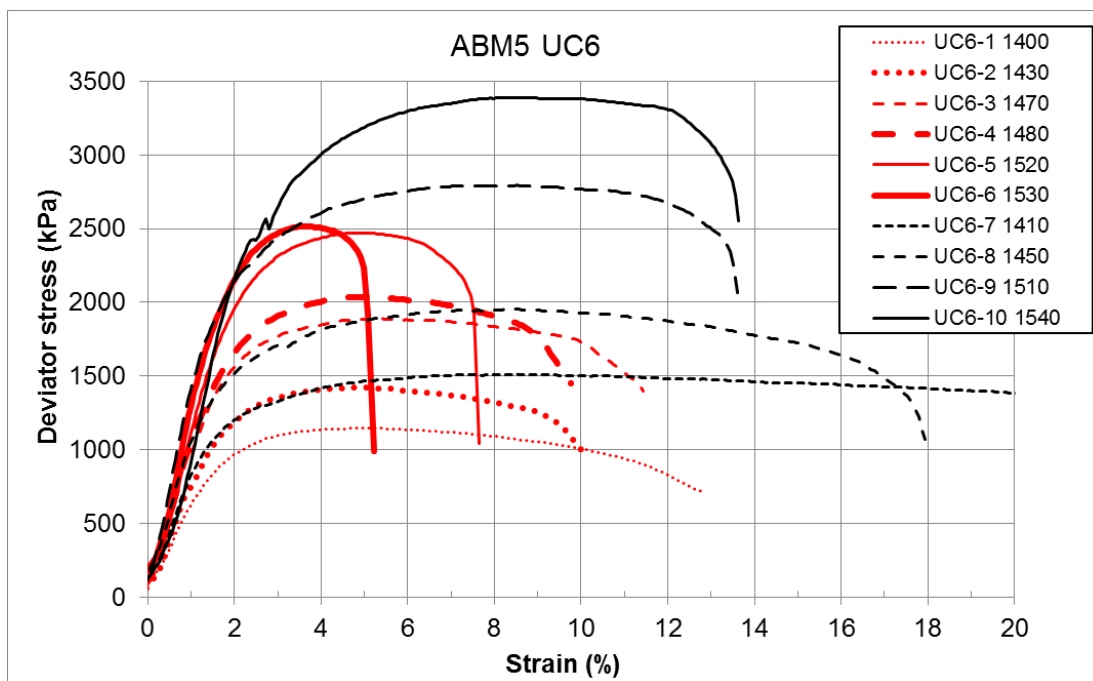


**Figure A2-3.** Evolution of deviator stress as a function of strain of Deponit CA-N specimens saturated with ABM-water. The colours red and black denote specimens from block 26 and reference material, respectively. The labels contain Test ID and dry density ( $\text{kg/m}^3$ ).

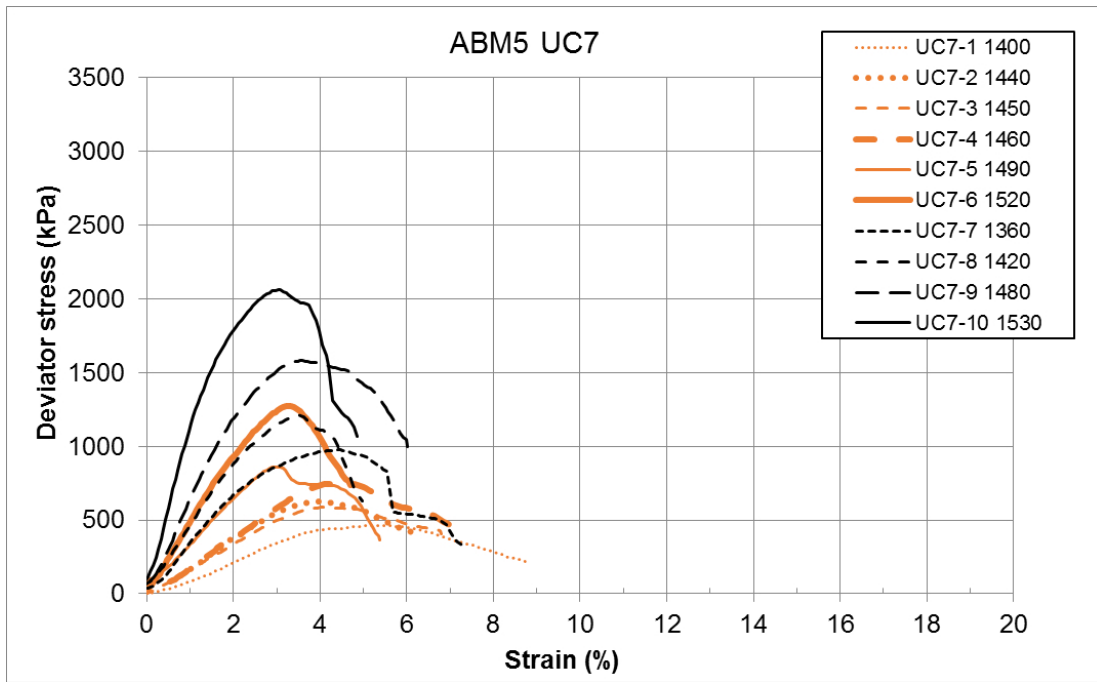


**Figure A2-4.** Evolution of deviator stress as a function of strain of Calcigel specimens saturated with ABM-water. The colours orange and black denote specimens from block 27 and reference material, respectively. The labels contain Test ID and dry density ( $\text{kg/m}^3$ ).

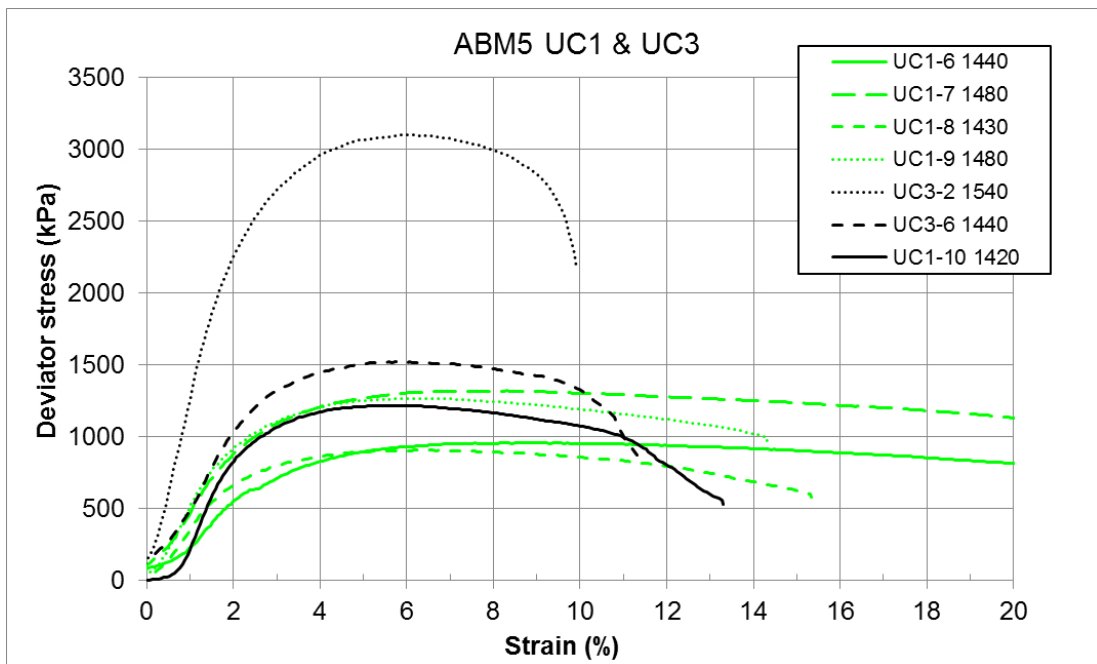


**Figure A2-5.** Evolution of deviator stress as a function of strain of Asha505 specimens saturated with ABM-water and ion-exchanged with  $\text{CaCl}_2$ . The colours green and black denote specimens from block 16 and reference material, respectively. The labels contain Test ID and dry density ( $\text{kg/m}^3$ ).

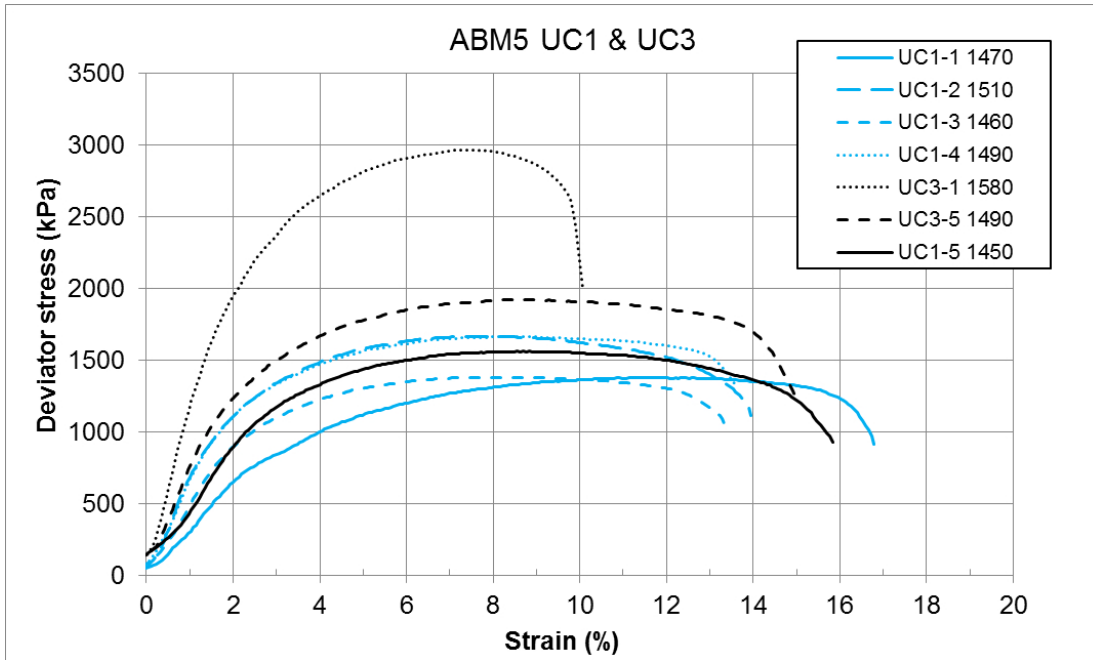


**Figure A2-6.** Evolution of deviator stress as a function of strain of MX-80 specimens saturated with ABM-water and ion-exchanged with  $\text{CaCl}_2$ . The colours blue and black denote specimens from block 20 and reference material, respectively. The labels contain Test ID and dry density ( $\text{kg/m}^3$ ).

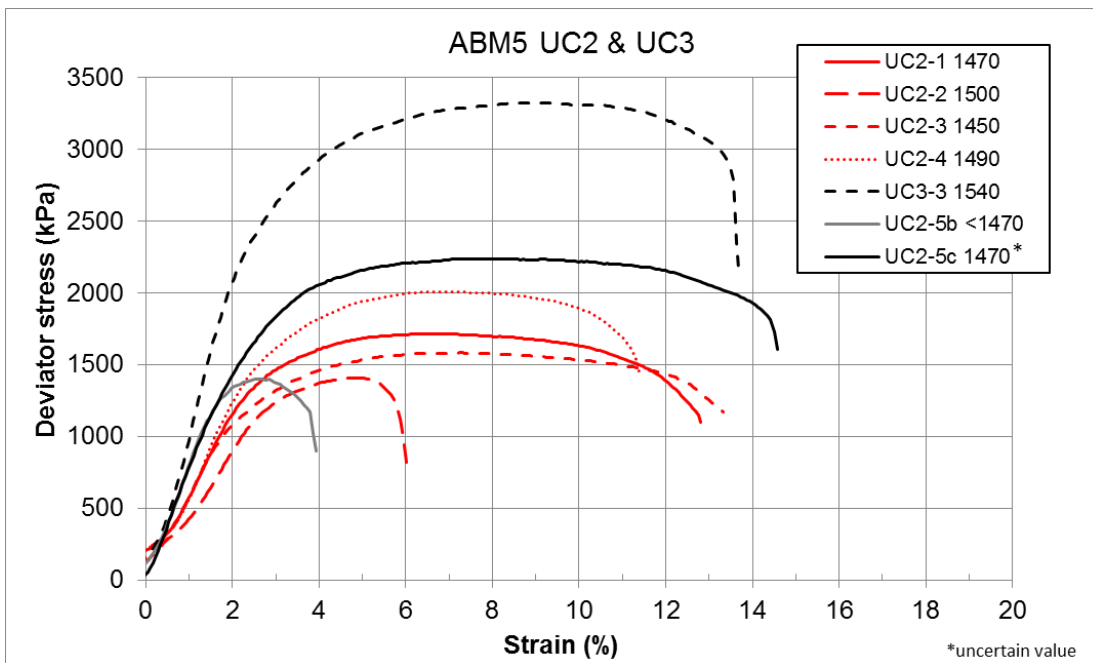


**Figure A2-7.** Evolution of deviator stress as a function of strain of Deponit CA-N specimens saturated with ABM-water and ion-exchanged with  $\text{CaCl}_2$ . The colours red and black denote specimens from block 26 and reference material, respectively. The labels contain Test ID and dry density ( $\text{kg/m}^3$ ). Specimen UC2-5 was tested twice. The higher  $q_{\text{max}}$  was used in the report, however marked as uncertain.

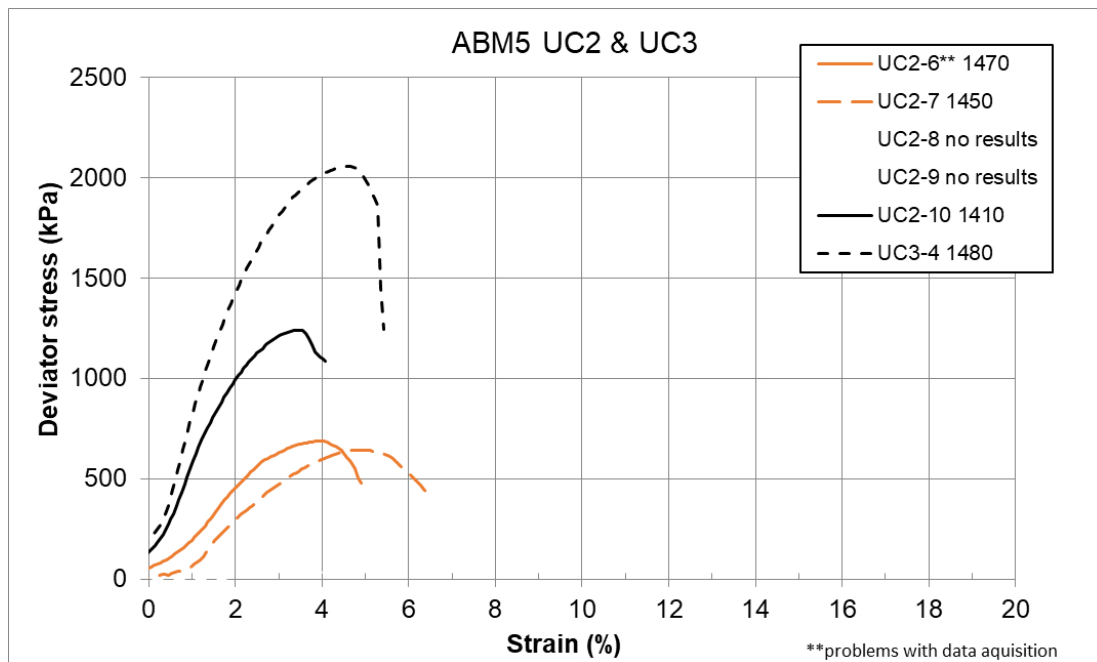


**Figure A2-8.** Evolution of deviator stress as a function of strain of Calcigel specimens saturated with ABM-water and ion-exchanged with  $\text{CaCl}_2$ . The colours orange and black denote specimens from block 27 and reference material, respectively. The labels contain Test ID and dry density ( $\text{kg/m}^3$ ).

In the test series the failure surface through specimens prepared from field experiment material differed somewhat from the failure surfaces through reference specimens. Theoretically the failure is assumed to take place along a plane inclined  $45^\circ$  to the horizontal plane. Examples of failure surfaces from some of the references are shown in Figure A2-9 and Figure A2-10. The vertical failure surface seen to the right in Figure A2-10 was in this study only seen in specimens of Calcigel. However, it was seen both in specimens from the field experiment and reference specimens and no coupling to the degree of saturation could be seen.



**Figure A2-9.** Photo after unconfined compression tests on ion-exchanged specimens of Asha 505 and MX-80 with dry densities  $1550 \text{ kg/m}^3$  and  $1490 \text{ kg/m}^3$  respectively.

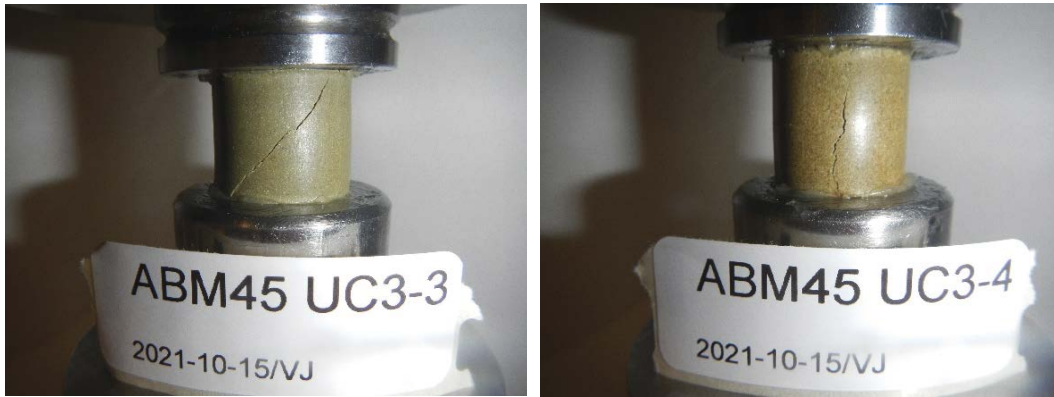


**Figure A2-10.** Photo after unconfined compression tests on ion-exchanged specimens of Deponit CA-N and Calcigel with dry densities  $1540 \text{ kg/m}^3$  and  $1480 \text{ kg/m}^3$  respectively.

SKB is responsible for managing spent nuclear fuel and radioactive waste produced by the Swedish nuclear power plants such that man and the environment are protected in the near and distant future.

**skb.se**